Erick Alejandro Gonzalez Olivares

Hybridization between Plasma and MIG Processes in a Tandem Configuration for Aluminum Joints

Aachener Berichte Fügetechnik
Herausgeber: Prof. Dr.-Ing. U. Reisgen

Band 2/2022 Shaker Verlag

Hybridization between Plasma and MIG Processes in a Tandem Configuration for Aluminum Joints

Hybridisierung zwischen Plasma- und MSG-Prozessen in einer Tandemkonfiguration für Aluminiumverbindungen

Von der Fakultät für Maschinenwesen der Rheinisch-Westfälischen Technischen Hochschule Aachen zur Erlangung des akademischen Grades eines Doktors der Ingenieurwissenschaften genehmigte Dissertation

vorgelegt von

Erick Alejandro Gonzalez Olivares

Berichter: Universitätsprofessor Dr.-Ing. Uwe Reisgen

Universitätsprofessorin Dr.-Ing. Kirsten Bobzin

Tag der mündlichen Prüfung: 29.11.2021

Diese Dissertation ist auf den Internetseiten der Universitätsbibliothek online verfügbar.

Erick Alejandro Gonzalez Olivares

Hybridization between Plasma and MIG Processes in a Tandem Configuration for Aluminum Joints

Aachener Berichte Fügetechnik
Herausgeber: Prof. Dr.-Ing. U. Reisgen

Band 2/2022 Shaker Verlag

Bibliographic information published by the Deutsche Nationalbibliothek
The Deutsche Nationalbibliothek lists this publication in the Deutsche Nationalbibliografie; detailed bibliographic data are available in the Internet at http://dnb.d-nb.de.

Zugl.: D 82 (Diss. RWTH Aachen University, 2021)

Printed in Germany.

ISBN 978-3-8440-8639-3
ISSN 0943-9358

Shaker Verlag GmbH • Am Langen Graben 15a • 52353 Düren
Phone: 0049/2421/99011-0 • Telefax: 0049/2421/99011-9
Internet: www.shaker.de • e-mail: info@shaker.de

Danksagung

Diese Dissertation wurde mit finanziert durch ein Forschungsprojekt der Arbeitsgemeinschaft industrieller Forschungsvereinigungen (AiF) „Otto von Guericke“ e.V. und das Stipendium für ein Doktorat im Ausland wurde von der Nationalen Kommission für wissenschaftliche und technologische Forschung (CONICYT) vergeben.

Ich danke dem Institutsleiter, Prof. Dr.-Ing. U. Reisgen, für die Aufnahme als Doktorand und die Möglichkeit, mein Forschungsprojekt in den Einrichtungen des Instituts zu entwickeln.

Besonderer Dank geht an Dr. Lars Stein für die Hilfe bei meiner Dissertation zu korrigieren. Ich danke meiner Freundin Jenny Kinable, dass er mir bei der englischen Korrektur geholfen hat.

Ich danke auch meinen Freunden C. Hernandez, V. Celva, G. Truppel, J. Dornelles, G. Bernhard, N.C. de Amorim, C. Kammers, P. Jeager, G. Faustini, D. Ribeiro, T. Calegari, T. Franca und B. Elias, mit denen ich meine Freizeit verbracht habe und mir die Möglichkeit gaben, als Person zu wachsen.

Aachen, November 2021

Acknowledgements

This dissertation was financed by a research project of the Arbeitsgemeinschaft industrieller Forschungsvereinigungen (AiF) „Otto von Guericke“ e.V. and the scholarship for doctoral studies abroad was granted by the National Commission for Scientific and Technological Research (CONICYT).

I thank the Head of the Institute, Prof. Dr.-Ing. U. Reisgen, for accepting me as a PhD student and being able to develop my research project within the institute’s facilities.

Special thanks to Dr. Lars Stein for helping me to correct my thesis. I thank my friend Jenny Kinable for helping me with the English correction.

I also thank my friends C. Hernandez, V. Celva, G. Truppel, J. Dornelles, G. Bernhard, N. C. de Amorim, C. Kammers, P. Jeager, G. Faustini, D. Ribeiro, T. Calegari, T. Franca, and B. Elias who were with me in my spare time and with whom I had the opportunity to grow as a person.

Aachen, November 2021

Content

I. List of figures

II. List of tables

III. List of abbreviations

AC	Alternating Current
ASTM	American Society for Testing and Materials
BM	Base Metal
CTWD	Contact Tip-to-Workpiece Distance
DC	Direct Current
DCEN	Direct Current Electrode Negative
DCEP	Direct Current Electrode Positive
DIN	Deutsches Institut für Normung
EN	Europäische Norm
HAZ	Heat Affected Zone
MIG	Metal Inert Gas
PMZ	Partial Melted Zone
SSC	Static Source Characteristic
SAC	Static Arc Characteristic
TIG	Tungsten Inert Gas
VPPA	Variable Polarity Plasma Arc
WM	Weld Metal

IV. List of symbols

L_{el}	Wire-electrode extension	[mm]
L_a	Arc extension	[mm]
R^2	Coefficient of determination	[-]
a	MIG arc length	[mm]
V_M	MIG voltage	[V]
I_M	MIG current	[A]
I_P	Plasma current	[A]

V. Abstract

Welding is one of the key manufacturing processes in the metal mechanic industry, for this reason, any improvement in quality and efficiency leads to enhanced overall productivity. On the other hand, aluminum alloys are increasingly becoming a fundamental part of the task of reducing the weight of metal structures in means of transport, as a means of reducing CO_2 emissions. The union or hybridization between two welding processes as a means of increasing productivity in joint applications is a widely used and studied technique. An alternative hybrid process that is being studied in recent years is the Plasma-MIG process in a tandem configuration. This process is characterized by having a torch arrangement on the same axis (paraxial) with a distance between them. With this configuration it is guaranteed that each one of its processes maintains its unique properties. However, problems and phenomena such as current transfer between the welding arcs which affects the measurement of electrical signals have been vaguely commented on in the scarce literature on the subject.

In this investigation the Plasma-MIG in tandem configuration is characterized by gradually bringing their torches closer together in order to observe the behavior of their electrical signals as the arcs are coupled. In addition, the Plasma process is configured with direct and alternating current, in order to observe the need for cathodic cleaning when the hybrid process is used in aluminum alloys. Once the phenomena that occur when hybridizing the processes are known, the interaction between the welding processes is studied, from an energy point of view. The objective is to observe if there is an exchange of current between the welding processes and, if it exists, how this affects the welding processes. The results showed that it is possible to couple the Plasma and MIG processes in a paraxial (tandem) configuration to make aluminum joints, with a stable arc and greater penetration than the single processes. The establishment of a "current path" between the MIG and plasma arcs was noticed, which allows the current flow between the welding process, influencing directly the MIG arc length behavior. Moreover, it was concluded that it is not necessary to configure alternating current in the Plasma process to weld aluminum, because the MIG process does the cathodic cleaning. It was also concluded that an external magnetic field is not necessary to stabilize the behavior of the welding arcs. The joints of 10 and 15 mm

thickness presented good surface appearance, although the hybrid process demonstrated superiority only for the 15 mm thick joints.

Kurzfassung

Schweißen ist einer der wichtigsten Herstellungsprozesse in der Metallmechanik. Aus diesem Grund führt jede Verbesserung der Qualität und Effizienz zu einer Steigerung der Gesamtproduktivität. Auf der anderen Seite werden Aluminiumlegierungen immer mehr zu einem grundlegenden Bestandteil der Aufgabe, das Gewicht von Metallstrukturen in Transportmitteln zu reduzieren, um so die CO2-Emissionen zu verringern. Die Vereinigung oder Hybridisierung zwischen zwei Schweißprozessen als Mittel zur Produktivitätssteigerung bei Verbindungsanwendungen ist eine weit verbreitete und untersuchte Technik. Ein alternativer Hybridprozess, der in den letzten Jahren untersucht wird, ist der Plasma-MIG-Prozess in einer Tandemkonfiguration. Dieses Verfahren zeichnet sich dadurch aus, dass die Brenner auf derselben Achse (paraxial) mit einem Abstand zueinander angeordnet sind. Mit dieser Konfiguration ist gewährleistet, dass jeder seiner Prozesse seine einzigartigen Eigenschaften beibehält. Probleme und Phänomene, wie z.B. die Stromübertragung zwischen den Schweißlichtbögen, die die Messung der elektrischen Signale beeinträchtigt, sind jedoch in der spärlichen Literatur zu diesem Thema nur vage kommentiert worden.

In dieser Untersuchung wird das Plasma-MIG in Tandemkonfiguration dadurch charakterisiert, dass sich ihre Brenner allmählich einander annähern, um das Verhalten ihrer elektrischen Signale bei der Kopplung der Lichtbögen zu beobachten. Darüber hinaus wird der Plasmaprozess mit Gleich- und Wechselstrom konfiguriert, um die Notwendigkeit einer kathodischen Reinigung zu beobachten, wenn der Hybridprozess bei Aluminiumlegierungen eingesetzt wird. Sobald die bei der Hybridisierung der Prozesse auftretenden Phänomene bekannt sind, wird die Wechselwirkung zwischen den Schweißprozessen unter energetischen Gesichtspunkten untersucht. Ziel ist es, zu beobachten, ob es einen Stromaustausch zwischen den Schweißprozessen gibt und, falls vorhanden, wie sich dieser auf die Schweißprozesse auswirkt. Die Ergebnisse zeigten, dass es möglich ist, die Plasma- und MIG-Prozesse in einer paraxialen (Tandem-)Konfiguration zu koppeln, um Aluminiumverbindungen mit einem stabilen Lichtbogen und einer größeren Eindringtiefe als die Einzelprozesse herzustellen. Es wurde die Etablierung eines "Strompfades" zwischen dem MIG- und dem Plasmalichtbogen festgestellt, der den Stromfluss zwischen den Schweißprozessen

ermöglicht, was sich direkt auf das Längenverhalten des MIG-Lichtbogens auswirkt. Darüber hinaus wurde der Schluss gezogen, dass es nicht notwendig ist, Wechselstrom im Plasmaprozess zu konfigurieren, um Aluminium zu schweißen, da der MIG-Prozess die kathodische Reinigung übernimmt. Man kam auch zu dem Schluss, dass ein externes Magnetfeld nicht notwendig ist, um das Verhalten der Schweißlichtbögen zu stabilisieren. Die Verbindungen von 10 und 15 mm Dicke wiesen ein gutes Oberflächenaussehen auf, obwohl der Hybridprozess nur für die 15 mm dicken Verbindungen eine Überlegenheit zeigte.

1 Introduction

One of the constant challenges in the construction of means of transport is the reduction of the weight of the structures that compose them, and in this way improve the fuel economy of vehicles in order to reduce CO_2 emissions for the sake of preserving the global environment. New materials and process technologies are being developed for application to vehicles in this regard. One effective way to achieve weight reductions is to apply aluminum alloys to the car body. In order to apply aluminum alloys to structural components, they should be joined with sufficient strength and quality at the highest welding speed possible. Traditional welding processes such as MIG and TIG have been used for years and, therefore, their production and quality capabilities are recognized and limited. For this reason, hybridization between conventional processes is an alternative that has been studied over the last decades, highlighting the Laser-MIG-hybrid-processes. However, its high cost of implementation makes its massification in the industry difficult.

Recent advances in hybridization between plasma and MIG processes offer an innovative option to increase productivity in welded joint tasks. This new commercial option offers high productivity through the reduction in the number of passes to complete the joint, because it takes advantage of the high penetration of the plasma process, while the high deposition rate of the MIG process completes the joint. This new version of the plasma-MIG process, in which the torches are arranged on the same axis (paraxial), offers the advantage that the torches of both welding processes are independent. Therefore the characteristic properties of each of them remains without significant changes, compared to past versions such as the coaxial plasma-MIG process.

While this version of the plasma-MIG process has shown an increase in productivity compared to processes such as MIG and the submerged arc, in applications with steel alloys, there have not been many studies for aluminum. The interaction between the welding arcs, and how this interaction influences the electrical parameters of each process does not yet have a clear explanation. In addition, joining aluminum alloys presents its own challenges such as the removal of the oxide layer and the internal porosities in the weld beads.

The present work contributes to a better understanding of the hybrid plasma-MIG process and its application in aluminum joints, especially the interaction between the welding arcs during their hybridization and their effect on the electrical signals and the microstructure of aluminum.

2 State of the art

2.1 Hybrid welding processes

In a new approach in the search for welding processes with greater capacities of production and productivity, arise the so-called "hybrid welding processes". This combination is regarded in the physical association of 2 welding processes, for example the MIG-Laser or the plasma-MIG, as a manner to exploit the most attractive sides of each one. In the case of MIG-Laser, it is possible to reach a greater geometrical and chemical control of the weld bead, although still maintaining (or increasing) the productive capacity of each welding process individually.

The MIG-Laser process limitations (mainly the higher investments and request of super-specialized workers to regulation, operation and maintenance) stimulated the development of another hybrid welding process, the plasma-MIG. The idea of using plasma instead of the laser comes from the high penetration offered by the plasma process, for a much lower installation and operational cost than the laser [1]. An alternative to plasma-MIG is the TIG-MIG process, which has shown good results in conjunction with different thicknesses and materials, although there is no commercial version yet.

These hybrid processes combine their advantages to increase the welding speed with low thermal stresses and, at same time, break off the oxide layer on aluminum alloys. When combining two different processes it is necessary to investigate their interaction. The principle of operation, the sources behavior for each welding process will be detailed in the following subchapters, mainly highlighting its operation with aluminum alloys.

2.1.1 Plasma-MIG hybrid welding process

The equipment necessary for the plasma-MIG process is composed by conventional MIG and plasma welding sources, with a welding torch that allows the internal coupling of the arcs of each welding process with a control system to synchronize them. The first plasma-MIG welding torch was proposed by Essers et al. [2] where a tungsten electrode was used to establish the arc that is coupled with the MIG arc (Figure 2.1). In this version the welding processes had a tandem or paraxial configuration with a certain distance between them. However, this torch did not

show good operational characteristics. Its size was bigger and not so easy to manipulate in complex geometries of the workpieces [1].

Improving the weaknesses of the first proposed concept of plasma-MIG, a commercial version appeared in the market, with several and important changes (Figure 2.2). The main difference of this version of the hybrid process is in the torch, where the tungsten electrode of the Plasma process is replaced by an annular copper electrode, where the wire-electrode of the MIG process passes concentrically through it. As in this hybrid torch the constricting hole of the plasma process is larger than in a conventional plasma torch, to allow the passage of the wire-electrode, the constricting effect of the arc is practically null, leaving the plasma process only as a mechanism of preheating the wire-electrode of the MIG process. This version of the hybrid process is called plasma-MIG concentric arcs [1].

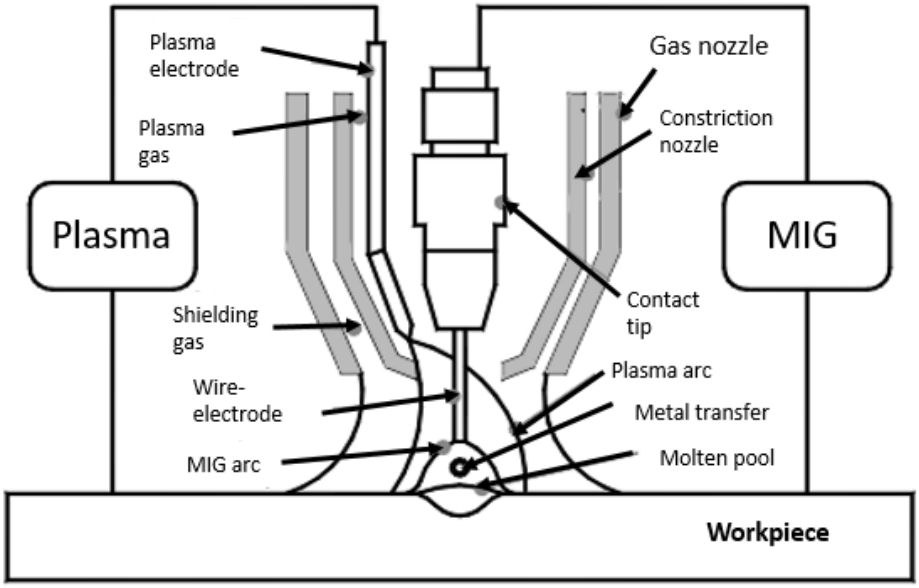

Figure 2.1 – Schematic design of the plasma-MIG welding process [2].
Schematischer Aufbau des Plasma-MIG-Schweißprozesses.

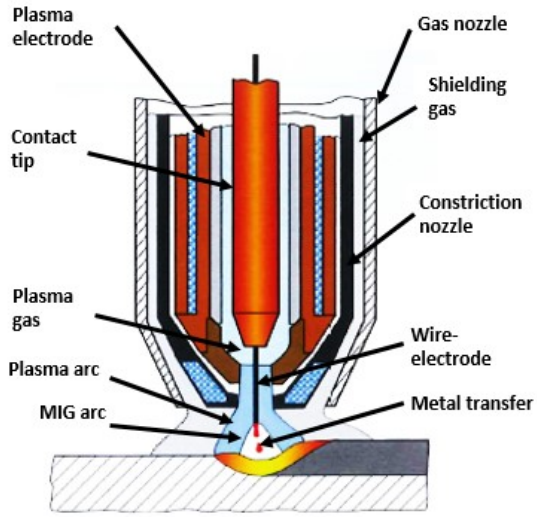

Figure 2.2 – Schematic representation of the plasma-MIG concentric arcs welding process [3].

Schematische Darstellung des Plasma-MIG-Lichtbogenschweißprozesses.

The plasma-MIG concentric arcs offer a certain independence between the addition of material (MIG process) and the additional energy provided by the plasma process. This hybrid process presented interesting advantages in the welding of thick plates, mainly in aluminum [4]. However, its application did not have a significant place among the welding processes most used by the industry, possibly due to its complexity. Oliveira et al. [5] mention that one of the reasons for the low use of this process may be the lack of arc stability under certain conditions which causes unstable metal transfer, irregular geometry of the weld bead and even destruction of some internal parts of the welding torch.

A second commercial version of the plasma-MIG process appeared on the market in 2018, with the name of SuperMIG. This version is characterized by a torch where the MIG and plasma processes are not in a concentric configuration, the torches of each process are independent, both aligned on the same axis (paraxial) (Figure 2.3). In the literature there is no agreement about how to refer to this hybrid welding process configuration. Some terms found are plasma-MIG [3], KPAW-GMAW-P [6] and VPPA-GMAW [7]. In the present investigation the hybrid process will be mentioned as paraxial plasma-MIG due to the arrangement of the two torches on the same axis.

In this version of the plasma-MIG, the paraxial arrangement of the welding torches allows each welding process characteristics to be maintained, such as the high penetration of the plasma process. However, due to the negative polarity of the tungsten electrode and the positive polarity of the MIG wire-electrode, the resulting electromagnetic fields cause both arcs to repel each other. The manufacturer of the SuperMIG proposes that the repel behavior between the arcs can be counteracted by an overlain magnetic field [8]. For that, they developed a “magnetic deflection” or “magnetic level compensation” device (depending on the SuperMIG unit model), which consists of a magnet coil and two pole shoes (Figure 2.3). The pole shoes are attached to the left and right side of the shielding gas nozzle of the SuperMIG torch. The magnetic deflection device can be adjusted in its intensity and the pole shoes are designed to apply the required magnetic force to push the plasma back to the impingement spot and hold it in place during the welding process. The pole shoes create 2 forces and the direction is based on the interaction of two magnetic fields. One force keeps plasma in center, and the other one “returns” the plasma to counteract the MIG forces [8]. Han et al. [7] worked with the SuperMIG unit with variable polarity plasma arc (VPPA), noticing that arcs repel each other during the DCEN period and attract each other during the DCEP period, resulting from the effect of magnetic field coupling due to the ampere force of the hybrid arc magnetic field [9]. Figure 2.4 shows the electromagnetic coupling mechanism of the VPPA-MIG hybrid arc. This mechanism influences the shape of each arc, compressing the MIG arc during the VPPA DCEN period by the repulsion force, but the degree of arc compression is smaller. Meanwhile, the MIG arc is subjected to the ampere force in the left direction and the force of the coupling region in the right direction, rendering the MIG arc contraction more obvious during the DCEP period. However, Han et al. [7] did not mention the influence or requirement of an external magnetic deflection device to improve the interaction in the arcs.

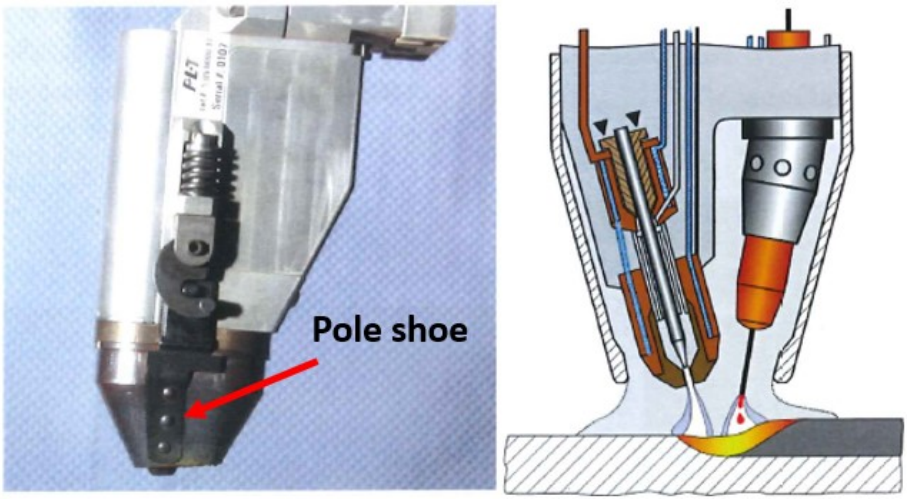

Figure 2.3 – SuperMIG torch with pole shoes for the magnetic deflection (left) and torch arrangement (right) [10].

SuperMIG-Brenner mit Polschuhen für die magnetische Ablenkung (links) und Brenneranordnung (rechts).

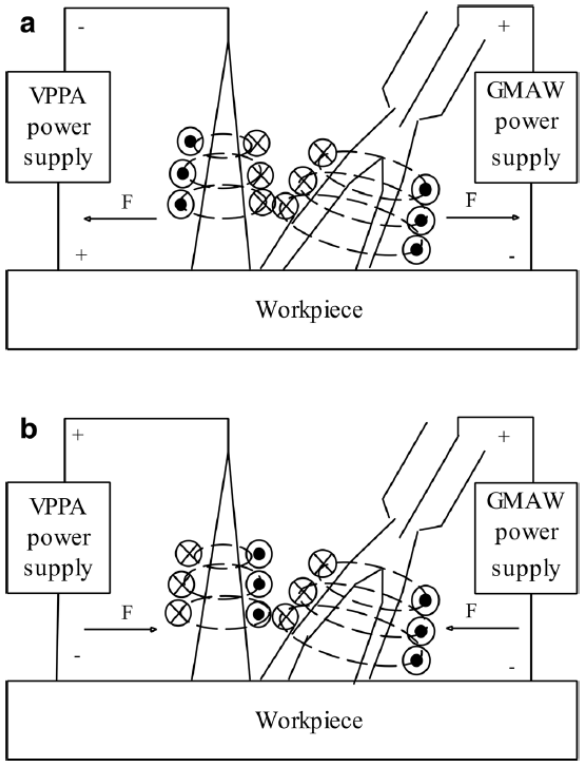

Figure 2.4 – Magnetic induction line distribution of the VPPA-MIG hybrid arc (a) during the VPPA DCEN period; (b) during the DCEP period [7].

Verteilung der magnetischen Induktionslinie des VPPA-MIG-Hybridlichtbogens (a) während der VPPA-DCEN-Periode; (b) während des DCEP-Zeitraums.

Figure 2.5 shows a simulation of the effect of an external magnetic field of 0 mT, 5 mT and 10 mT on the MIG and plasma arcs in the SuperMIG [3]. In contrast to the MIG arc, the plasma process is hardly affected by the external magnetic field. The great inherent stability of a constricted plasma arc prevents the deflection of the arc by the external magnetic field. However, the MIG arc is strongly deflected toward the plasma process by the external magnetic field. As a result, metal vapor is increasingly pressed into the arc of the plasma process on the workpiece, whereby the stability of the plasma process can be deteriorated. Contrary to expectations, the shielding gas cover is not affected by the effect of the external magnetic field on the arcs.

With weak external magnetic fields (B < 5 mT) the numerical investigations show hardly any change on the MIG arc. Only with strong external magnetic fields (B > 5 mT) can significant changes occur. The model calculations cast doubt on whether a sufficiently strong magnetic field can be generated with the installed coil in the SuperMIG torch, in order to be able to influence the arcs sufficiently strong in the investigated processes [3, 10].

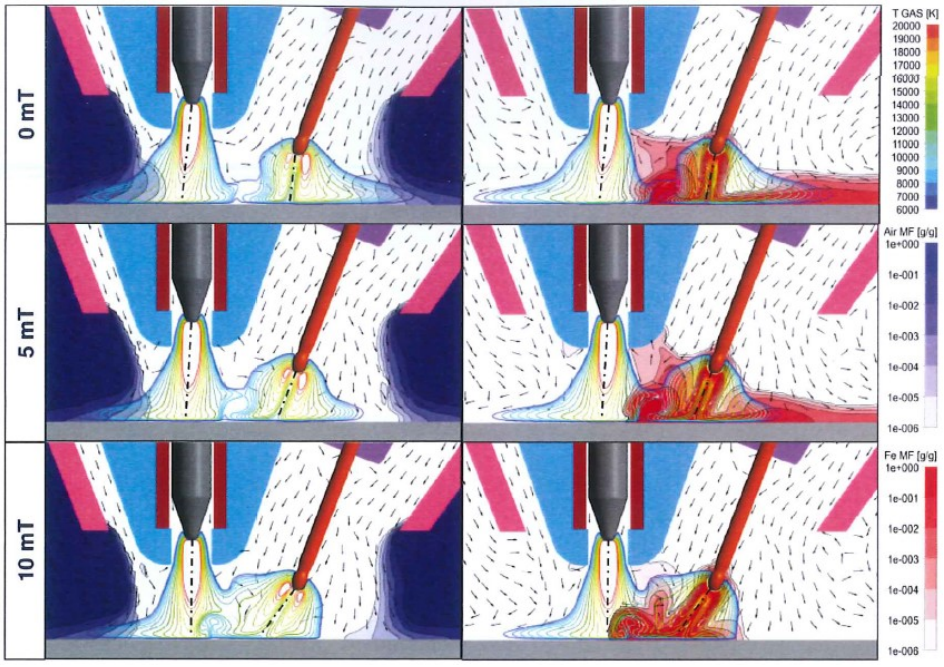

Figure 2.5 – Variation of the external magnetic field. Left: Shielding gas; Right: Metallic vapor concentrations in the arc [3].

Variation des externen Magnetfeldes. Links: Schutzgas; Rechts: Metallische Dampfkonzentrationen im Lichtbogen.

During the experimental test of the simulation showed in the Figure 2.5, it was noticed the mutual repulsion of the two arcs due to their different polarity, as is shown in Figure 2.6. During the (late) switching on of the MIG current in the ignition phase, the plasma arc deflects forwards (right) (Figure 2.6a), while during welding phase of MIG process with a long arc is blown back (left) by plasma arc, who is without a deflection (Figure 2.6b). However, the high-speed images also show that hybrid welding with 100% magnetic deflection control and optimally adjusted arcs cannot prevent a mutual repulsion of the two arcs (Figure 2.7). Transverse discharges can be seen between the arcs. This means that a part of the welding current does not flow to the workpiece, but it is flowing between the two arcs establishing a “path” or “bridge”. This current path causes a reduced heat input through the plasma arc in the weld zone [3]. This current path was also noticed by Han et al. [7] and Guo et al [11] working with the SuperMIG and VPPA, mentioning that “coupling area” is formed by the greater quantity of metallic vapor product of the keyhole made by the plasma process and the wire-electrode melted by the MIG process. The metallic vapor reduces the ionization potential of the shielding gas and, therefore, it establishes the plasma state easier and current flow between the welding processes.

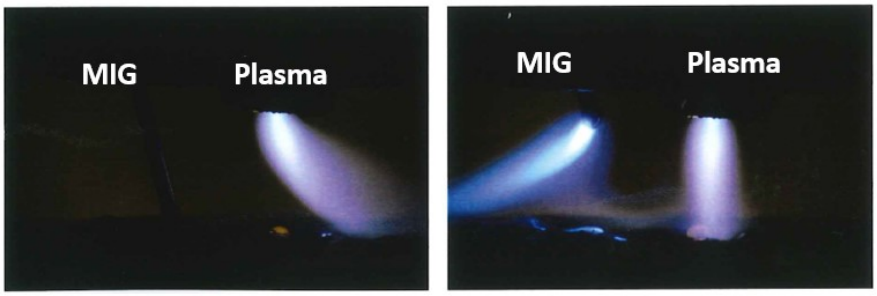

Figure 2.6 – Mutual influence of the two arcs due to their different polarity (a) deflection of the plasma arc by (too late) switching on the MIG current in the ignition phase MIG; (b) deflection of a long MIG arc during hybrid welding without magnetic deflection on plasma process [3].

Gegenseitiger Einfluss der beiden Lichtbögen aufgrund ihrer unterschiedlichen Polarität (a) Ablenkung des Plasmabogens durch (zu spätes) Einschalten des MIG-Stroms in der Zündphase MIG; (b) Ablenkung eines langen MIG-Lichtbogens während des Hybridschweißens ohne magnetische Ablenkung beim Plasmaprozess.

Figure 2.7 – Mutual arc interference at 100% magnetic deflection control [3].

Gegenseitige Lichtbogeninterferenz bei 100% magnetischer Ablenkungskontrolle.

Another influence of the major quantity of metallic vapors is the voltage drop in the MIG voltage. Figure 2.8 shows that increasing the plasma current, the MIG voltage decreases. This behavior is due to high-temperature environment of the plasma keyhole and the large number of metal ions and electrons. These provide an excellent discharge environment for the arc. Moreover, the charged particles in the coupling region spread to the MIG arc region, replenish the lost charged particles and energy, and improve the electrical conductivity of the MIG arc. The ionizing potential of metal atoms (5.96 V of Al, 7.61 V of Mg) is lower than the inert gas atom (15.69 V of argon); hence, the metal atoms produced by the vaporization are more easily ionized [11]. Therefore, the power supply compensation is correspondingly reduced and the MIG arc voltage is decreased. With increasing plasma current, the temperature and metal vapor in the keyhole increase, which causes the MIG arc conductivity to increase and the arc voltage to decrease more substantially. On the other hand, the study made by Wu et al. [6] shows that the arc length of the MIG-Pulsed process increases when it is coupled to the plasma process. It also mentions that the droplet velocity and the metal transfer frequency are higher than the single MIG-Pulsed process, while the droplet diameter decreases. Furthermore, the temperature measurements of the molten pool show that the single MIG-Pulsed process is slightly higher by 91°C compared to the hybrid process. This study is the only one that has made an arc length measurement of the MIG process during the hybrid process, however, it does not make the relation with the electrical signals or the static curves of the welding source.

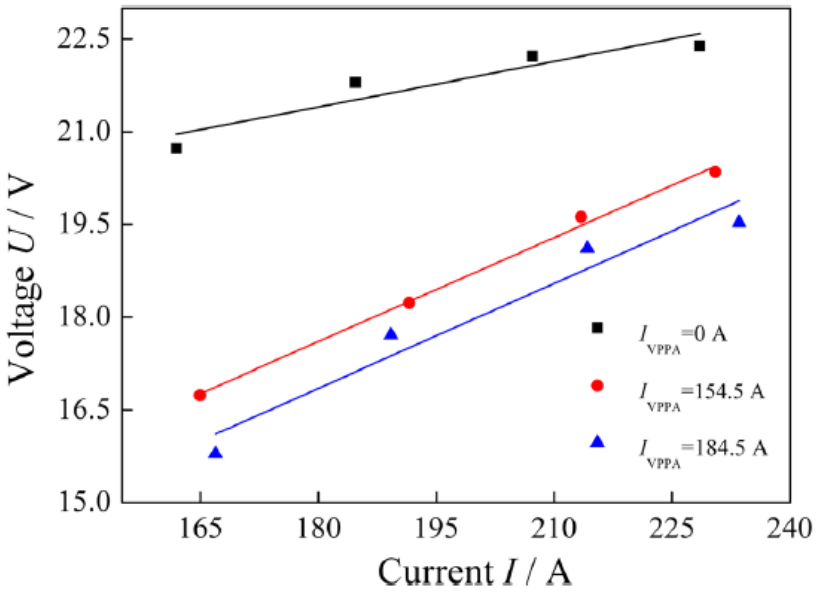

Figure 2.8 – Voltage-current characteristics of the MIG arc during the hybrid welding [7].

Strom- Spannung -Eigenschaften des MSG-Lichtbogens beim Hybridschweißen.

The plasma-MIG paraxial hybrid process was used in several alloys mainly in steel. Joints are the main application of this hybrid process being an alternative to the submerged arc or the MIG process. Huber et al. [10] concluded that SuperMIG offers economic advantages in comparison with MIG process, giving the possibility to finish a joint more quickly and with higher process reliability with regard to the penetration weakness at the start of the weld and to the avoidance of a lack of interpass fusion. Han et al. [7] compared the SuperMIG and MIG process in 7A52 high-strength aluminum alloy joints of 11 mm thickness, concluding that with single MIG process it was necessary a multilayer joint, while with SuperMIG the joints were completed in one pass. Welding solution Inc. [12] compared the submerged arc welding (SAW) with SuperMIG, concluding that this last one reduces the overall processing by 75% compared to SAW. In addition, the observed degree of post weld deformation with the hybrid process was considerably less than the SAW process due to the reduced heat input.

This hybrid process offers several benefits, however, there are several factors without a proper explanation. The effect of the magnetic deflection device is not completely clear and the studies made with the SuperMIG welding source do not mention its configuration (intensity), only the work made by GSI SLV München [3]

gave a proper explanation, however, the results were not conclusive. On the other hand, how the discharge or bridge between the welding arcs influences the electrical signals of each process, has not been sufficiently studied by the current bibliography.

2.1.2 TIG-MIG process

The TIG-MIG hybrid process is an alternative to the plasma-MIG paraxial hybrid process, which has begun to be studied in more detail in recent years. The advantage of this process is the simplicity offered by the TIG process compared to the plasma process, not requiring complex torches or expensive consumables. In addition, the operation principle of the TIG process is simpler, requiring less hours of training for operators. In the case of the TIG-MIG hybrid process, Kanemaru et al. [13] comments that unlike other hybrid processes, no special properties of welding sources or special circuits are necessary. However, the principle of operations of the TIG and plasma processes are similar. Both use a welding source with constant current static characteristic, which allows direct comparison of the electrical signals with the paraxial hybrid plasma-MIG process.

There is currently no commercial version of the hybrid TIG-MIG process, as is the case of the paraxial plasma-MIG with the SuperMIG. The investigations are made with a single MIG and TIG torches. The first simulations made for this process show that there is a repulsion between the welding arcs (Figure 2.9a), as was observed for the paraxial plasma-MIG process. In addition, the numerical results of the current density distribution show that a current path between the tungsten electrode and the wire-electrode of the MIG process was established, and that a current of 32 A is flowing between them (Figure 2.9b).

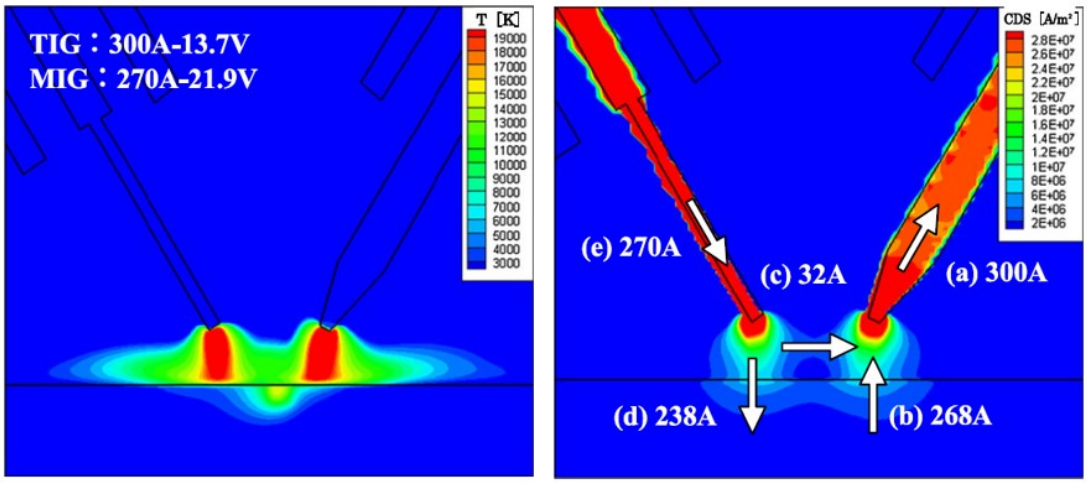

Figure 2.9 – Simulation of the arcs interaction for the hybrid process TIG-MIG (a) Temperature distribution of each process (b) current density distribution and current path [13].

Simulation der Lichtbogenwechselwirkung für den Hybridprozess WIG-MSG (a) Temperaturverteilung jedes Prozesses (b) Stromdichteverteilung und Strompfad.

The experimental results showed effectively the current flows from one process to the other [14]. However, this current flow is not possible to estimate or predict accurately. The current path observed in Figure 2.10b is similar to that observed for the paraxial hybrid plasma-MIG process, however, in the investigations it is not mentioned that any of the processes increase the welding current. Figure 2.10c shows how the voltage of the TIG process is reduced when the MIG arc is ignited. Similar behavior was noticed for paraxial plasma-MIG in the MIG process and the explanation for this phenomenon is the expansion of the plasma arc (current path), this increases the amount of metal vapor produced by TIG-MIG hybrid process, causing change in the electric potential of the welding arc [14].

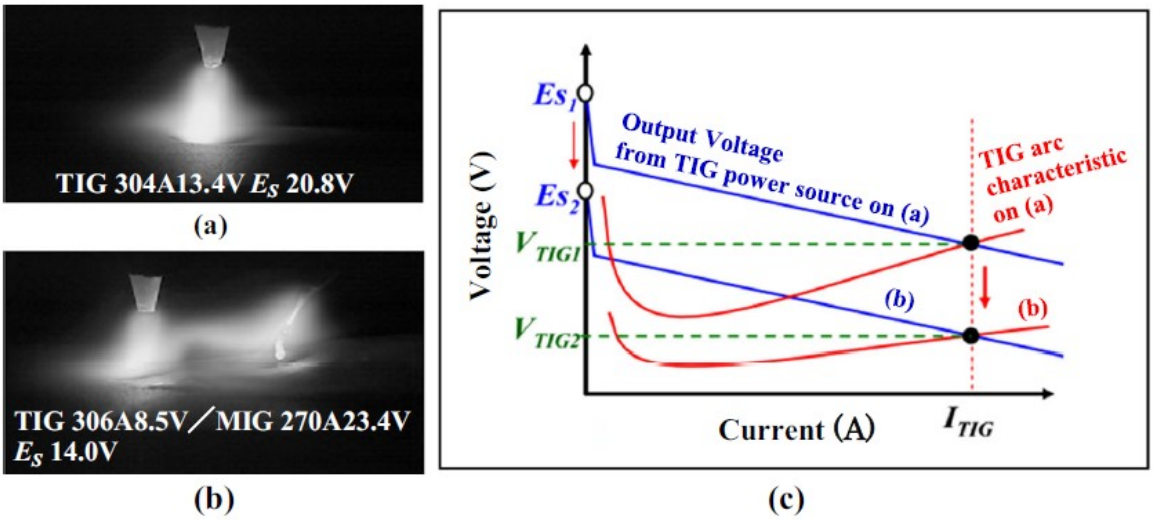

Figure 2.10 – Comparison and analysis for arc shape and voltage on each state of arc (a) TIG arc, (b) TIG-MIG hybrid arc, (c) TIG arc characteristic and output voltage from TIG power source corresponded to state of (a) and (b) [14].

Vergleich und Analyse der Lichtbogenform und -spannung in jedem Zustand des Lichtbogens (a) WIG-Lichtbogen, (b) WIG-MIG-Hybridlichtbogen, (c) WIG-Lichtbogencharakteristik und Ausgangsspannung von der WIG-Stromquelle entsprachen dem Zustand von (a) und (b).

The thermal efficiency of the TIG-MIG hybrid process is about 70%, while the efficiency of the single TIG and MIG processes is about 80% [14]. The lower efficiency of the hybrid process is due to the current path established between the welding processes, changing the current flow towards the TIG process and not flowing to the base material. However, the thermal efficiency of the process is lower, its productivity is higher in around 17- 44% compared to the single TIG process. Although there is no study on the efficiency of the paraxial plasma-MIG process, it can be suggested that its efficiency must be lower than single processes, because it also has a "current path" between its welding arcs.

The studies on the TIG-MIG hybrid process show that its stability depends on a proper energy balance between the TIG and MIG process. Kanemaru et al. [13] observed that for TIG current range from 150 to 200 A, TIG current is less than MIG current (270 A), and the MIG arc was unstable, producing much spatter. Thus, in range of TIG current less than MIG current, the penetration depth was independent of TIG current. These results suggest that the TIG current needs to be greater than the MIG current for arc stability. Therefore, it is recommended that TIG current be

greater than the MIG current to guarantee penetration and stability of the hybrid process.

2.2 Aluminum and its influence on the automotive industry

The European automotive industry has more than doubled the average amount of aluminum used for the construction of passenger cars [15]. Determining the right alloy for the body structure and hang-on panels has been the subject of considerable development effort and most of the activity is concentrated on a relatively small number of alloys [16]. The main aluminum alloy classes for automotive sheet application are the non-heat treatable Al-Mg (EN 5000 series) and the heat treatable Al-Mg-Si (EN 6000 series). Undoubtedly, aluminum is more expensive to be manufactured than steel [17]. Aluminum alloys offer a wide range of properties that can be engineered precisely to the demands of specific automotive applications, through the choice of alloy, temper and fabrication process. The key characteristics of aluminum in the automotive use are lightweight, high strength to weight ratio, resilience, corrosion resistance, forming and fabricating, joining, crashworthiness, cold resistance, recyclability, thermal conductivity and reflectivity [18].

In respect to limited resources of fossil fuels and global environmental concerns, it will be necessary to reduce the fuel consumption for passenger cars, as shown in Figure 2.11. There are different strategies to reach the prospected requirements for maximum carbon dioxide emissions, and one obvious solution is to substitute the traditional combustion engine with electric battery technology or other alternative driveline concepts. But another problem to solve this challenge is spelled “lightweight engineering”, which for the car body will mean the introduction of other materials than the traditional zinc-coated steel sheets. Lately we have seen full aluminum bodies as well as complete fiber reinforced plastic solutions. The drawback of these concepts is that they are extremely expensive and will require big modifications of the industrial structure and the body shops. Therefore, today’s body engineers work according to the principle “the right material at the right place”, which will mean that different material types will be mixed in the body structure [19].

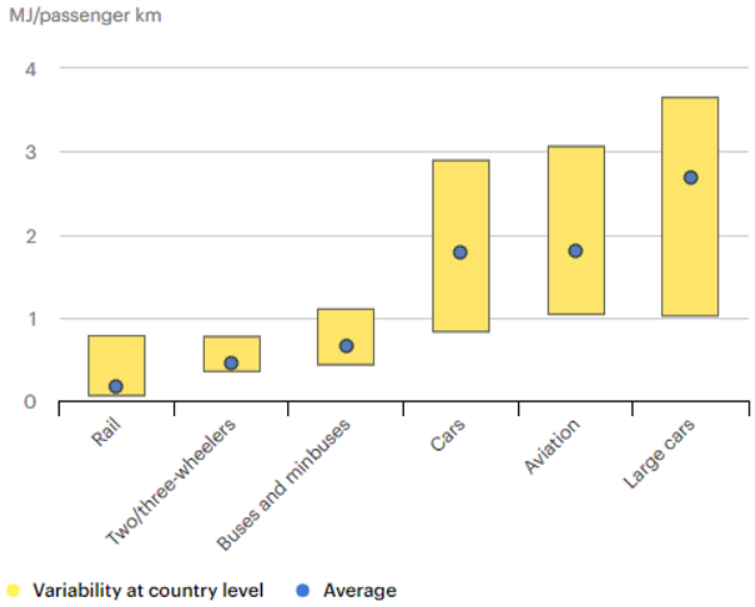

Figure 2.11 - Energy intensity of passenger transport modes (2018) [20].

Energieintensität der Personenverkehrsträger (2018).

A general evolution of steel/aluminum mixing starts with the manufacture of all hang-on parts, such as doors, hoods, trunk lids and tailgates, in aluminum, while maintaining the body structure in steel. The next step is to introduce less load sensitive areas in the body, such as floor pans and roof panels. And finally, also load carrying components are made out of aluminum. Figure 2.12 illustrates the growth of the quantity of aluminum used per vehicle over the last 50 years, an eightfold increase, and according to Santos Jr. et al. [21], today figures are about 180 kg per passenger vehicle with an estimation of 70% increase up to 2025 (or 250 kg per vehicle).

With these statistics in mind it is natural to seek continuous improvement of the manufacturing processes in the different aluminum alloys, which each one presents its own difficulties associated with its weldability. In the following subchapters, it will be described the main characteristics of aluminum alloys and its influence on their weldability and the stability of the welding processes.

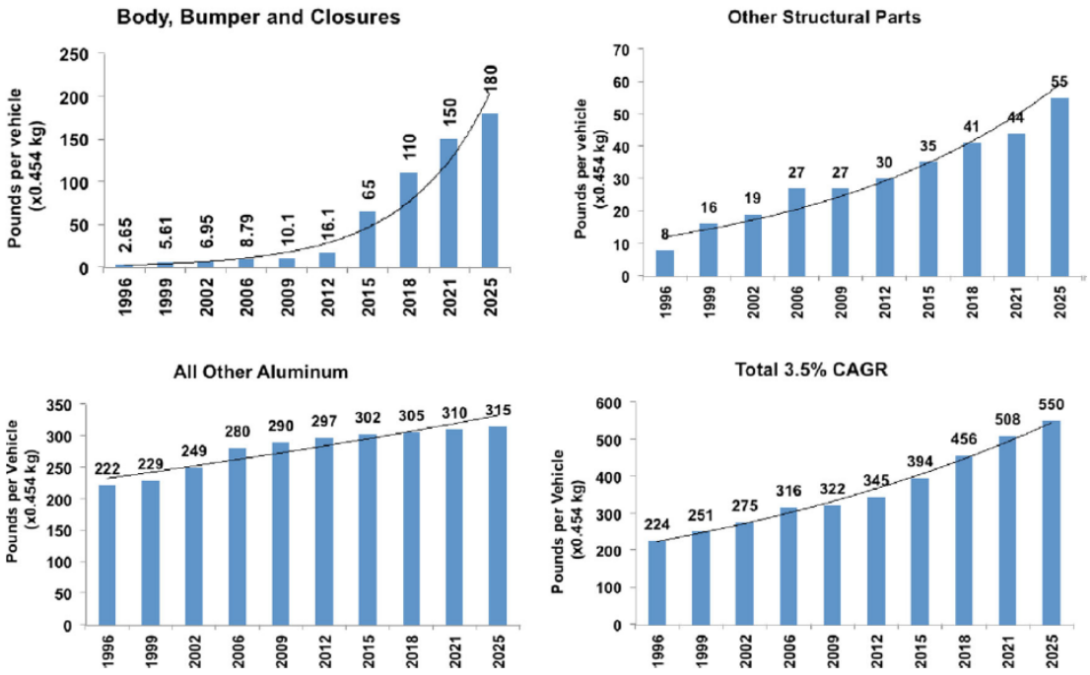

Figure 2.12 – Average use of aluminum in the car industry [21].

Durchschnittliche Verwendung von Aluminium in der Autoindustrie.

2.2.1 Aluminum properties and weldability

In this investigation, the heat treatable aluminum alloy EN AW 6060-T66 will be used. The alloys of the 6XXX series are widely used as medium-strength structural alloys which have the additional advantages of good weldability and corrosion resistance. The nomenclature used to classify the aluminum alloys in DIN EN 573 norm [22], mention that prefix “AW” means that the alloy is a wrought product and it is followed by four digit which uniquely identifies the alloy. The first digit indicates the main alloying element, that in this case is 6, meaning an aluminum–magnesium–silicon alloy. Moreover, the letter “T” after the 4 numbers indicates that the alloy was thermally treated. This identifies the alloys that are aged to produce a stable condition. The ‘T’ is always followed by one or more numbers to identify the specific heat treatment, in this case by “66”. The norm DIN EN 515 [23] mentions that first six means that the alloy was solution heat treated and artificially aged, while the second six means that it passed for a temper treatment (mechanical property level higher than T6 achieved through special control of the process 6000 series alloys).

Al–Mg–Si alloys are widely used as medium-strength structural alloys which have the additional advantages of good weldability and corrosion resistance. Just as the 5XXX series of alloys comprise the bulk of sheet products, the 6XXX series are used

for the majority of extrusions, with smaller quantities being available as sheet and plate. However as shown in Figure 2.13, aluminum alloys from the 6XXX-series have a stronger tendency to form hot cracks, which are dependent on a number of factors, such as alloying content, solidification rate, constraint, etc [19].

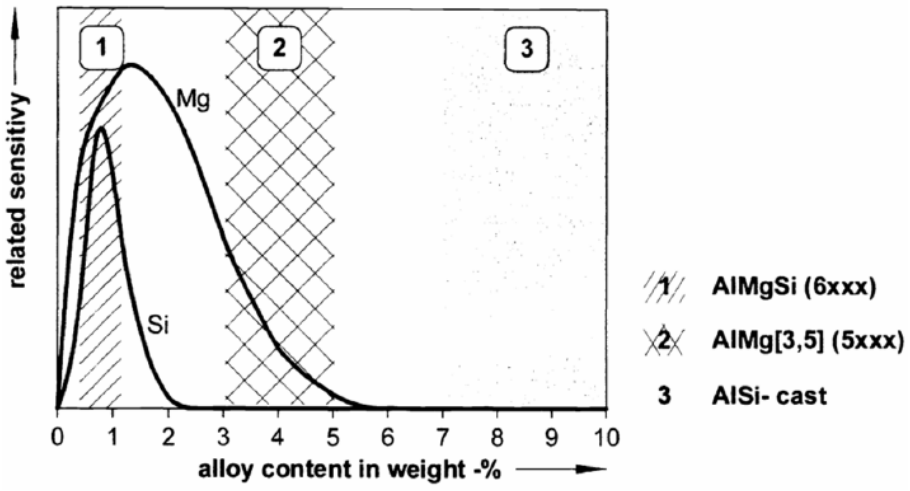

Figure 2.13 – Hot crack sensitivity of aluminum alloys dependent on Si and Mg content [19].

Heißrissempfindlichkeit von Aluminiumlegierungen in Abhängigkeit vom Si- und Mg Gehalt.

The welding of aluminum alloys has some peculiarities in relation to the welding of steels, mainly due to their physicochemical properties, despite being a technique already considered practically dominated. These properties include low melting point, high coefficient of linear expansion, high thermal conductivity, formation of a thin oxide layer and low electrical resistivity, which will influence the appearance of the weld bead, the formation of defects and varying arc height. Therefore understanding their properties and how they can influence the hybrid process is of vital importance.

2.2.1.1 Thermophysical properties and the influence on the weldability

In a first analysis, due to the melting point of aluminum being lower than steel, it is assumed that the heat required to perform welding is lower. However, thermal conductivity has a great influence on weldability, as it is about five times higher than steel. This means that in practice aluminum alloys require a higher thermal input. Therefore, the high thermal conductivity of aluminum acts as a deadlock for formation of the molten pool, since at the beginning of the bead, the high conductivity

dissipates heat quickly, making it difficult to penetrate depth and to wet the base and weld metal. However, the high thermal conductivity of aluminum alloys helps to solidify the molten pool and, consequently, facilitates out-of-position welding [24].

The coefficient of linear thermal expansion is another physical property of importance when considering weldability, this indicates the change in length of a material with a change in its temperature [24, 25]. The coefficient of linear thermal expansion for aluminum is twice that for steel [26]. Thus, there is a risk of crack formation triggered by obstruction of shrinkage after the welding. This means that the heat input should be kept to a minimum during joining. For the joint space to remain uniform, extra care must also be taken in welding aluminum. This may necessitate preliminary joining of the parts of the assembly by tack welding prior to the main welding operation. The combination of high coefficient of thermal expansion and high thermal conductivity would cause considerable distortion of aluminum during welding, however, a high welding speed is a solution to avoid this type of defects [19, 24].

Another important problem is the low electrical resistivity. Welding source that imposes the current (constant current static characteristic), the electric arc tends to randomly vary its length, that is, for a given current the arc may assume different voltage values. This behavior can be better understood by Figure 2.14, verified in the work of Kiyohara et al. [27] that interprets the melting characteristics of aluminum electrodes in MIG welding and which have a direct connection with the arc length. Figure 2.14 shows their results for the aluminum wire-electrode ER 5183 where average voltage curves are plotted by average current, called by Quites and Dutra [28] as iso-consumption curves. For a high arc voltage, the welding current is practically constant regardless of the arc voltage increase. In this region, where spray transfer occurs, the voltage increase may have the same current value (vertical line), this phenomenon being associated with arc instability. For lower voltages, where the transfer occurs by short circuit, for each current value there is a corresponding voltage value. These problems related to varying arc height often end up making welding difficult or even unfeasible. This behavior is relevant according to the study of Wu et al. [6] about the change in the arc length of the MIG-

Pulse process when it is coupled to the plasma-DC process in steel joints, therefore, it is expected that in aluminum this behavior would be intensified.

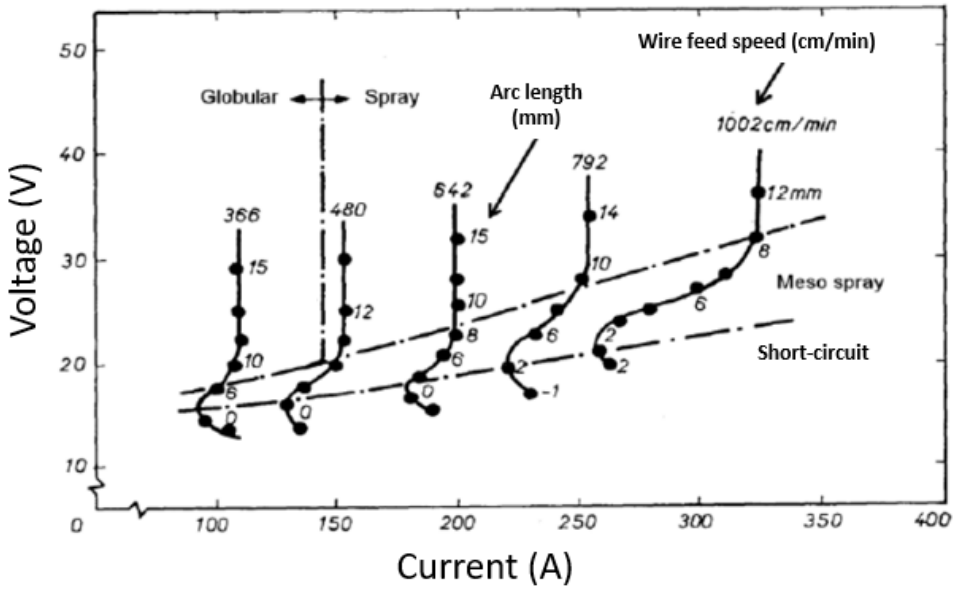

Figure 2.14 – MIG arc behavior in aluminum weld [27].

MSG-Lichtbogenverhalten bei Aluminiumschweißungen.

2.2.1.2 Oxyde layer

Another aluminum characteristic concerns the high reactivity with oxygen, forming on its surface a layer of aluminum oxide (Al_2O_3). In a dry environment, the layer stabilizes at about 25 – 50 Å and in damp conditions, or anodizing, the layer can grow up to a thousand times [24, 29]. This layer, although very thin, is enough to protect the metal in various corrosive media, which explains its excellent corrosion resistance. However, all metals form oxides on their surface, in the case of aluminum there is a particularity due to its difference in melting temperature. While alumina (Al_2O_3) melts at 2052 °C, the melting point of aluminum is around 660 °C [30, 31]. At first this would not be a problem as the electric arc reaches temperatures up to 6000 °C, but due to the high thermal conductivity of aluminum there is rapid heat dissipation, causing only the metal to melt and the oxide layer to remain intact. In addition, Al_2O_3 is electrically nonconductive which causes a difficulty of current flow, resulting in arc instability, so it is necessary to remove this oxide layer.

This oxide layer must be removed mechanically by machining, wire brushing, scraping, or chemical cleaning in order to achieve defect-free joints of aluminum by fusion methods. If oxides are not removed, oxide fragments may be entrapped in

the weld and will cause a reduction in ductility, a lack of fusion, and possibly weld cracking [29, 32, 33]. During welding, the oxide must be prevented from re-forming by shielding the joint area with a non-oxidizing gas such as argon, helium or chemically by use of fluxes [24]. In welding procedures, the removal of the oxide layer is a mixture of mechanical, chemical and cathodic cleaning. Firstly, the union is brushed (mechanical cleaning) and then any oil or impurity is removed using a chemical cleaning product, usually alcohol. However, the most effective cleaning process is the cathodic, which is done during welding time.

The cathodic cleaning results when the electrode is connected to the positive pole of the welding power source, and direct current (DC) is passed there is a flow of electrons from the workpiece to the electrode with ions travelling in the opposite direction and bombarding the workpiece surface. This ion bombardment breaks up and disperses the oxide film and permits the weld metal to flow and fuse with the parent metal. For example, the MIG welding process uses DC with electrode positive (EP), using DC electrode negative (DCEN) results in an unstable arc, erratic metal transfer and poor weld quality. Oxide film removal is therefore an intrinsic part of welding processes as MIG and submerged arc.

On the other hand, welding processes as TIG or plasma, conventionally uses DCEN, which, if used on aluminum, can result in poor weld quality. Using DCEP with TIG, however, results in the tungsten electrode overheating as some 60–70% of the heat generated in a TIG welding arc may be produced at the positive pole [34]. This can cause melting of the electrode and bring the welding operation to a premature end. A compromise is therefore reached by using alternating current (AC), where oxide film removal takes place on the positive half cycle and electrode cooling on the negative half cycle. TIG and plasma welding of aluminum is therefore normally carried out with AC, although there are a couple of techniques that use either DCEP or DCEN. Using helium as shielding and plasma gas is an alternative to weld aluminum alloys with DC [16], although the removal action of the cathodic cleaning is absent, it is thought that the higher temperature reached by the arc with helium as shielding gas will melt the oxide layer making it possible to establish a molten pool (Figure 2.15) [17]. However, this is not a technique frequently used for the high risk to produce imperfections, and it is preferred use AC [18]. One feature

seen with helium as shielding gas, which often gives cause for concern, is the formation of a black ‘soot’ along the heat affected zones of the weld. This ‘soot’ is not detrimental to the weld quality and can easily be removed by stainless steel wire brushing. If left in place between passes it can affect arc stability and is unsightly on a completed weld [17].

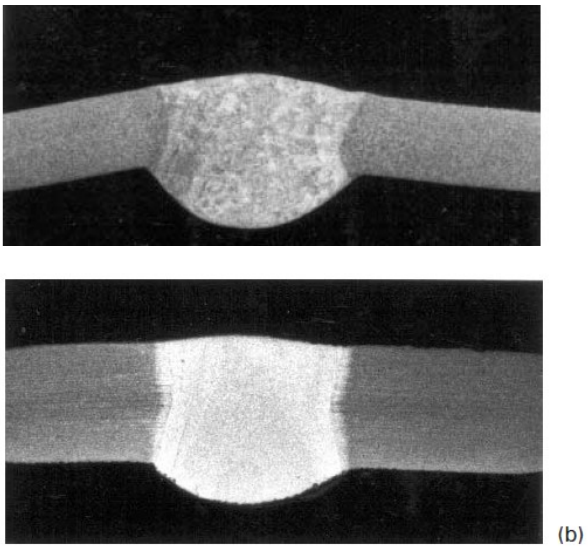

Figure 2.15 – Aluminum joints made by TIG with direct current (DC) and helium as shielding gas in plates thickness of (a) 3 mm (b) 6 mm [29].

Aluminiumverbindungen von WIG mit Gleichstrom (DC) und Helium als Schutzgas in Plattendicken von (a) 3 mm (b) 6 mm.

The use of alternating current (AC) in the plasma process or also called variable polarity plasma arc (VPPA), is generally used with the "keyhole" technique in aluminum alloys. The alternating current in the plasma process follows the same principle as in the TIG process. It is recommended a ratio of 20% of the time in positive polarity of the electrode to maintain an adequate balance between cathodic cleaning and tungsten electrode life [19]. The application of the AC keyhole plasma has demonstrated excellent quality, using it to manufacture space shuttle external tanks construction [20]. However, the large number of parameters and the constant change of tungsten electrodes make this manufacturing process expensive compared to other arc processes.

As it was mentioned in the subchapter of hybrid processes, currently the hybrid paraxial plasma-MIG process is used on aluminum alloys by means of alternating current (AC) in the plasma process or VPPA [7], showing excellent results. However,

the possibility of using a configuration with plasma-DC has not been studied, which would reduce the complexity of the hybrid process.

2.2.1.3 Hydrogen and oxygen on the weld bead quality

The porosity formation mechanism is a problem confined to the weld metal and is associated with the high thermal conductivity, which allows no time for gases to escape from the weld metal since cooling is fast, and also to trap gases during welding solidification, mainly related to hydrogen [29, 35, 36]. According to Woods [37] the solubility of hydrogen in aluminum is higher than in any other material, and small concentrations of hydrogen are enough to form gas bubbles. Porosity can range from being extremely fine micro-porosity, to coarse pores 3 or 4 mm in diameter (Figure 2.16). The main responsible in the case of aluminum alloys is hydrogen, which has high solubility in molten aluminum but very low solubility in the solid state, as shown in Figure 2.17. This shows a decrease of solubility to the order of 20 times as solidification takes place, a drop in solubility so pronounced that it is extremely difficult to produce a porosity-free weld in aluminum [29, 38]. Other gases such as oxygen and nitrogen present lower solubility in molten aluminum in comparison to hydrogen and, as a consequence, they usually play no important role in porosity generation [39]. However, in a micro-gravity environment with vacuum, these gases can assume importance. Fuji et al. [40] also found a link between the porosity and the formation of Al_2O gas bubbles at high vacuum (the oxygen would come from the superficial oxide layer).

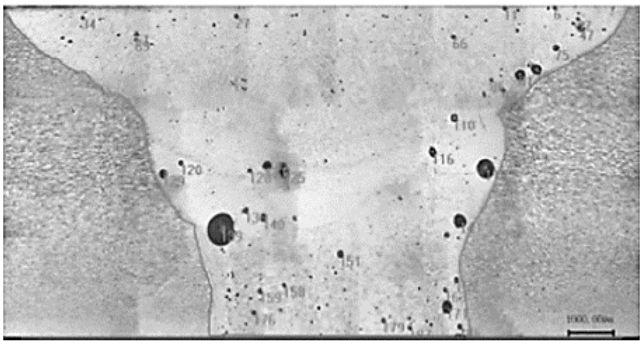

Figure 2.16 - Optical macrograph showing porosity in MIG welded Al-Zn-Mg alloy [41]. Note: porosity amount is about 1.6%.

Optische Makroaufnahme der Porosität in einer MIG-geschweißten Al-Zn-Mg-Legierung [23]. Hinweis: Die Porositätsmenge beträgt ca. 1,6%.

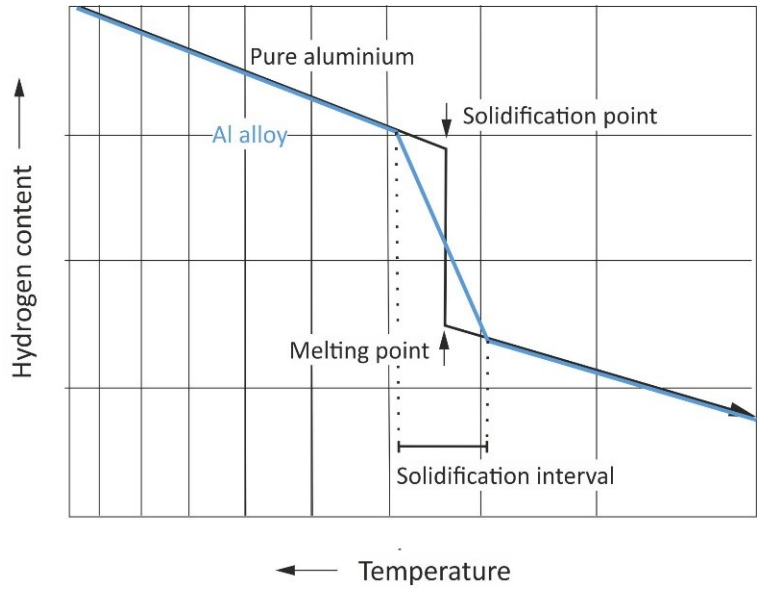

Figure 2.17 - Solubility of hydrogen in aluminum [38].

Löslichkeit von Wasserstoff in Aluminium.

Porosity tends to be lowest in autogenous welds in comparison with process with material addition, due to high hydrogen content in the wire-electrode. Reisgen et al. [42] find that condensation on the wire-electrode surfaces leads to pores in the weld metal even if the wire is dry at the moment of processing. To welders who are working with aluminum, it is suggested that fast climate changes, especially caused by transport of the welding wires, even within the factory premises, are to be avoided since they bear the risk of condensation. Moreover, the change of specific welding wire properties (such as hydrogen quantity and the adhesion factor) are due to substance changes on the welding wire surfaces rather than aging of the welding wires by means of a natural oxide layer growth in a constant climate without condensation [33]. Welding processes such as manual metal arc (MMA) and submerged arc welding (SAW) are not recommended to weld aluminum, due to moisture being an intrinsic part of the flux used for producing the shielding gas [29].

Some methodologies to reduce the entry of hydrogen during the open arc period are through of metal transfer in the MIG process. Morais [43] concluded that controlled metal transfer, specifically MIG-Pulsed, leads to lesser porosity than welds carried out with the standard transfer modes. The worst results were found with short-circuiting transfer. Da Silva and Scotti [32] made a comparison between MIG-Pulsed and MIG-Double pulsed concluding that this last process in spite of

having theoretically higher potential for porosity generation, does not increase the porosity susceptibility in aluminum welding, when compared with the MIG-Pulsed.

Other methods that can be used to suppress the hydrogen sources include controlling the ambient humidity [44], vacuum heat treatment [45] and removing the surface contamination and the oxide film [46]. Among the methods to remove the oxide film, chemical and mechanical surface cleaning are the most effective ones [47]. A novel laser beam welding (LBW) method has been proposed recently by Chen et al. [48] to eliminate hydrogen porosity without any surface pretreatment: a defocused laser beam is applied for surface re-melting ahead, followed by a focused laser beam for deep penetration welding. Hence, proper cleaning and shielding must be utilized to ensure the production of welds free of gas porosity. In addition, hydrogen porosity can be effectively reduced when welding at a higher welding speed [49]. It is assumed that there is not enough time for the accumulation of hydrogen due to rapid cooling and solidification at a higher welding speed. Measurements or comparison of hydrogen quantities in the weld beads made by paraxial hybrid plasma-MIG process on aluminum alloys were not possible to find.

3 Statement of the problem and goals

Based on the analysis of the state of the art performed, few studies were found on the principle of operation of the paraxial hybrid plasma-MIG process, however, there are still questions that have not been clarified. It should be mentioned that the coaxial hybrid plasma-MIG process was widely studied during a time, however, its operating principle is completely different to the paraxial plasma-MIG process, therefore, the arc physics between them cannot be compared.

Although the idea of the paraxial hybrid plasma-MIG process is to maintain the characteristics of each single welding process, these are influenced by the magnetic interactions that the magnetic fields of each welding process produces. In addition, the production of metallic vapors influences the ionization potential of the shielding gas, affecting the electrical signals of each process. However, on this last fact the conclusions found are diffuse and it is not possible to understand the real influence that one process has on the other, specifically on issues such as the length of the arc for different types of metal transfers in the MIG process.

The objective of this work is to characterize the paraxial hybrid plasma-MIG process, from its behavior with the electrical signals of each welding process to its influence on the gases diffused in the weld bead. For this, a comparative analysis between the single plasma and MIG processes, studying their gradual hybridization will be made, including a comparison with the current commercial version of the paraxial plasma-MIG process, called SuperMIG. In order to achieve the proposed objectives, the following procedures are necessary:

1. Observe the behavior of the plasma and MIG processes gradually approaching between them until the minimum distance. Plasma process will be configured to use alternating and direct current, this in order to observe the behavior of the electrical signals of each welding process and the phenomena in the welding arc. In addition, the base parameters (distance between torches) for the next experiments will be established.
2. The influence that each welding process has on the other, has not yet been studied in detail in the literature. In this case, the electrical signals of both welding processes will be measured, while one of them increases its current.

The MIG process will be studied using a pulsed and spray metallic transfer, with the aim to observe the influences on the hybrid arc behavior.

3. The results acquired with the paraxial plasma-MIG process will be compared with the commercial option “SuperMIG”, determining if there is any significant difference between them. In addition, the "magnetic deflection device" possessed by the SuperMIG will be studied in detail, in order to determine if an external magnetic field is necessary to obtain a stable hybrid process.
4. Which type of current (alternating or direct) in the plasma process is most effective in aluminum joints, when they are made by the paraxial hybrid plasma-MIG process will be studied. The level of oxygen and hydrogen in the joints will be measured, as a means of obtaining an indicator of the level of porosity inside of the joints.
5. Finally, the productivity of the plasma-MIG paraxial process will be compared with the conventional MIG process and the SuperMIG, through the task of completing 10 mm and 15 mm thick joints under the same welding conditions. Microhardness, tensile strength and amount of oxygen-hydrogen will be part of the analysis. This aim to determine if the hybridization between MIG and plasma process is an alternative to improve considerably the productivity.

4 Experimental set-up and consumables

In this chapter are described the equipment, materials and methodologies of the experiments made throughout this work. Given the exploratory and comparative nature of the experiments, several destructive and non-destructive tests were used, which are described sequentially.

4.1 Equipment

For this investigation, a workbench was implemented with the equipment indicated in Figure 4.1 and Table 4.1. A more detailed description of each of them will be given in the next sub-chapters.

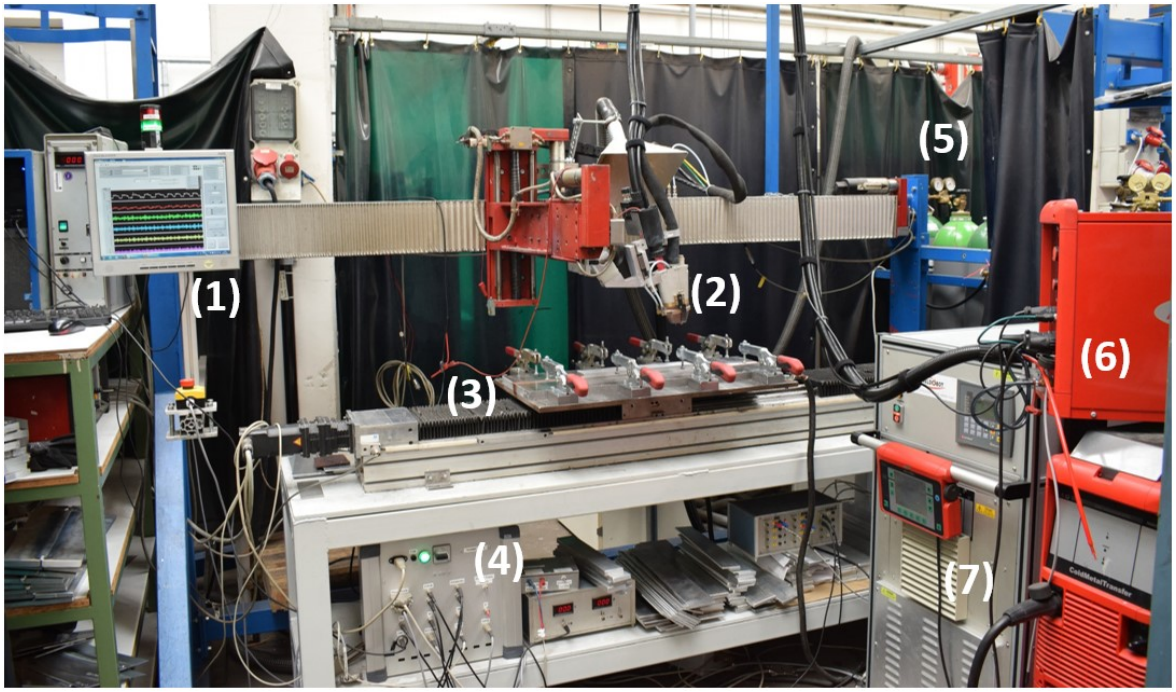

Figure 4.1 – Welding workbench.

Schweißversuchsstand.

Table 4.1 – Equipment of the workbench.

Ausstattung der Versuchsstand.

Item	**Equipment**
1	Display of the signal analysis and control software
2	Welding torch
3	Displacement device
4	Signal acquisition and control system
5	Shielding gases
6	MIG welding source
7	SuperMIG or plasma welding source

4.1.1 Welding sources

In this research, three different welding sources were used, in addition to their corresponding peripherals to ensure their correct operation. In the first stages, the single MIG source (Fronius) and the single plasma source (EWM) will be used, where the effects of the gradual coupling between the welding arcs will be studied. Then, a comparison between the commercial option, SuperMIG, and the single processes coupled will be made.

4.1.1.1 SuperMIG hybrid welding system

SuperMIG is a hybrid welding system that combines two welding processes, plasma and MIG, by means of a specially designed welding torch to optimize the addition of the filler material and the interaction between the welding arcs that compound each process. The main structure of the SuperMIG equipment (Figure 4.2) consists of three levels inside. The upper one is the plasma process and external magnetic field control unit. The second level has the plasma welding source, which is from Fronius brand, model MagicWave 3000, with a capacity of 300 A (35% duty cycle) and the option to work with direct current (DC) and alternating current (AC). On the other hand, the MIG welding source is not provided with the SuperMIG package and the SuperMIG control panel does not control MIG process parameters.

Figure 4.2 – SuperMIG equipment and its structure.

SuperMIG-Ausrüstung und -Struktur.

The welding torch provided with the SuperMIG unit was the "Heavy-duty" model (Figure 4.3). This torch has the shielding gas nozzle cooled, to which a black structure is connected; who corresponds to the electromagnets (pole shoes) that induce the magnetic field to stabilize the welding arcs of the MIG and plasma processes (Figure 4.3). The torch in its normal working position has the plasma torch at an angle of 90 degrees with respect to the base material, while the MIG torch is at 20 degrees with respect to the plasma torch. A constrictor plasma nozzle with a diameter of 3.2 mm was used for all the tests performed.

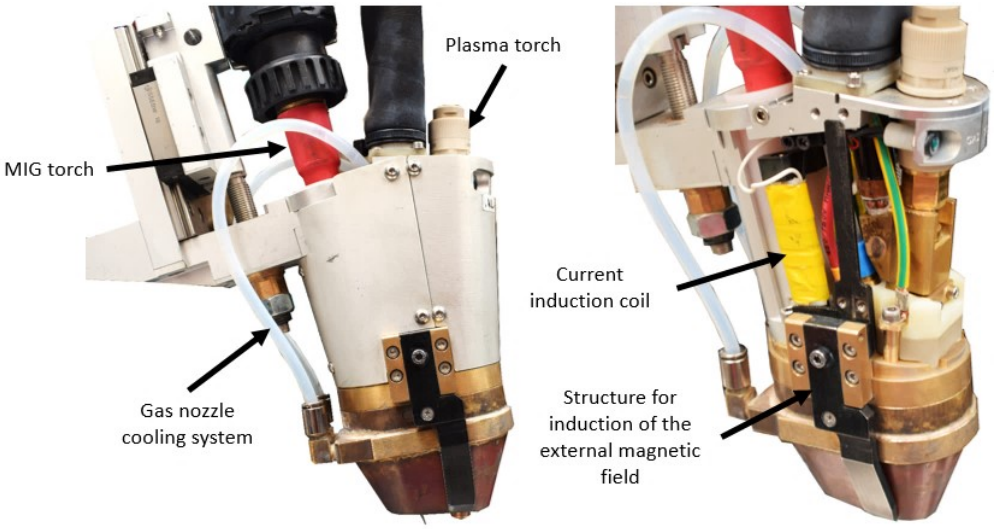

Figure 4.3 – SuperMIG torch heavy duty model.

SuperMIG-Brenner "Heavy-Duty" Modell.

4.1.1.2 MIG welding source

The welding source for the MIG process was a Fronius CMT Advance 4000R with a wire feeder model VR 7000-CMT and control panel model RCU 5000i. This model has different synergic curves for several alloys, and it has a capacity of 400 A (40% duty cycle). Although this welding source is characterized by its CMT (Cold Metal Transfer) system, who is a variant of the controlled short circuit metal transfer. In this research it will not be used, because the short circuit metal transfer has a low deposition rate, which would make it infeasible to complete a joint in one pass. The metallic transfers used in this work will be the "free flight" type, that is, spray and pulsed transfer. The main objective of using these two metallic transfers is because they use different types of welding source control. A constant voltage source is used for transfer of spray type, while a constant current source is used for pulsed transfer. With this, it will be observed which type of MIG welding source is more convenient for hybridization.

As this welding source is a synergic type, the parameters that can be adjusted are limited, and for this investigation only the wire feed speed was altered. The rest of the parameters were kept constant. In addition, the welding source is self-regulated for each situation, thus its static source characteristic (SSC) curve does not follow the normal pattern found in the books of classical literature. The SSC curve of the welding source changes according to the synergic curve to be used.

4.1.1.3 Plasma welding source

The plasma welding source used was from EWM company, model Tetrix 350 AC/DC Comfort. It is characterized by working with DC and AC with a capacity of 350 A (40% duty cycle).

The plasma torch used is from the company Autogen-Ritter GmbH, which has a capacity of 350 A (100% duty cycle). A constrictor nozzle with a diameter of 3.2 mm was used for all the tests performed.

4.1.2 Linear manipulator

In this investigation only linear welds were performed, therefore the linear manipulator Weltron WSC-3D model was used (Figure 4.1). The welding speeds required were from 15 cm/min to 80 cm/min, depending on the thickness of the joints

to be welded. Therefore, the welding torches were maintained fixed and the base material was displaced.

4.1.3 Measuring devices

The voltage and current electrical signals were acquired through a system developed for this work (hardware and software), in addition to the recording of high-speed videos.

4.1.3.1 Measurement of electrical signals

In order to obtain the electrical behavior of the welding processes, the voltage and current were measured as in the Figure 4.4 is presented. The current was measured at an arbitrary location of the ground cable. The sensors were connected to the computer through National Instruments acquisition cards (Figure 4.5a), which have an acquisition rate of 20 kHz. Upon entry of the acquisition cards, a low pass filter was implemented. The sensor used to measure the current was a LEM HTA-500S (Figure 4.5b), this sensor is characterized by using the hall effect, and can measure up to 500 A.

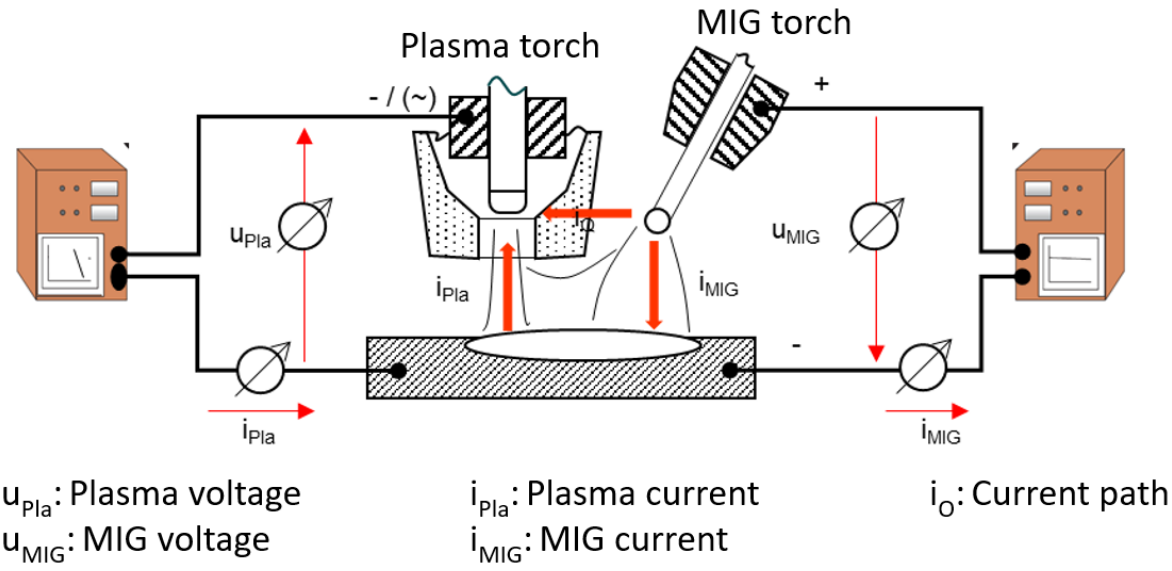

Figure 4.4 – Scheme of the measurement system of the electrical signals of the welding processes.

Schema des Messsystems der elektrischen Signale der Schweißprozesse.

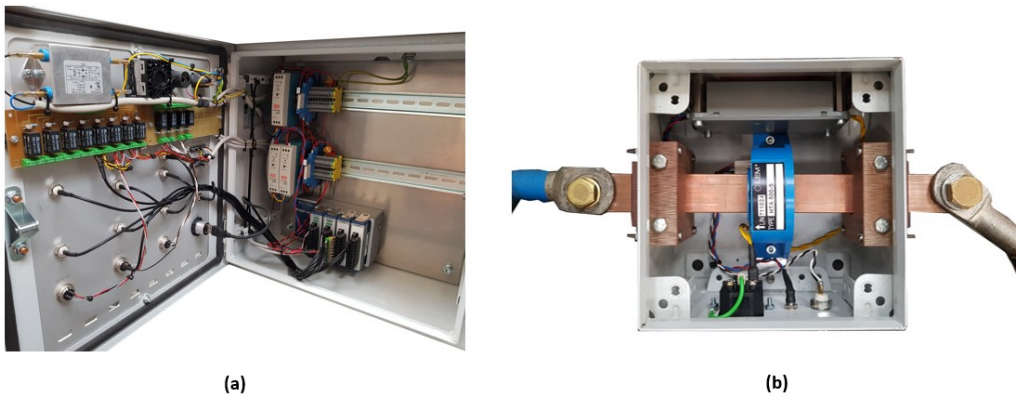

Figure 4.5 – Devices used for measuring electrical signals (a) NI cards with low pass filter (b) LEM HTA 500-S.

Geräte zur Messung elektrischer Signale (a) NI-Karten mit Tiefpassfilter (b) LEM HTA 500-S.

To measure the arc voltage drop, in the case of the MIG process, the measurement point was after the traction rollers positioned in the welding torch (Figure 4.6). The ideal measuring point would be directly on the wire-electrode, however, this is practically impossible. In the case of the plasma process, the measuring point was inside the torch body (Figure 4.6), which is in direct contact with the clamp that holds the tungsten electrode.

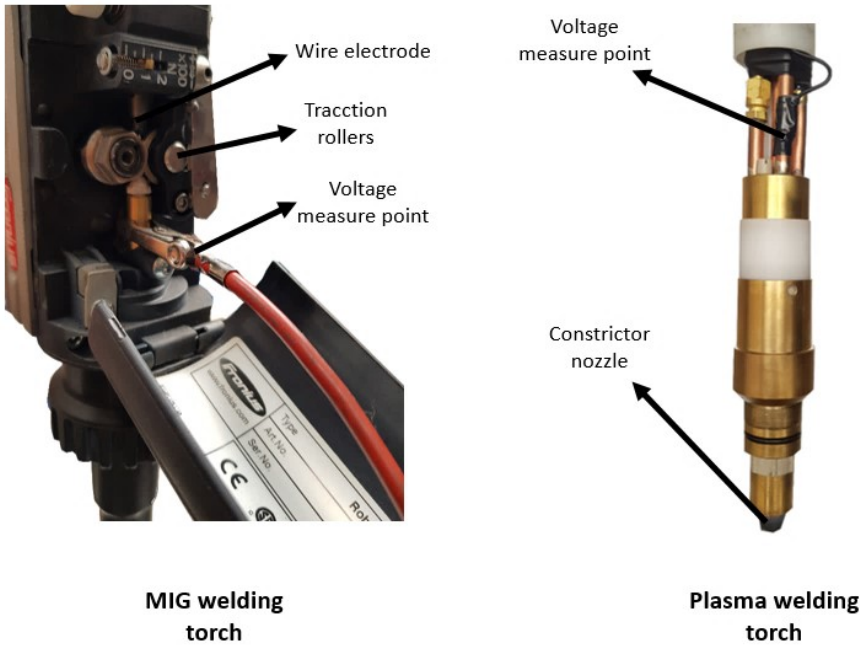

Figure 4.6 – Position of the voltage measurement points in the torches of each welding process.

Position der Spannungsmesspunkte in den Brennern jedes Schweißprozesses.

A software made by Labview for this investigation allows the visualization, analysis and storage of the electrical signals of the welding processes (Figure 4.7). It also allows to control the speed of the displacement device of the base material and the ignition of the welding processes.

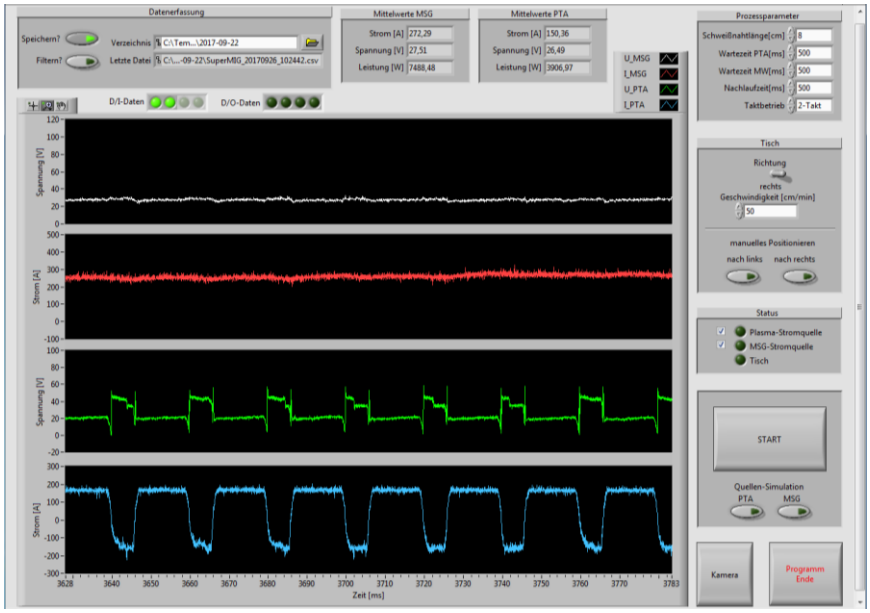

Figure 4.7 – Software for control, visualization and storage of the electrical signals.

Software zur Steuerung, Visualisierung und Speicherung der elektrischen Signale.

4.1.3.2 High speed video recording

High-speed videos were made using the Photron camera model SA4, which has a 12-bit ADC sensor (Bayer color, single sensor) with 20 µm pixel size. Its acquisition rate is adjustable from 1000 fps with 1024 * 1024 pixels, up to 500.000 fps with 128 × 16 pixels.

The recordings made in this study were at 20,000 fps at a resolution of 704x272. In addition, to improve the visualization of the arcs during the recordings, a light source opposite to the high-speed camera was used (Figure 4.8). This technique is used to reduce the influence of the great intensity of the light coming from the welding arc. The model of the light source is LSH 601 Hg which is able to produce high irradiance on small targets as a result of the concentrated arc.

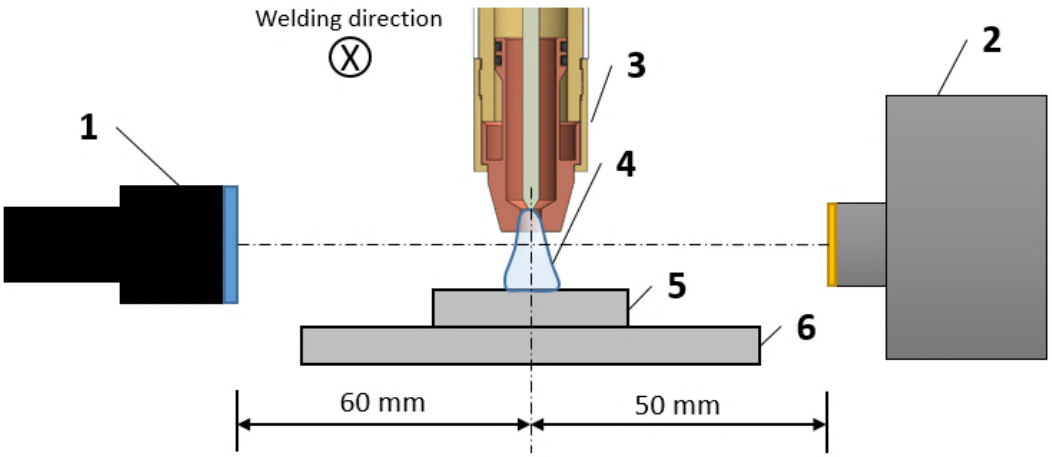

1 High speed camera
2 UV light
3 Plasma-MIG torch
4 Arc column
5 Base material
6 Table

Figure 4.8 – Video recording setup.

Videoaufzeichnungseinrichtung.

The software to control the camera is called Photron FASTCAM Viewer (PFV). It can adjust the parameters of the camera, as are the frames per second, shutter speed, duration of recording and image size among others. The shutter speed was set to 0.1 µs and the duration of recording was 250 ms.

4.1.3.3 Arc length measurements

To study the influence of the coupling between the welding processes on the arc length of the MIG process, the Photron FastCam Anlysis (PFA) software was used (Figure 4.9). With PFA, it is possible to analyze motion within an image sequence imported from Photron FastCam Viewer (PFV) in order to obtain values for displacement, velocity and acceleration. Following analysis, it is possible to achieve synchronized playback of the data graphs and images.

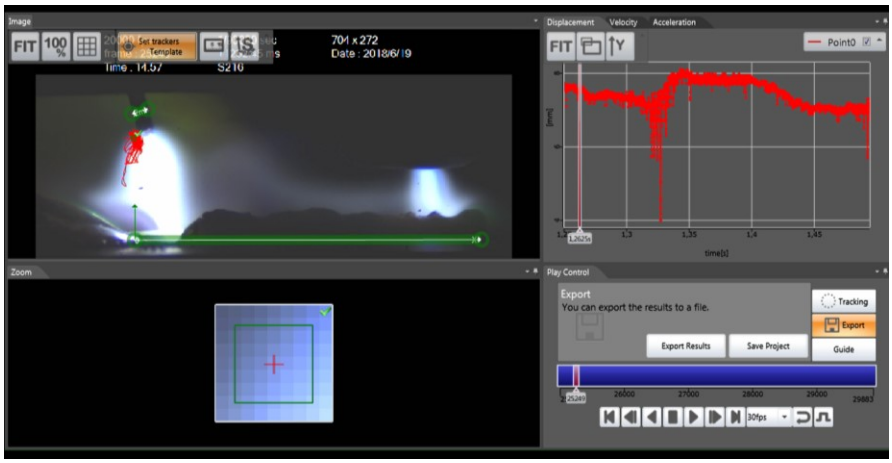

Figure 4.9 – Photron FastCam Analysis (PFA) software interface in the measurement of the MIG process arc length.

Photron FastCam Analysis (PFA) -Softwareschnittstelle zur Messung der MIG-Prozessbogenlänge.

4.2 Materials

The base material used to make this investigation was the aluminum alloy EN AW 6060-T66 in thicknesses of 10 mm and 15 mm. While the filler material was the wire-electrode EN ISO 18273 S Al 4043 (AlSi5) in a diameter of 1.2 mm. The chemical composition of the materials was obtained by means of an optical emission spectroscopy (OES) analysis and they are found in Table 4.2.

Table 4.2 – Chemical composition of the base metal and filler metal (wt%).

Chemische Zusammensetzung des Grundwerkstoff und des Zusatzwerkstoff (wt%).

Material	Si	Fe	Cu	Mn	Mg	Zn	Cr	Ti	Al
AW6060 (15 mm)	0.518	0.149	0.009	0.013	0.531	0.016	0.012	0.024	Bal.
AW6060 (10 mm)	0.433	0.195	0.006	0.032	0.466	0.007	0.009	0.019	Bal.
EN ISO 18273 S Al 4043 (AlSi5)	4.460	0.138	0.011	0.007	0.074	0.004	0.006	0.039	Bal.

Before welding, the base material was brushed to remove the oxide layer and after cleaned with acetone.

4.2.1 Metallography

In preparation for metallography, the specimens were polished to a mirror-like finish and then etched using 10% aqueous hydrofluoric acid.

4.2.2 Tensile test

Tensile tests of the welding joints were performed with an universal tester Instron 4210. The dimensions of the tensile test specimens were obtained by norm DIN EN ISO 4136:2013-02 and their final dimension is shown in Figure 4.10. The samples distribution in the welding joints are presented in Figure 4.11, it was followed by the norm DIN EN ISO 15614-1:2017-12.

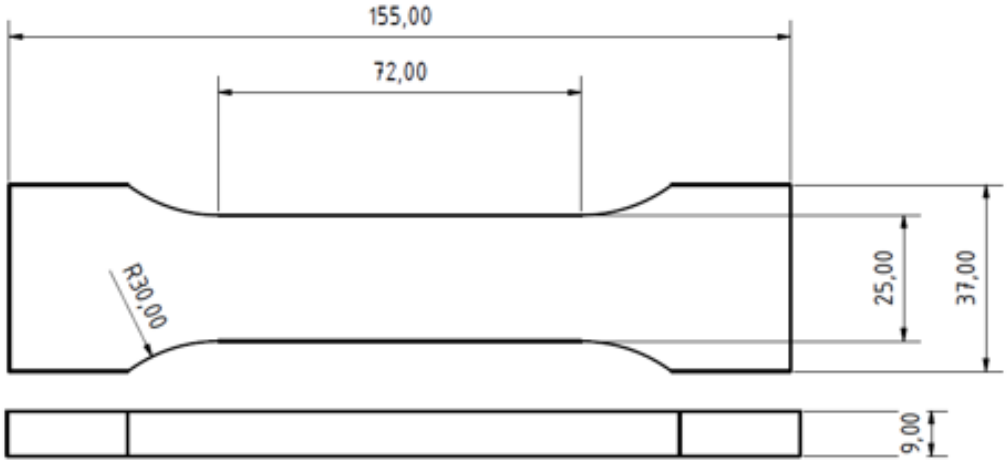

Figure 4.10 – Sample dimensions for tensile tests according to the norm DIN EN ISO 4136:2013-02.

Probenabmessungen für Zugversuche nach Norm DIN EN ISO 4136: 2013-02.

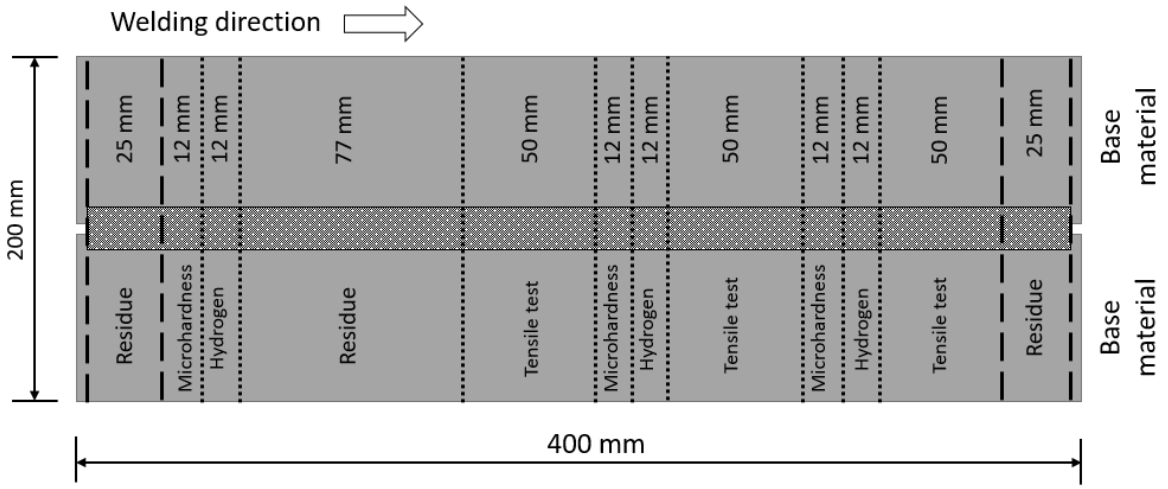

Figure 4.11 – Distribution of samples to be extracted from the joints to measure microhardness, diffusible hydrogen and tensile test.

Verteilung der Proben, die aus den Fugen entnommen werden sollen, um die Mikrohärte, den diffusionsfähigen Wasserstoff und die Zugfestigkeit zu messen.

4.2.3 Microhardness measurements

The microhardness of the welding joint was measured using Vickers hardness tester at 4.9 MPa load and 15 s dwell time. Two lines of hardness measurements were made, the first in the upper part and the second in the lower section of the joint (Figure 4.12). The objective is to observe the difference in hardness that exists between the regions of the joints, especially for joints 15 mm thick.

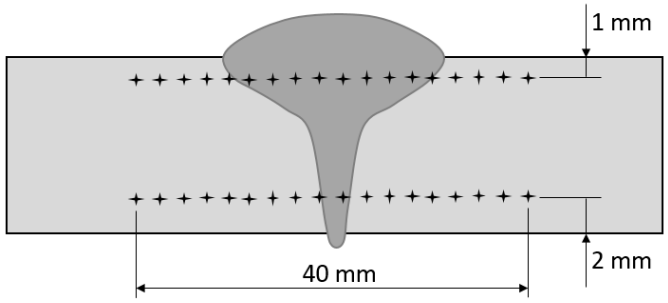

Figure 4.12 – Schema of the localization of the microhardness measurements.

Schema der Lokalisierung der Mikrohärtemessungen.

4.2.4 Temperature measurements

Temperature measurements were performed as described in Figure 4.13. Type K thermocouples connected to the Yokogawa DL850E oscilloscope were used for them. The thermocouples were attached in the molten pool when the plasma torch

of the hybrid processes traveled a distance of 150 mm from the beginning of the joint.

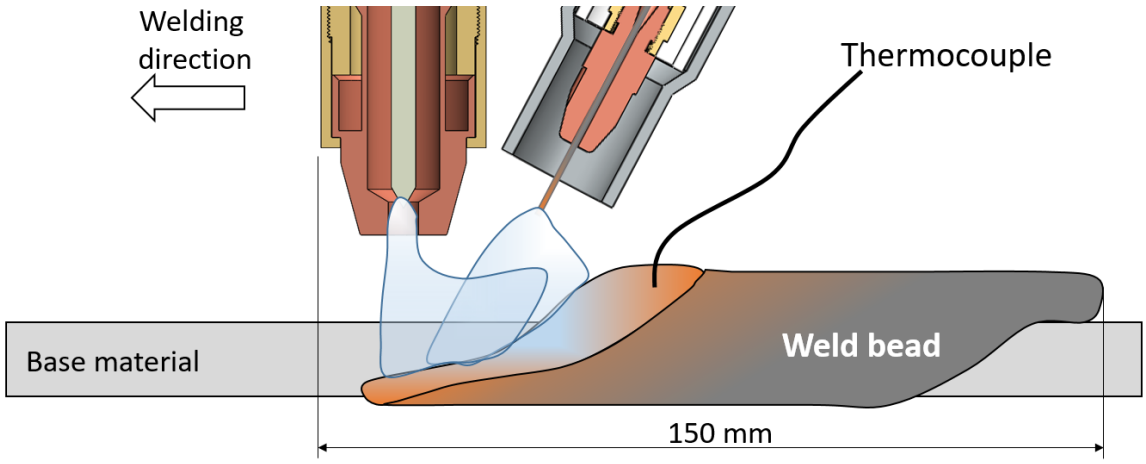

Figure 4.13 – Thermocouple positioning during the welding process to measure the temperature of the molten pool.

Thermoelementpositionierung während des Schweißprozesses zur Messung der Temperatur des Schmelzbades.

4.2.5 Hydrogen measurements

The hydrogen content of the filler material and welding joints were determined using the inert gas fusion (IGF) method. The measurements in the filler wires were made following the method described by DVS [50]. For this purpose, three samples of the welding wire were retrieved by cutting each into 12 pieces with a length of 8 mm, which was equivalent to a weight of 0.3 g.

The hydrogen amounts in the welding joints were measured following the method described in the norm ASTM E2792-13 [51]. For each welding joint were extracted 3 samples from the weld bead, as described in Figure 4.11, with a weight of 4 g. The extracted sample is divided into two sections, face and root, as shown in Figure 4.14.

All samples were placed into a carbon crucible and heated in a furnace. The outgassing hydrogen was absorbed by a carrier gas. By comparing the thermal conductivity of the mixture of outgassed hydrogen and carrier gas with a reference gas, the quantity of hydrogen was determined. The unit of the values is “parts per million” (ppm), the weight of hydrogen in micrograms in relation to the weight of the specimen in grams.

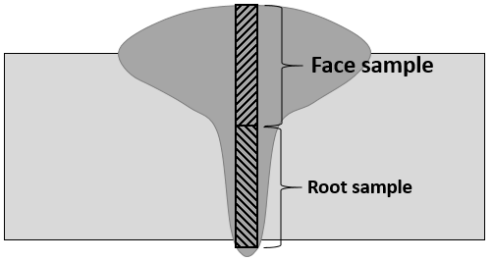

Figure 4.14 – Scheme of hydrogen samples distribution.

Schema der Wasserstoffprobenverteilung.

4.2.6 Oxygen, magnesium and silicon measurement in the weld beads.

To compare how the welding processes influence the properties of the weld beads, especially the oxygen (O), magnesium (Mg) and silicon (Si) contents, three different points along the cross section of the weld beads will be measured, as seen in Figure 4.15. These measurements were made with an Energy-dispersive X-ray (EDX) spectroscopy analysis.

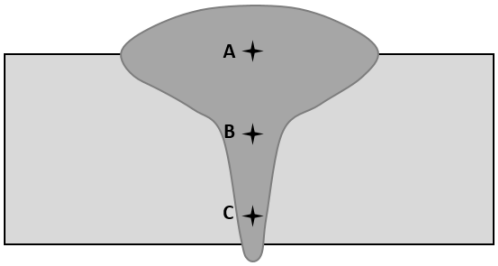

Figure 4.15 – Measurement points (A, B and C) of oxygen, magnesium and silicon concentration by EDX analysis.

Messpunkte(A, B und C) der Sauerstoff-, Magnesium- und Siliziumkonzentration mittels EDX-Analyse.

5 Methods

The methodology in this work was divided in two groups. The first relates to the study of the interaction between the welding arcs of the plasma and MIG welding processes, for different current polarities in the plasma process, in addition to different metal transfers in the MIG process. The second group deals with making applied comparisons between the MIG process, the paraxial hybrid plasma-MIG process and the commercial option SuperMIG. Figure 5.1 shows a schematic representation of the stages in which the work was structured.

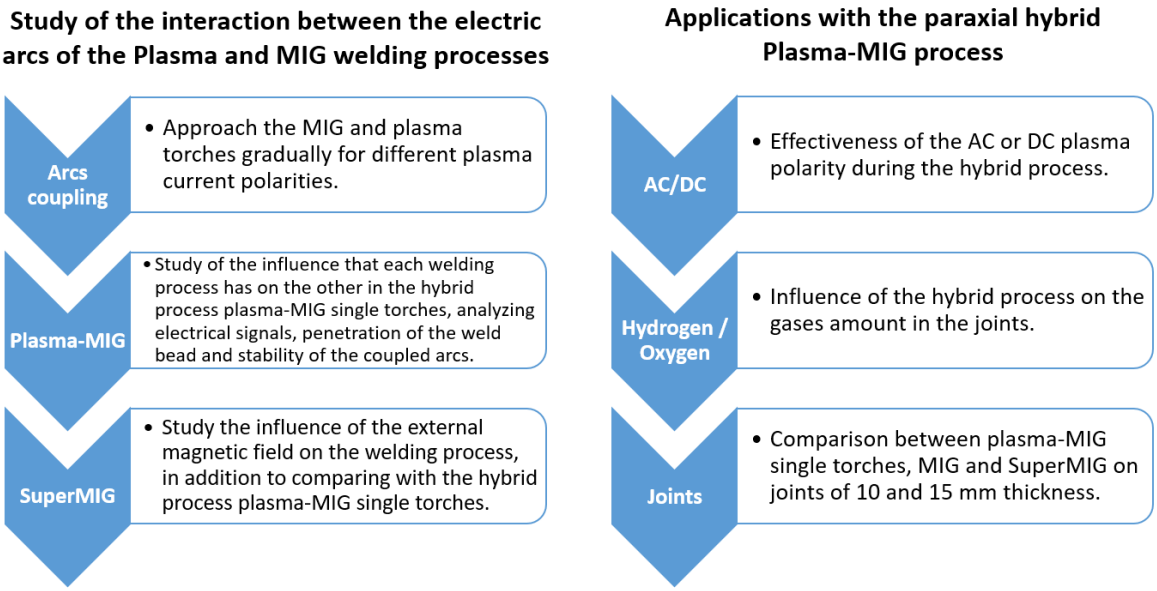

Figure 5.1 – Schematic representation of the methodology of experiments.

Schematische Darstellung der Methodik der Experimente.

Some of the welding parameters used in the tests performed were kept constant as plasma gas flow in 3.2 l/min, plasma shielding gas flow in 15 l/min, electrode setback (R) in 3 mm, plasma arc length (A) in 5 mm, CTWD in 14 mm, argon as MIG shielding gas, MIG shielding gas flow in 25 l/min, argon as shielding and plasma gas with plasma-AC process, ArHe30 as shielding and plasma gas with plasma-DC process, AC frequency in 50 Hz, AC balance in 70% and welding speed in 50 cm/min.

5.1 Arcs coupling

The coupling between the MIG and plasma welding processes were studied setting different distances between the torches of each welding process. Figure 5.2 describes the position of each welding torch and Table 5.1 describes the welding

parameters used in this experiment. The plasma process was configured with direct and alternating current in order to observe its influence on the arc of the MIG process (magnetic deflection), molten pool temperature and weld bead geometry. In this study the MIG welding source was configured in the “Standard” mode (constant voltage static characteristic).

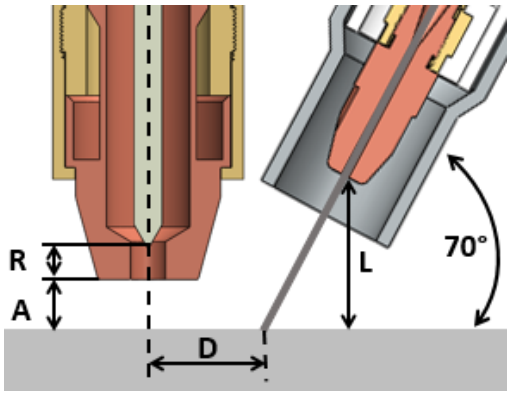

Figure 5.2 – Welding torches configuration.

Schweißbrennerkonfiguration.

Table 5.1 – Welding conditions for MIG and plasma processes coupling study.

Schweißbedingungen für die Kopplungsstudie zu MSG- und Plasmaprozessen.

Parameter	**Plasma DC**	**Plasma AC**
Plasma current [A]	100	150
MIG wire feed [m/min]	16	12
Distance between torches (D) [mm]	50, 40, 30, 20, 10	50, 40, 30, 20, 10
MIG welding source mode	Standard	Standard

5.2 Influence of the plasma process current and MIG current on the hybrid process

In order to study the influence of the plasma process on the behavior of the paraxial plasma-MIG processes, different current intensities were configured, keeping the wire feed speed of the MIG process constant. In addition, four levels of wire feed speed were also tested maintaining plasma current constant. The objective is to

observe the influence of the plasma process for different current of the MIG process. With electrical signals analysis of each welding process and high-speed videos, the influence of plasma current on the formation and establishment of the current path between the two welding processes will be studied. Table 5.2 describes the welding parameters and the torches configuration (Figure 5.2) used for this experiment. The MIG process was configured in “Standard” and “Pulsed” modes with the aim to observe how the welding source characteristic influences the current and voltage measurements.

Table 5.2 - Welding condition for the study of the influence of the Plasma and MIG processes current on the hybrid process.

Schweißbedingungen für die Untersuchung des Einflusses der aktuellen Plasma- und MSG-Prozesse auf den Hybridprozess.

Parameter	**Plasma DC**	**Plasma AC**
Plasma current [A]	50, 100, 150, 200, 250, 300	50, 100, 150, 200, 250, 300
MIG wire feed [m/min]	8, 12, 14, 16	12, 14, 16
Distance between torches (D) [mm]	20	20
MIG welding source mode	Standard, Pulsed	Standard, Pulsed

5.3 Study of the SuperMIG equipment and the magnetic level compensation

The commercial option to paraxial hybrid plasma-MIG process is called SuperMIG and its main characteristic is a device that regulates the stability between welding arcs. Different plasma current intensity and wire feed speeds will be tested, with the aim to compare with the results obtained by the paraxial plasma-MIG process. In addition, the influence of the parameter called "Magnetic level compensation" on the stability of the hybrid welding process will also be analyzed. Table 5.3 shows the parameters used for the study.

Table 5.3 - Welding condition for the study the SuperMIG welding process.

Schweißbedingungen für die Untersuchung des SuperMIG-Schweißprozesses..

Parameter	**Plasma DC**
Plasma current [A]	100, 150, 200, 250, 300
MIG wire feed [m/min]	5, 8, 12, 14, 16
Distance between torches (D) [mm]	20
MIG welding source mode	Standard
Magnetic compensation level [%]	5, 10, 20, 40, 50, 60, 70

5.4 Applications of plasma-MIG hybrid process

To work with joints of different thicknesses, the workbench table was adapted as shown in Figure 5.3, in which a copper backing is observed to ensure sustainability of the molten pool at the joint root. The tests were performed with 10 and 15 mm plates. In the 15 mm joints, the use of bevels to complete the joints was compared. A different configuration was used for each situation and it was indicated in the description of each test plan, following the scheme presented in Figure 5.4.

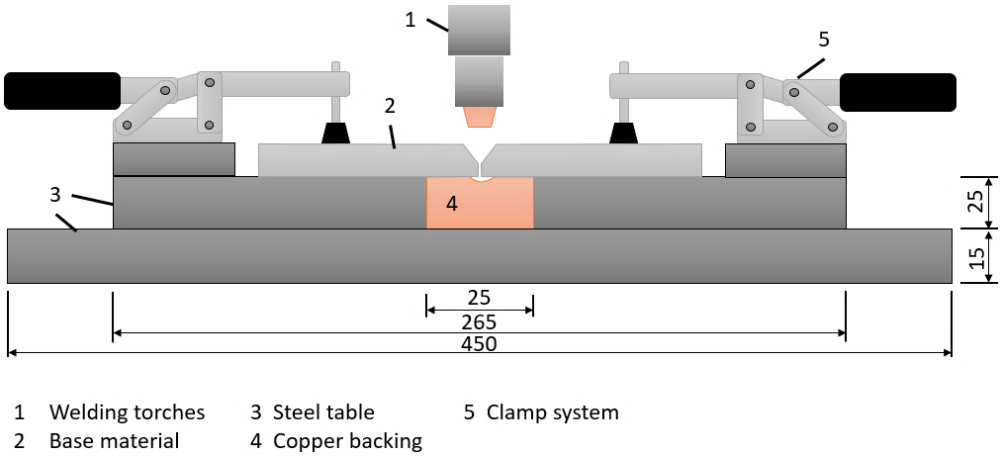

Figure 5.3 – Workbench configuration to study the hybrid and singles processes when they complete joints of 10 and 15 mm.

Werkbankkonfiguration zur Untersuchung der Hybrid- und Einzelprozesse, wenn Verbindungen von 10 und 15 mm ausgeführt werden.

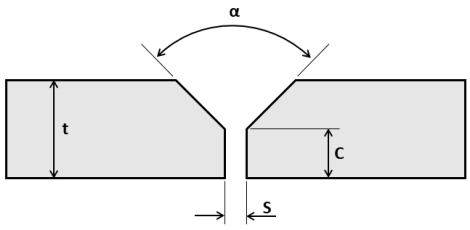

Figure 5.4 - Scheme of dimensions used in joints 10 and 15 mm.

Maßschema für 10 und 15 mm Fugen.

The first comparison is between plasma processes with alternating current (AC) and direct current (DC), in order to compare the mechanical properties that each of these variants offers to the welded joint. The test plan used is presented in Table 5.4.

Table 5.4 – Welding condition to compare paraxial hybrid Plasma-MIG process with alternating current (AC) and direct current (DC) in joint applications.

Schweißbedingung zum Vergleich des paraxialen Plasma-MSG-Hybridprozesses mit Wechselstrom (AC) und Gleichstrom (DC) in gemeinsamen Anwendungen.

Parameter	**Plasma DC**	**Plasma AC**
Plasma current [A]	100	100
MIG wire feed [m/min]	15	15
Distance between torches (D) [mm]	20	20
MIG welding source mode	Standard	Standard
Joint configuration	α=0° t=10 mm s= 0 mm c= 0 mm	α=0° t=10 mm s= 0 mm c= 0 mm

With 15 mm thick joints, beveled joints were used as presented in Figure 5.4. In addition, different joint gaps were used to guarantee total penetration. The test plan is presented in Table 5.5.

Table 5.5 - Welding condition to study the influence of the gap joint with the paraxial hybrid plasma-MIG.

Schweißbedingung zur Untersuchung des Einflusses der Spaltverbindung mit dem Plasma-MSG-Paraxialhybrid.

Parameter	**Plasma DC**
Plasma current [A]	100
MIG wire feed [m/min]	14, 16
Welding speed [cm/min]	30
Distance between torches (D) [mm]	20
MIG welding source mode	Standard
Joint configuration	α=0°, 30°; t=15 mm; s= 0, 1.6, 2 mm; c= 0, 5 mm

All welding processes (MIG, plasma-MIG and SuperMIG) were compared in 15 mm joints, in order to measure the amount of hydrogen and oxygen that each of these processes provide to the joints, in addition to measure their mechanical properties by tensile tests. The test plan is presented in Table 5.6.

Table 5.6 - Welding condition to compare the MIG, paraxial plasma-MIG and SuperMIG in joint of 15 mm thickness.

Schweißbedingungen zum Vergleich von MSG, Plasma-MSG paraxial und SuperMIG in einer 15 mm dicken Verbindung.

Parameter	**Plasma DC**
Plasma current [A]	200
MIG wire feed [m/min]	18
Welding speed [cm/min]	40
Distance between torches (D) [mm]	20
MIG welding source mode	Pulsed
Joint configuration	α=0°; t=15 mm; s= 2 mm; c= 0 mm

6 Experimental Researchs and Discussions

6.1 Coupling between plasma and MIG processes

To study the coupling between MIG and plasma processes, the welding torches were approached gradually, in order to observe the behavior of the welding arcs, electrical signals and their influence on the penetration profile of the weld beads. The welding conditions are described in Table 5.1.

Figure 6.1 shows the voltage curves for plasma-DC and AC during welding time for different torch distances. A drop voltage in the plasma-DC process is noticed when the arc of MIG process is ignited and the distance between the torches is equal and minor than 20 mm. Changing the plasma current type to alternating (AC) a disturbance in the electrical signals was also noticed when MIG arc was ignited. In both cases the disturbance began when the distances between torches were equal and lower than 20 mm. In Figure 6.1b, it is observed that as the torch distance decreases, the amplitude of the plasma voltage curve increases. The voltage drop observed in the plasma-DC process starts exactly when the welding arcs are close enough to interact with each other, which happens for distances less than 20 mm (including). This voltage drop is around 10 V.

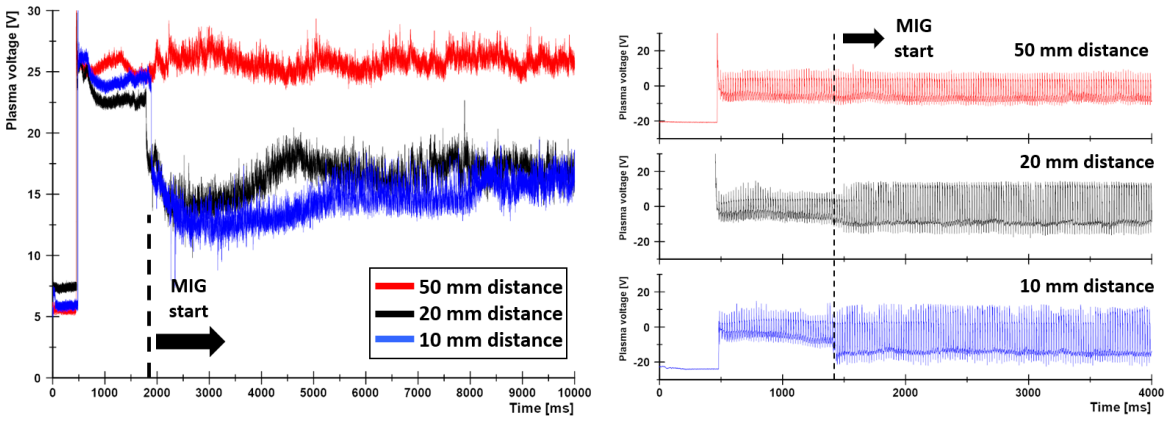

Figure 6.1 – Plasma voltage for different distances between torches (a) direct current (b) alternating current. Plasma-DC: 100 A, Wire feed speed: 16 m/min; Plasma-AC: 150 A, Wire feed speed: 12 m/min.

Plasmaspannung für unterschiedliche Abstände zwischen Brennern (a) Gleichstrom (b) Wechselstrom. Plasma-DC: 100 A, Drahtvorschubgeschwindigkeit: 16 m/min; Plasma-AC: 150 A, Drahtvorschubgeschwindigkeit: 12 m/min.

The current signal of the plasma process in AC and DC were not influenced by the coupling of the welding arcs (Figure 9.1 and Figure 9.2). This behavior is expected from a welding source that controls the output current (constant current static characteristic). On the other hand, the electrical signals of the MIG process did not show any influence or alteration in their behavior (Figure 9.3 and Figure 9.4), especially the current, which is the response signal when the welding source is a constant voltage characteristic.

Analyzing in detail the voltage curves of the plasma-AC in Figure 6.2, it is observed that the amplitude increases, however, it is the negative polarity of the curve where a strong influence is noticed, increasing the voltage in this polarity by approximately 7 V. A histogram of the plasma voltage curves of Figure 6.2 is presented in Figure 6.3, observing that the voltages in negative polarity increase while the torches distances are reduced, although, this effect is not as pronounced for the positive polarity. An increase of the plasma voltage in the negative polarity of 8 V is noticed, while in the positive polarity the voltage decreased by 1 V.

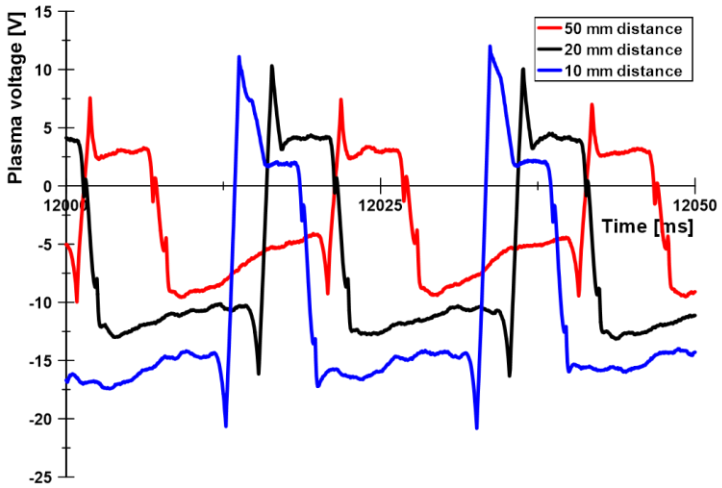

Figure 6.2 - Comparison of voltage signals for plasma-AC process for different distances between welding torches. Plasma AC: 150 A; MIG wire feed speed: 12 m/min.

Vergleich der Spannungssignale des Plasma-Wechselstromprozesses für unterschiedliche Abstände zwischen Schweißbrennern. Plasma-Wechselstrom: 150 A; MSG-Drahtvorschubgeschwindigkeit: 12 m/min.

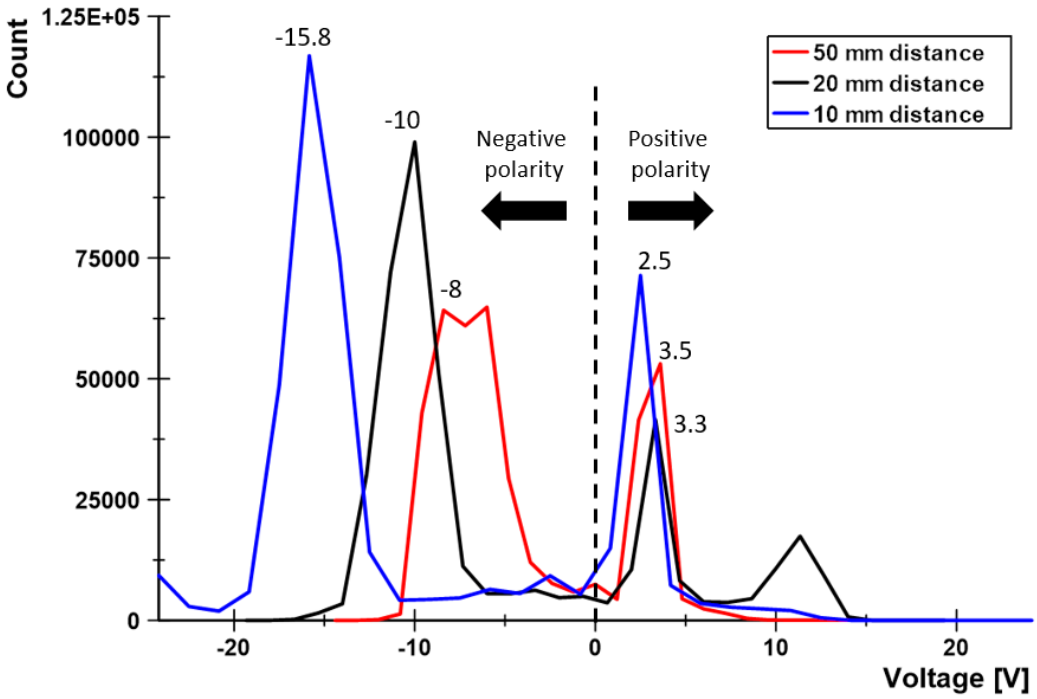

Figure 6.3 - Comparative histogram between plasma voltages for different distances between welding torches. Plasma AC: 150 A; MIG wire feed speed: 12 m/min.

Vergleichshistogramm zwischen Plasmaspannungen für unterschiedliche Abstände zwischen Schweißbrennern. Plasma-AC: 150 A; MSG-Drahtvorschubgeschwindigkeit: 12 m/min.

As the voltage of the plasma-AC was influenced and the current was kept undisturbed by coupling the arcs, the power of the process was affected. The power in the negative polarity increased by approximately 1000 W when a distance of 10 mm is used. In positive polarity, power had no clear trend and just a variation of approximately 200 W (Figure 9.5)

By means of images obtained by high-speed camera, it is observed that there is a magnetic deflection in the arcs of both processes, which is more intense for shorter distances between the torches (Figure 6.4). Although, when the polarity of the plasma arc is positive, an attraction between the arcs is noticed, while with negative polarity, the arcs tend to repel each other. This effect was also observed by Han et al. [7] in the paraxial VPPA-MIG and by Kanemaru et al. [13] with the hybrid TIG-MIG welding processes, where they concluded that the phenomenon is resulting from the effect of magnetic field coupling due to the ampere force produced by the arc magnetic field of both welding processes. Quantify the intensity of the magnetic deflection in the plasma process between the polarity change is difficult, however,

based on the behavior observed in the voltage histogram in Figure 6.3, it is possible to say that the magnetic deflection is more intense when the arcs repel each other (DCEN). This conclusion is based on the fact that the arc length is considered proportional to the plasma process voltage, thus, the higher the voltage, the longer is the arc column.

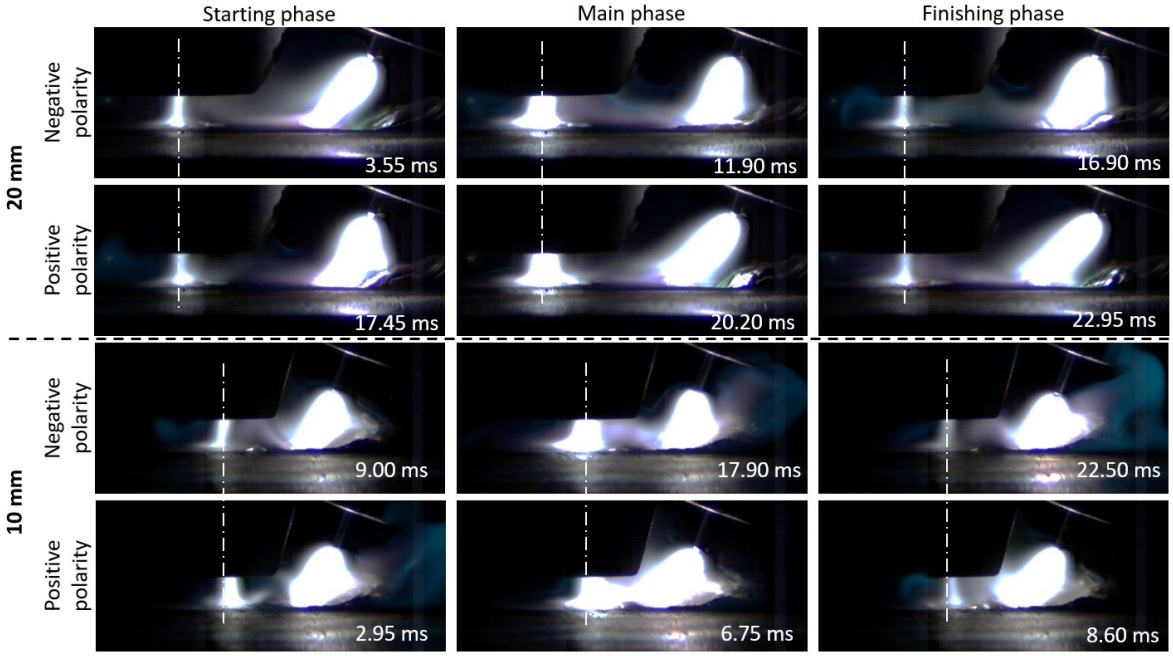

Figure 6.4 - Intensity of the magnetic deflection in the arcs of the plasma-AC and MIG processes for distances of 10 and 20 mm between torches. Plasma AC: 150 A; MIG wire feed speed: 12 m/min.

Intensität der magnetischen Ablenkung in den Lichtbögen der Plasma-AC- und MIG-Prozesse für Abstände von 10 und 20 mm zwischen den Brennern. Plasma-AC: 150 A; MSG-Drahtvorschubgeschwindigkeit: 12 m/min.

Magnetic deflection was also observed when direct current was used in the plasma process, however, in comparison with plasma-AC, it causes a constant repulsion between the plasma and MIG arcs (Figure 6.5). Moreover, for torch distances minor than 20 mm, the arcs establish a plasma “bridge” or “path” between them. In the study on the hybrid TIG-MIG process with direct current, Kanemaru et al. [13, 14] also noticed this "current path", which influences the voltage and current lectures. Han et al. [7] observed the current path in the paraxial hybrid VPPA-MIG, mentioning that the metallic vapors produced by the hybrid arc are responsible for the voltage drop in the welding processes.

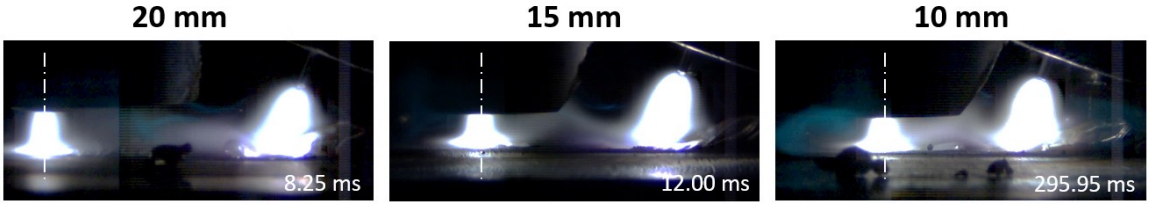

Figure 6.5 - Intensity of the magnetic deflection in the arcs of the plasma-DC and MIG processes for distances of 10, 15 and 20 mm between torches. Plasma DC: 100 A; MIG wire feed speed: 16 m/min.

Intensität der magnetischen Ablenkung in den Lichtbögen der Plasma-DC- und MIG-Prozesse für Abstände 10 und 20 mm zwischen den Brennern. Plasma DC: 100 A; MSG-Drahtvorschubgeschwindigkeit: 16 m/min.

The average voltage of the plasma process shows different behaviors depending on the type of current configured (Figure 6.6). When AC is used, the RMS voltage increases while the torch distance decreases, this raised in the RMS voltage is around 5 V. On the other hand, when direct current is used, the average plasma voltage decreases by 10 V. The studies made by Kanemaru et al. [13, 14] propose that the voltage drop for the TIG-MIG process is due to a combination of 2 main factors: 1. exist a current flow between the welding process when a current path is stablished between the arcs; 2. the metal vapor reduces the ionization potential of the shielding gas. Han et al. [7] proposed that the metal vapors are the main responsible for the voltage drop in the paraxial hybrid plasma-MIG process with alternating current, while, Hong et al. [9] noticed that the voltage drop in the plasma-AC is stronger when MIG current is higher. However, the behavior observed in the plasma-AC voltage in the Figure 6.6 does not match with the explanation made by Kanemaru et al. [13, 14]. It is suggested that in the case of plasma-AC voltage, there is not a voltage drop due to the intensity of the MIG current is not enough strong (around 280 A) as in the curve for plasma-DC (around 380 A). In addition, a strong alternated magnetic deflection reduces the efficiency of the arc; therefore, a minor amount of metallic vapors would be produced, which would diminish the effect of reduction of the ionization potential of the shielding gas. The current path, as was observed in Figure 6.4, is intermittent for plasma-AC, which would influence the voltage drop of the plasma process, due to the current flow between processes is not constant. In the subchapter 6.2.2, this phenomenon will be studied in detail for different levels of current.

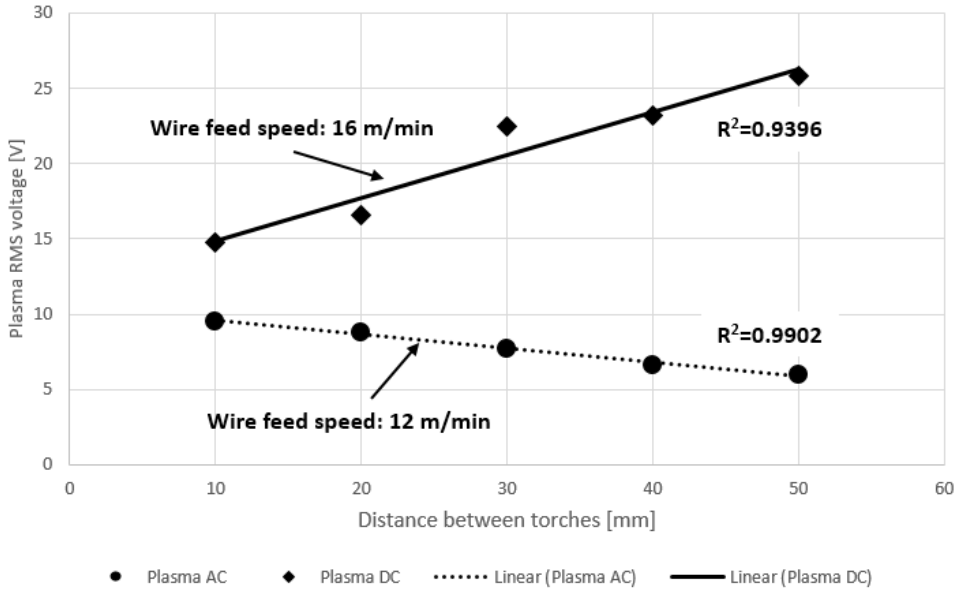

Figure 6.6 – Plasma RMS voltage and power for different plasma polarity current and torches distances. Plasma DC: 100 A; Plasma AC: 150 A.

Plasma-RMS-Spannung und -Leistung für unterschiedliche Plasmapolaritätsströme und Brennerabstände. Plasma DC: 100 A; Plasma-AC: 150 A.

The average MIG current, on the other hand, has a similar behavior with plasma direct and alternating current (Figure 6.7). For plasma-DC, the average MIG current has a defined tendency to increase, while for plasma-AC it is less pronounced. The increase in MIG current, when it is coupled to the plasma-DC, is around 14 A. The MIG voltage was not influenced by the torch distances (Figure 6.8), due to the MIG process works with a welding power source with constant voltage static characteristic.

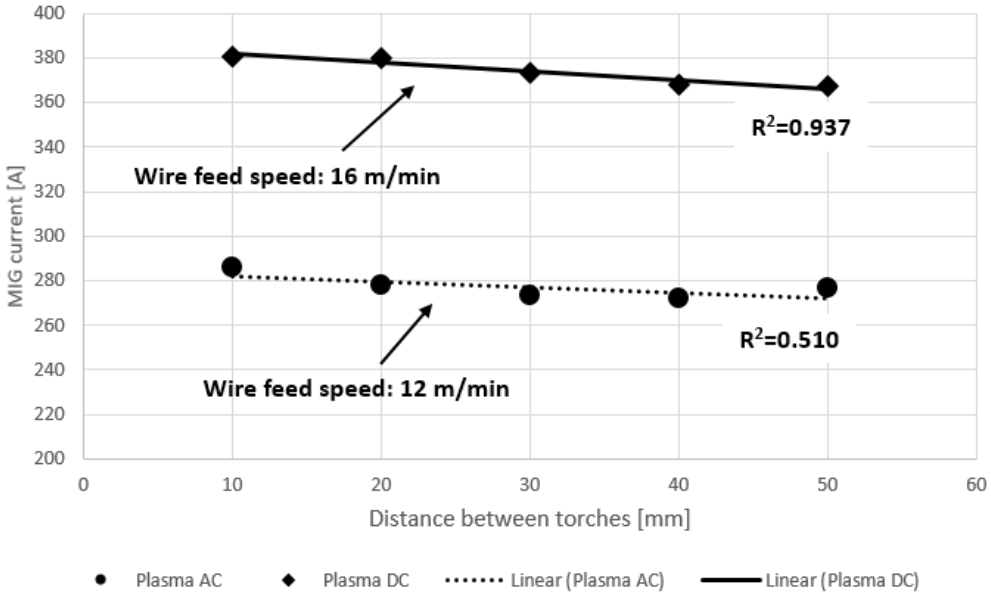

Figure 6.7 – MIG average current for different plasma polarity current and distances between torches. Plasma DC: 100 A; Plasma AC: 150 A.

Durchschnittlicher MSG-Strom für unterschiedliche Plasmapolaritätsströme und Abstände zwischen Brennern. Plasma DC: 100 A; Plasma-AC: 150 A..

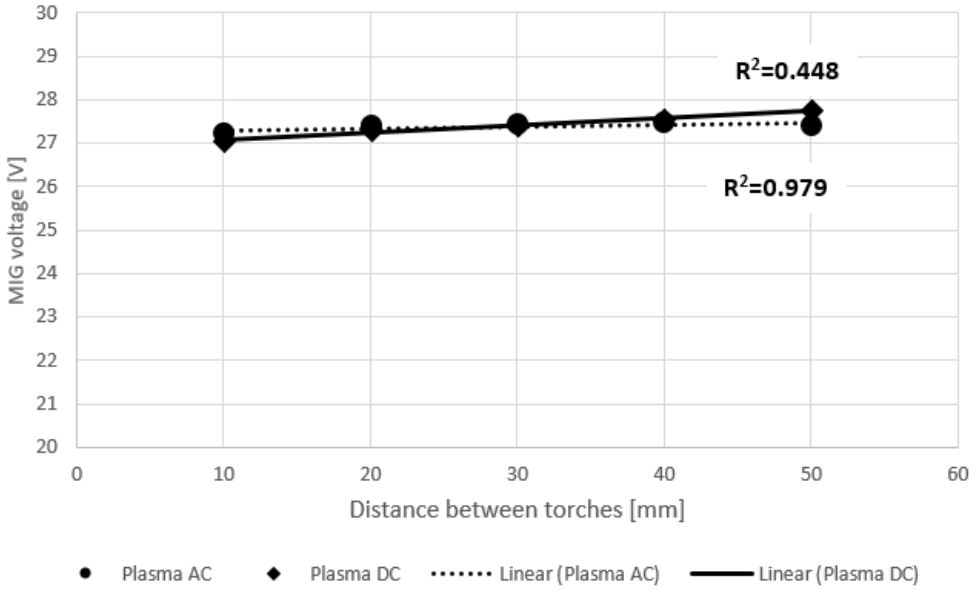

Figure 6.8 – MIG average voltage for different plasma polarity current and distances between torches. Plasma DC: 100 A; Plasma AC: 150 A.

Durchschnittliche MSG-Spannung für unterschiedliche Plasmapolaritätsströme und Abstände zwischen Brennern. Plasma DC: 100 A; Plasma-AC: 150 A.

The average current in the MIG process is a consequence of the voltage and the wire feed speed, therefore, if the voltage and wire feed speed are constant, then the variables that could influence the MIG current are the arc length and the stick-out [1, 52]. As was explained in the study made by Silva et al. [52], the MIG current increase when the stick-out is reduced and the arc length is maintained constant. On the other hand, when the arc length is increased and the stick-out is constant, the current is reduced [1]. However, this explanation does not agree with the behavior observed in the MIG process when the torches distances are reduced. The MIG arc length increased and, as a consequence, the stick-out was reduced. The arc length is proportional to the MIG voltage [1], therefore, it is expected that the MIG voltage increases, but this was not observed in Figure 6.8. It is suggested that the main responsible for this phenomenon is the electrical current flow between the processes plasma and MIG through the current path established, noticed by several authors [3, 7, 11, 13, 14, 53]. Another possible explanation is the deflection in the MIG arc by the influence of the magnetic field of the plasma process, which changes the arc length and increases the value of the MIG current. This interaction between the welding processes and their influences in the arc length will be studied in detail in the subchapter 6.2.1.1.

Analyzing the weld beads cross sections is noticed that in the samples made with plasma-AC, their penetration profiles are not symmetrical, especially for the distance between torches of 10 mm (Figure 6.9). This behavior is due to the alternating magnetic deflection observed between the welding arcs, who disrupts the molten pool and the metal transfer. On the other hand, in the samples with plasma-DC this defect is not strong and, as was observed in Figure 6.5, the magnetic deflection is unidirectional, making the arc and the molten pool more stable in comparison with plasma-AC. The increase in the arc length or reduction in the stick-out, it is also a possibility, due to its influence in the momentum of the drop detached from the wire-electrode during the metal transfer [6, 52].

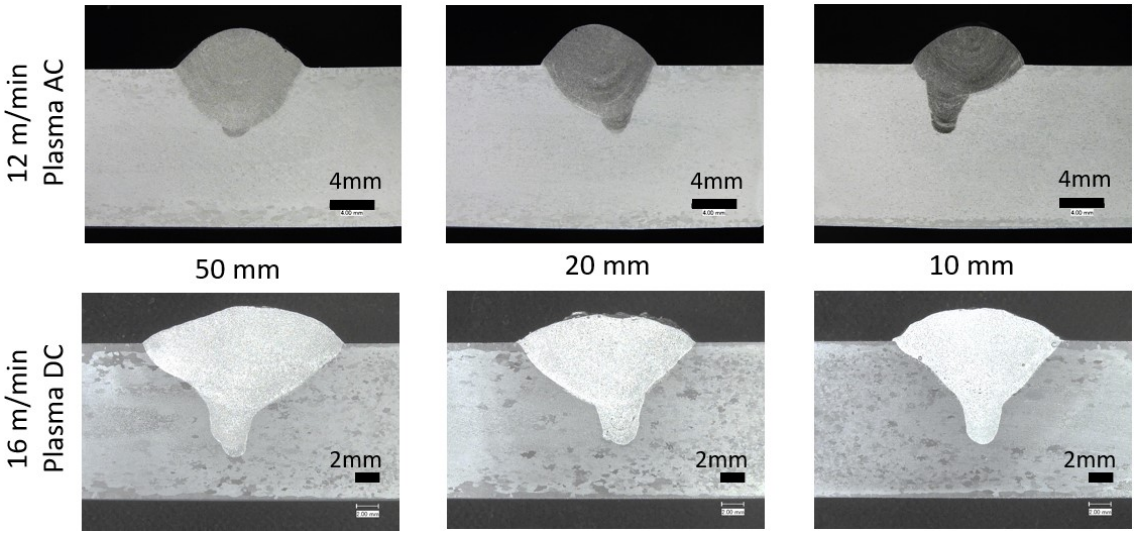

Figure 6.9 – Cross sections of the weld beads for plasma process with direct and alternating current for different distances between welding torches. Plasma AC: 150 A; Plasma DC: 100 A.

Querschnitte der Schweißraupen für den Plasmaprozess mit Gleich- und Wechselstrom für unterschiedliche Abstände zwischen Schweißbrennern. Plasma-AC: 150 A; Plasma DC: 100 A.

The Figure 6.10 and Figure 6.11 show that the coupling of plasma and MIG processes do not have a strong influence on the penetration of the weld beads. The weld beads made with plasma-AC had a penetration dispersion of 0.9 mm with no clear tendency to increase. Conversely, the samples made with plasma-DC had the tendency to reduce the penetration, around 1 mm. The arc deflection produced by the plasma with AC and DC explains the behavior in the penetration. With alternating current, the instability in the molten pool and the welding arcs produce irregular penetration profiles. While, the reduction in the penetration in plasma-DC is explained due to the increase in the permanent magnetic blow for shorter distances between the torches, which produces a reduction in the arc power towards the base material. The reduction in the current flowing to the base material was noticed by SLV München [3] and Kanemaru et al. [14], mentioning that formation of the current path between the welding arcs is responsible for this loss of current.

The coupling of the welding arcs did not influence the reinforcement of the weld beads, for both types of plasma currents. The width of the beads had a tendency to decrease its value, in plasma AC and DC, which could indicate a constriction of the welding arc, producing a narrow and long molten pool. The width dispersion (1.4

mm) in plasma-AC, is explained by the non-symmetric profile observed in Figure 6.9 produced by the arc deflection.

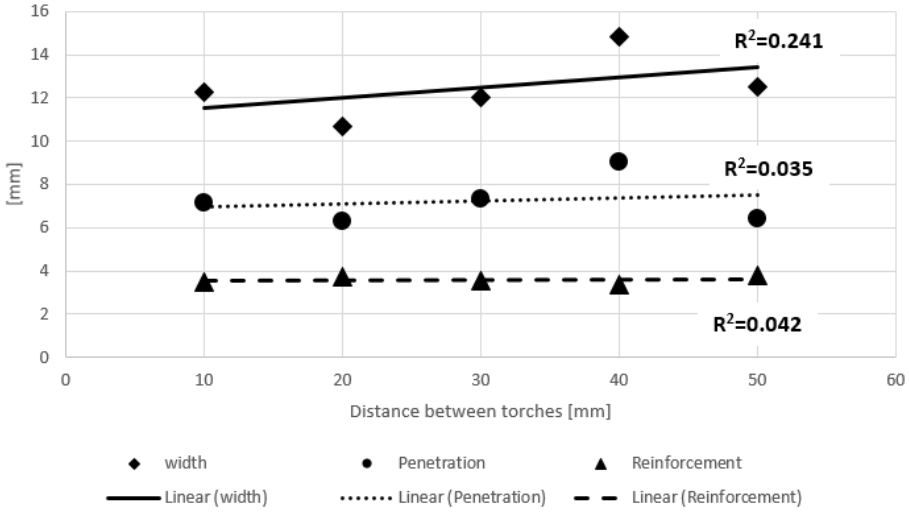

Figure 6.10 – Weld bead penetration, width and reinforcement for different torch distances with 12 m/min of wire feed speed and 150 A of plasma-AC.

Einbrand, Breite und Überhöhung der Schweißraupen für verschiedene Brennerabstände mit 12 m/min Drahtvorschubgeschwindigkeit und 150 A Plasma-AC.

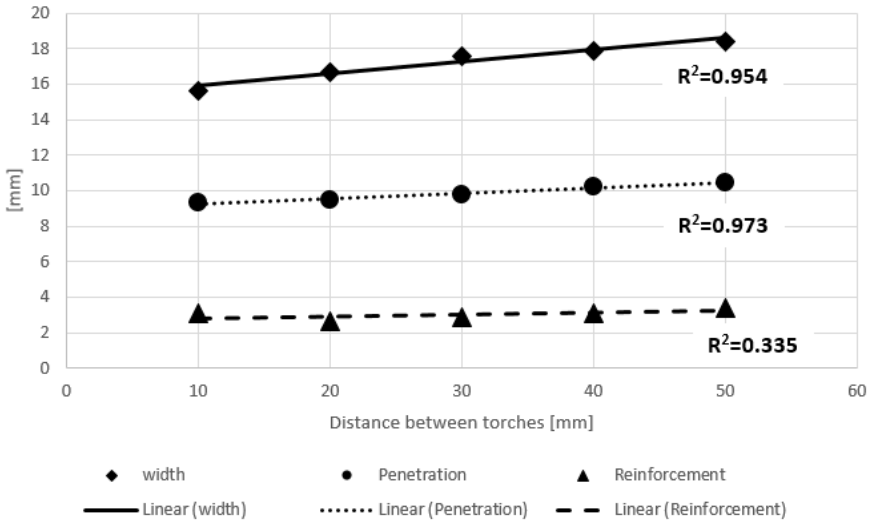

Figure 6.11 – Weld bead penetration, width and reinforcement for different torch distances with 16 m/min of wire feed speed and 100 A of plasma-DC.

Einbrand, Breite und Überhöhung der Schweißraupen für verschiedene Brennerabstände mit 16 m/min Drahtvorschubgeschwindigkeit und 100 A Plasma-DC.

Coupling the plasma and MIG processes was expected to obtain a significant increase in penetration, while as observed in Figure 6.10 and Figure 6.11 the penetration tends to decrease, which is explained by the strong interaction between the welding arcs. Temperature measurements of the molten pool, made according to the procedure described in subchapter 4.2.4, show that temperature for a torch distance of 20 mm is 52.6 °C higher than for a distance of 50 mm (Figure 6.12). Wu et al. [6] show that the maximum temperature in the paraxial hybrid plasma-MIG process was close to the MIG zone (2489 K), while the lowest was close to the plasma process in steel alloy. Thus, as the heat in the weld pool is transported from the high-temperature region to the low-temperature region, the molten metal temperature near the MIG process decreases, in comparison with the temperature of a single MIG process (2584 K). Moreover, the MIG arc expanded and the current density decreased because of the formation of the current path between the plasma and MIG processes. Therefore, the MIG heat transported to the weld pool decreased. Wu et al. [6] concluded that all the mechanism (arc interaction, droplet and keyhole) promoted the fluid flow and heat transfer in the weld pool and, therefore, decreased the weld pool temperature. On the other hand, Han et al. [7] mentioned that the paraxial hybrid plasma-MIG process with alternating current had a higher temperature than the single MIG process, however, it was noticed that the penetration was influenced by one of the welding processes (plasma or MIG) when its energy is too large in comparison to the other. Therefore, the penetration in the hybrid process depends strongly on the pressure that the arcs can generate on the molten pool [7], because the heat is strongly dissipated by the Marangoni effect [6], which is more intense in the aluminum and its strong heat transfer coefficient.

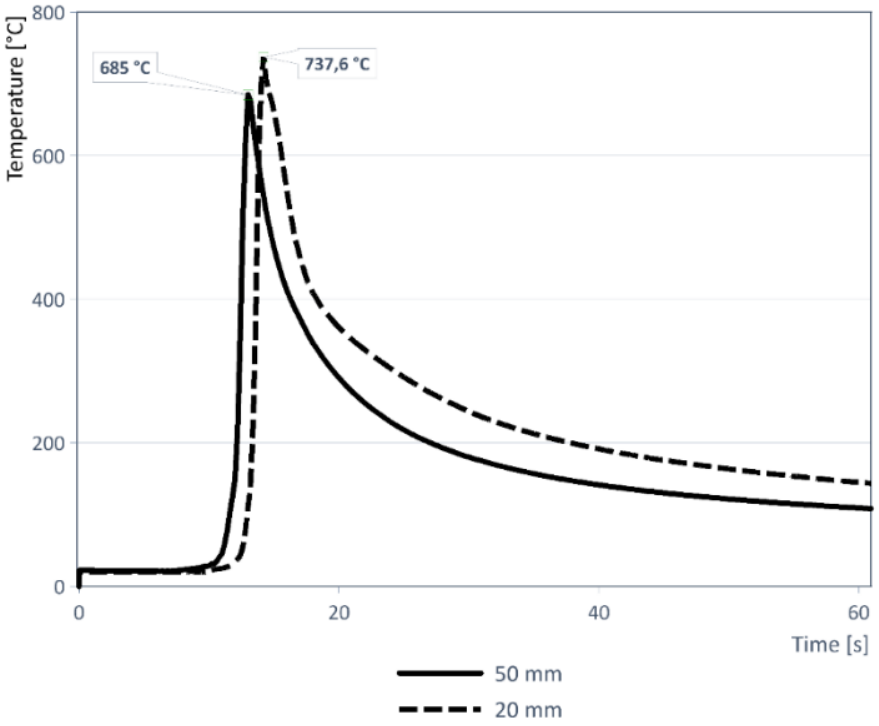

Figure 6.12 – Temperature measurement of the paraxial hybrid plasma-MIG process for 50 and 20 mm distances between torches. Plasma DC: 100 A; MIG wire feed speed: 16 m/min.

Temperaturmessung der Hybridprozess-Plasma-MSG-Einzelbrenner für Abstände von 50 und 20 mm zwischen Brennern. Plasma DC: 100 A; MSG-Drahtvorschubgeschwindigkeit: 16 m/min.

6.1.1 Conclusions

The coupling between the plasma and MIG process is possible, although the interaction between them depends on the type of current that the plasma process uses. The study of the interaction between the arcs through high-speed videos, revealed the formation of a current path between the arcs of each welding process for distance between torches lower than 25 mm. In the case of the plasma-AC configuration, this current path was not constant due to the polarity change. The coupling of the welding arcs produced a voltage drop in the plasma process, while in the MIG process a tendency to increase the welding current was observed. This due to the current flow that allows the established path between the arcs, which is formed by the metallic vapors that reduce the ionization potential of the shielding gas. It is proposed also that the arcs deflection could produce this change in the voltage and current measurements.

It is concluded that the use of alternating current in the plasma process when coupled with the MIG process is not necessary to weld aluminum alloys. No differences on the quality of the weld beads made by plasma DC or AC configuration were observed. The explanation lies in the fact that the cathodic cleaning is carried out by the MIG process, while the plasma process preheats the base material.

In general, the hybridization between the plasma and MIG processes showed good stability, although the penetration did not show significant changes while the distance between the welding torches was closer. In the next chapter, the influence of each welding process and its parameters on the stability and penetration of the paraxial hybrid plasma-MIG process will be studied in detail. Although it was concluded that the plasma-AC process does not have an influence on the weld beads, this variant will continue to be studied to determine its influence on the current path. Furthermore, based on the results of this chapter, a torch distance of 20 mm was found to be the most appropriate for the next chapters of the investigation, due to the low possibility of contamination of the plasma constriction nozzle and to offer the same properties as for smaller torch distances.

6.2 Influence of the welding current on the hybrid process

In this chapter the plasma current will be gradually increased while the MIG process parameters remain constant. The aim is to observe how each welding process influences the formation of the current path, as well as its influence on the penetration and stability of the welding process. On the other hand, the MIG process will be tested with spray (MIG-Standard) and pulsed (MIG-Pulsed) metal transfer.

6.2.1 Plasma direct current

6.2.1.1 MIG-Standard process

The pressure and temperature of the arc on the base material increases when the welding current rises, which favors the weld bead penetration. When the plasma current is increased the penetration of the hybrid process is enhanced, as shown in Figure 6.13. However, the finger shape penetration, typical of the MIG process, is strongly heightened. This behavior was observed for 12 m/min and 16 m/min of wire feed speed, although with 16 m/min the finger shape was maximized.

The Figure 6.14 shows that the weld beads penetration increased by 57% when a plasma current of 200 A was used with 16 m/min of wire feed speed, in comparison with the penetration by a single MIG process. In addition, with plasma current over 200 A the penetration stopped its enhancement, due to the instabilities observed during the coupling of the welding arcs. For 12 m/min of wire feed speed this behavior was stronger and no differences were observed in the penetration after 100 A. However, the weld bead penetration with 12 m/min increased around 127% when the plasma current was set up in 100 A. For both wire feed speed the linear regression had a good adjustment, with correlation coefficient of 0.93 for 16 m/min and 0.77 for 12 m/min. Gao et al [11] reached similar results using the hybrid plasma-MIG process on 5083 aluminum alloy, the penetration depth increased gradually with the increase of plasma current, due to its strong arc stiffness, reaching the complete penetration on a plate of 6 mm thickness with 110 A.

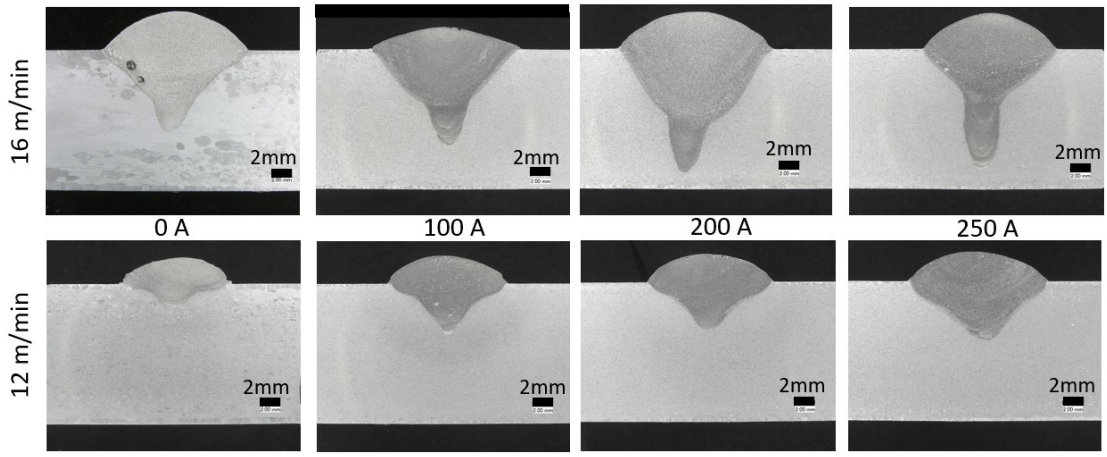

Figure 6.13 – Weld beads cross sections for different plasma currents with 16 m/min and 12 m/min of wire feed speed.

Schweißraupenquerschnitte für unterschiedliche Plasma-Gleichstromintensitäten mit 16 m/min und 12 m/min Drahtvorschubgeschwindigkeit.

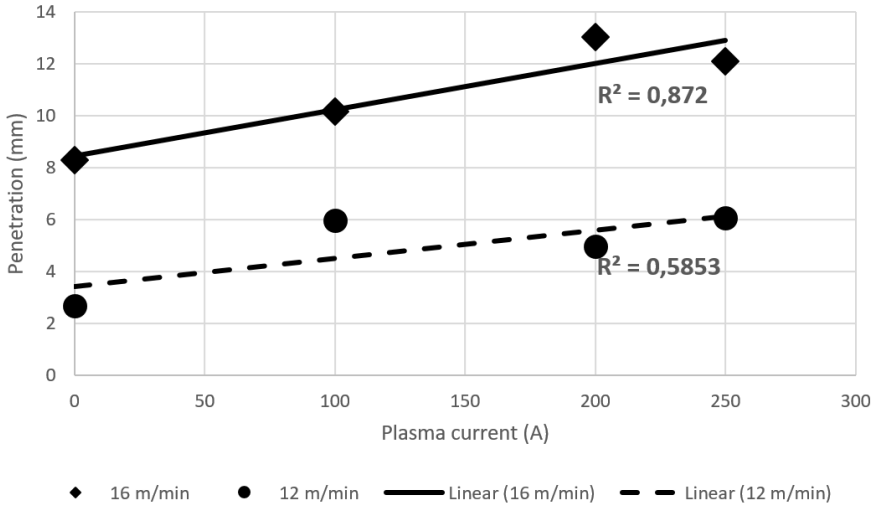

Figure 6.14 – Influence of the plasma direct current on the weld bead penetration for 16 m/min and 12 m/min of wire feed speed.

Einfluss der Plasma-Gleichstromintensitäten auf die Einbrand für 16 m/min und 12 m/min Drahtvorschubgeschwindigkeit.

In the previous chapter, where the coupling of the plasma and MIG processes were studied, an increase in penetration was not observed as the torches approached (Figure 6.10). However, in Figure 6.14 it shows a clear tendency to increase the penetration while the plasma current is higher, compared to a single MIG process. This difference between the results of both chapters is due to while the bigger is the plasma current, the bigger is the heat input and arc pressure towards the base material and, therefore, greater penetration is achieved. In addition, Figure 6.10 demonstrates that even with torch distances of 50 mm, the plasma process preheats the base material, which helps in increasing the penetration, without the problems of magnetic deflection. The studies conducted by Liang et al. [53, 54] demonstrate that with 30 mm distance between the TIG and MIG torches, the preheating effects of the TIG process are enough to increase the wettability and penetration of the weld beads. Therefore, the reason for the non-increase in penetration depth in the previous chapter was that the preheating advantage of the hybrid process was being used, even for torch distances of 50 mm.

With 16 m/min the weld bead width has not significantly changed, the standard deviation was 1.1 mm and the linear regression shows a low adjustment level, with a correlation coefficient of 0.02 (Figure 6.15). For 12 m/min, the width tendency is to increase with the plasma current, with a standard deviation of 1.5 mm and a

correlation coefficient of 0.95. The different behavior in widths for each wire feed speed is because the molten pool temperature with 12 m/min is influenced by the plasma process, which produces a reduction of the superficial tension of the molten pool, increasing the wettability of the weld bead and, therefore, the weld bead width. For 16 m/min, the plasma process has not had a strong influence in the molten pool temperature, due to the arc energy and temperature produced by the MIG process with this high wire feed speed, that overpasses the energy that the plasma process can supply. Similar explanation was described by Kanemaru et al. [13] with the hybrid TIG-MIG process, concluding that in configurations with MIG current superior than TIG current, the benefits of TIG process are not exploited.

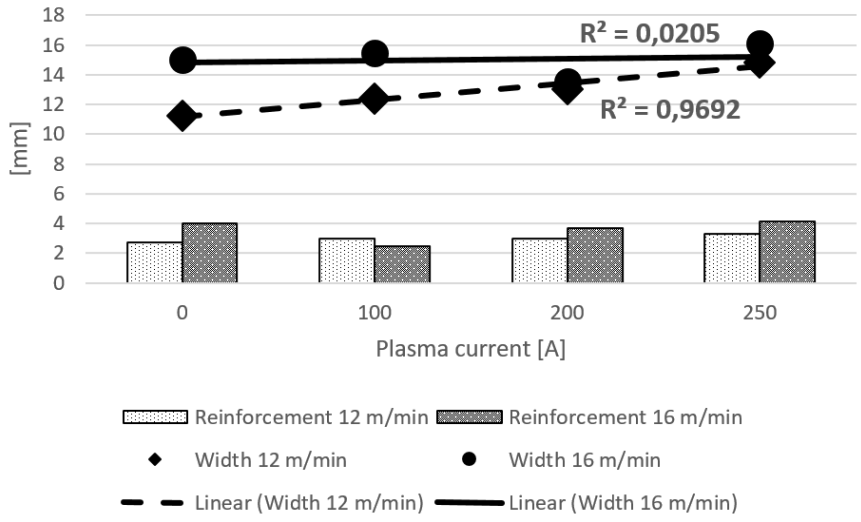

Figure 6.15 – Influence of the plasma current on the weld bead width and reinforcement for 16 m/min and 12 m/min of wire feed speed.

Einfluss des Plasmastroms auf die Schweißraupenbreite und -überhöhung für 16 m/min und 12 m/min Drahtvorschubgeschwindigkeit.

Comparing the cross sections in Figure 6.13 and geometric measurements Figure 6.15, it is observed how relevant the plasma process is to the penetration in the weld bead, however, this one does not influence its reinforcement and width. This phenomenon is explained by the keyhole established by the plasma process, who removes material from the base material and it is placed behind of the plasma process molten pool, this removed material is after re-melted by the MIG arc and added finally to the molten pool (Figure 6.16). Therefore, the plasma process is digging with the keyhole while the MIG process is filling the hole, thus the

reinforcement and width of the weld bead depend mainly on the MIG process and its wire feed speed.

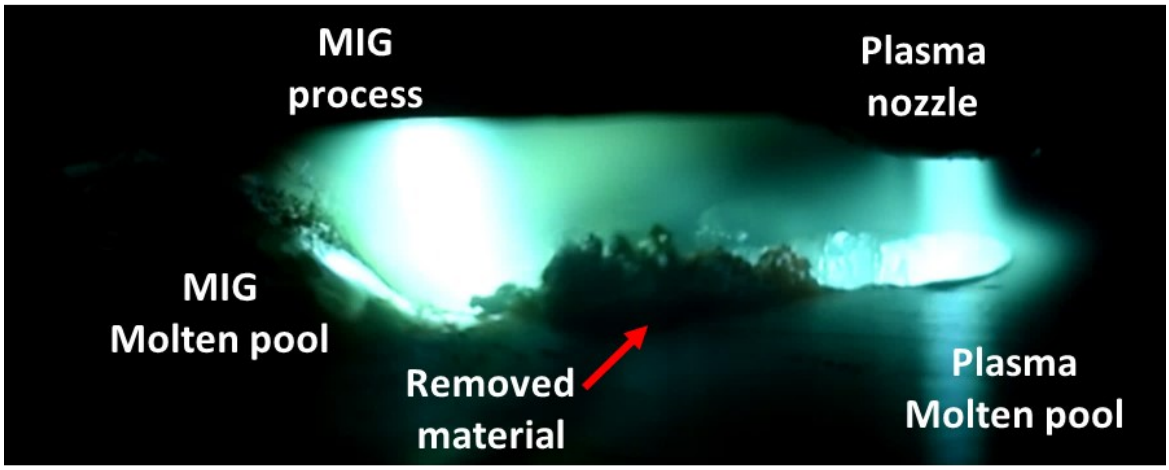

Figure 6.16 – Molten pool behavior of the hybrid process with a plasma current of 250 A and 16 m/min wire feed speed.

Verhalten des Hybridprozesses im geschmolzenen Pool mit einem Plasmastrom von 250 A und einer Drahtvorschubgeschwindigkeit von 16 m/min.

Analyzing the electrical signals of the MIG process, it is noticed that the voltage was not affected until 200 A of plasma current (Figure 9.6), with higher currents the interaction between the arcs became the MIG process unstable. On another hand, the MIG current signal was influenced by a 300 A of plasma current (Figure 6.17), showing erratic behavior and with a tendency to establish a rotating spray metal transfer.

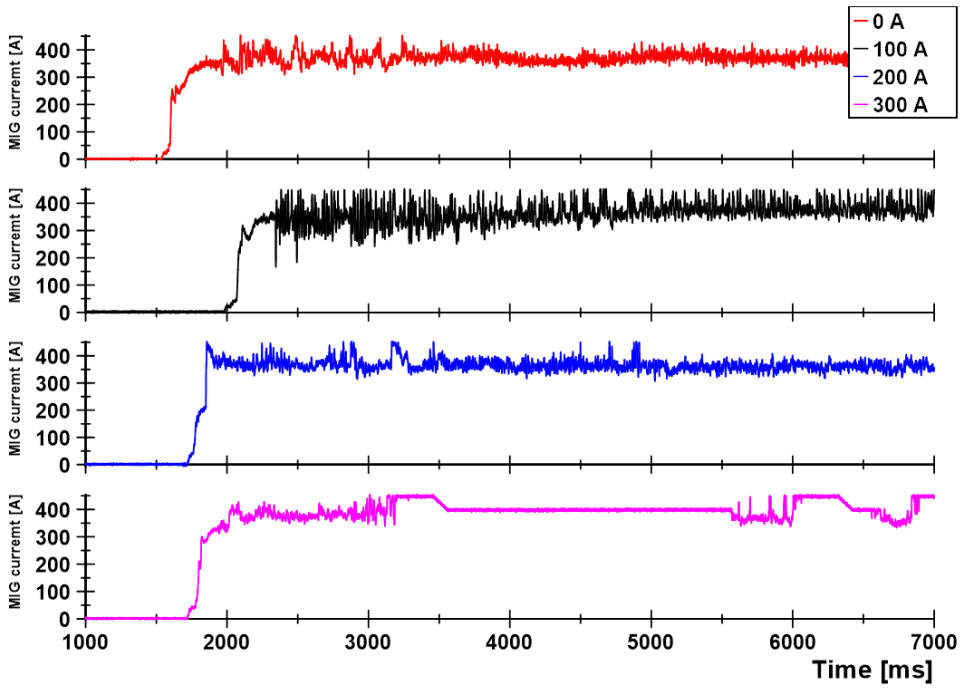

Figure 6.17 - MIG current for different plasma currents. MIG wire feed speed: 16 m/min.

MSG-Strom für verschiedene Plasmaströme. MSG-Drahtvorschubgeschwindigkeit: 16 m/min.

As plasma current increased, the average MIG current was influenced, although only for wire feed speeds greater than 12 m/min (Figure 6.18). With a wire feed speed of 16 m/min, MIG current increased by 20 A in comparison with a single MIG process, following a linear tendency with a correlation coefficient of 0.63 and standard deviation of 13.7 A. For wire feed speeds of 12 m/min and 8 m/min, the correlation coefficients are 0.14 and 0.29 respectively, denoting a low linear adjustment or that the plasma current has not an influence on the MIG current for these levels of wire feed speeds. The average MIG voltage measurements for the different wire feed speeds show a low level of variability, 0.6 V (16 m/min), 0.4 V (12 m/min) and 0.3 V (8 m/min) (Figure 9.7).

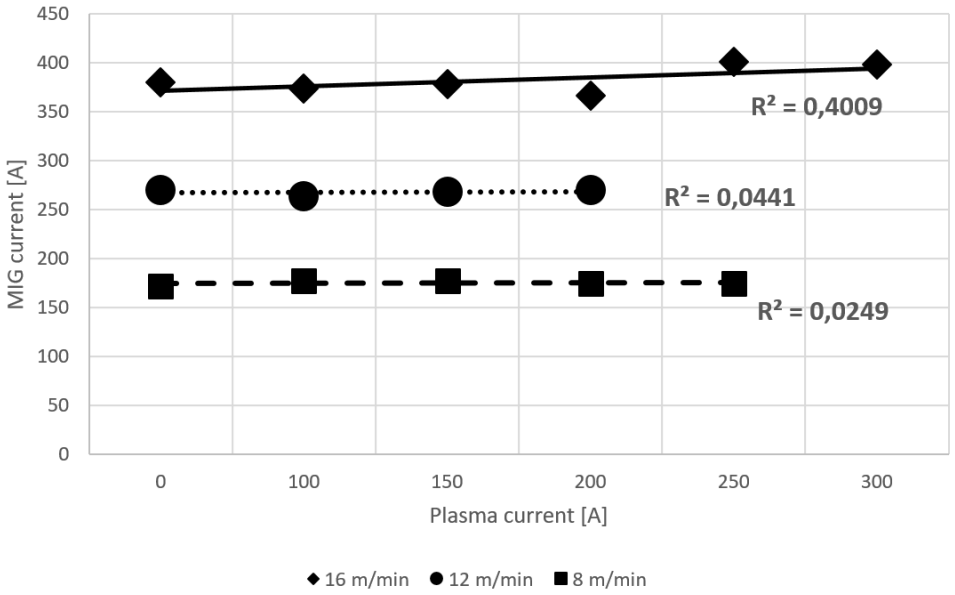

Figure 6.18 – Influence of the plasma current on MIG process current.

Einfluss des Plasmastroms auf den MSG-Prozessstrom.

The high speed video images with the influence of the plasma current on the hybrid process is shown in Figure 6.19, observing that as the plasma current rises, the arc length of the MIG process increases significantly. Measurements of the arc length are presented in Figure 6.20, showing a linear tendency to rise the MIG arc length when the plasma current increases. This behavior was also noticed by Wu et al [6], however, it was just to comment the phenomenon and not the complete relationship between the MIG arc length and the plasma current.

The establishment of the current path between MIG and plasma arcs was noticed, which becomes stronger while the plasma current increases. However, the stability between the welding arcs is compromised when the plasma current is greater than 200 A, observing a strong repulsion between both arcs. Similar behavior was commented by several authors [7, 11, 13, 14, 55] with paraxial hybrid plasma-MIG and TIG-MIG processes. Kanemaru et al. [13] and Han et al. [7] observed the instabilities when the plasma current is higher than MIG current, this happened also in the other way. In the situation of the TIG-MIG process, Kanemaru et al. [13] suggest that the TIG current needs to be greater than the MIG current for arc stability, then, increasing TIG current, increases the penetration depth. It is also observed that for plasma currents over 200 A the base material is being removed and placed beside the keyhole formed by the plasma process, this material is re-

melted again by the MIG process. For plasma current over 250 A was noticed that the material is expelled by the plasma arc due to the excessive arc pressure and the unstable interaction with the MIG arc.

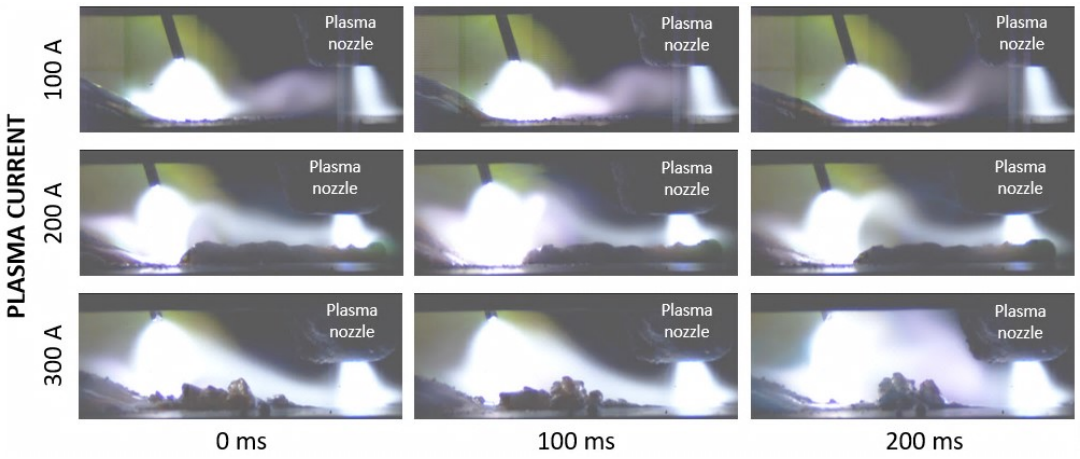

Figure 6.19 – MIG process behavior for different plasma current. MIG wire feed speed: 16 m/min; torch distances: 20 mm.

MSG-Prozessverhalten für unterschiedliche Plasmastromintensitäten. MSG-Drahtvorschubgeschwindigkeit: 16 m/min; Brennerabstände: 20 mm.

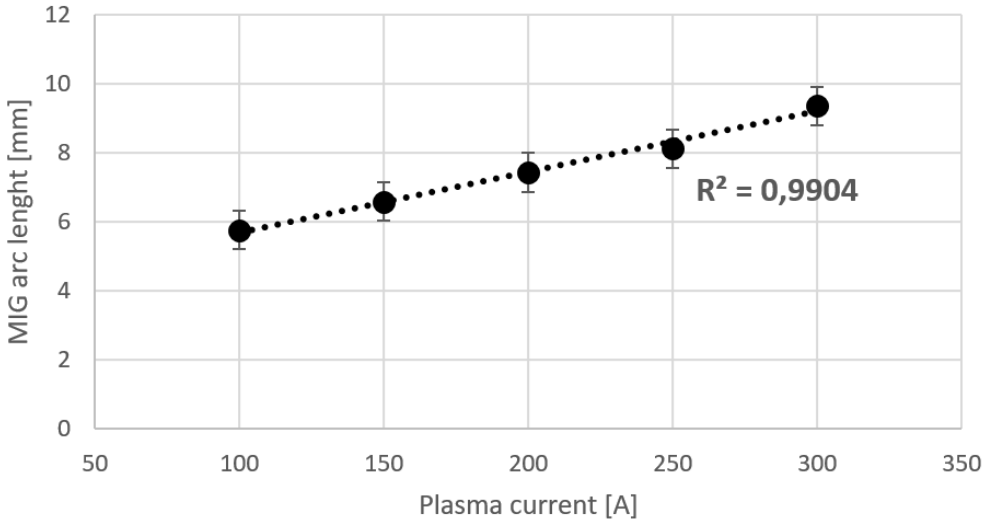

Figure 6.20 – MIG arc length for different plasma current. MIG wire feed speed: 16 m/min; torch distances: 20 mm.

MSG-Lichtbogenlänge für unterschiedliche Plasmastromintensitäten. MSG-Drahtvorschubgeschwindigkeit: 16 m/min; Brennerabstände: 20 mm.

The self-regulation arc length of the MIG-Standard process is based in that while the distance between MIG torch and base material increases, MIG current decreases, however the voltage and the wire feed speed are keep constant, with

which the wire feed speed becomes greater than the melt speed of the wire-electrode. Then, the tip of the wire-electrode approaches the base material again, progressively reducing the arc length. This reduction is also followed by a progressive increase in the MIG current, returning to the original state before increasing the distance between the MIG torch and the base material [1]. However, in this investigation the behavior is completely different, the MIG current increases when the arc length is longer (Figure 6.18 and Figure 6.19). This behavior can be explained by the current path, which provides an extra current to the MIG process, while the voltage and wire feed speed are maintained constant (Figure 9.6). This means an increase in the melting speed of wire-electrode, causing an increment in the MIG arc length because the self-regulation system has reached a new equilibrium point. Figure 6.21 proposes a new way of understanding the behavior of the self-regulation arc length of the MIG process when it is coupled with the plasma process in hybrid form. The scheme explains that by increasing the plasma current from I_{P1} to I_{P2}, the MIG current I_{M1} will be influenced by raising its value to I_{M2}, whereby the melting speed of the wire-electrode will exceed the wire feeding speed, displacing the static curve of the MIG arc a1 towards position a2. For higher plasma current values (I_{P3}), the behavior described above is stronger. This behavior is for constant wire feed speed and voltage.

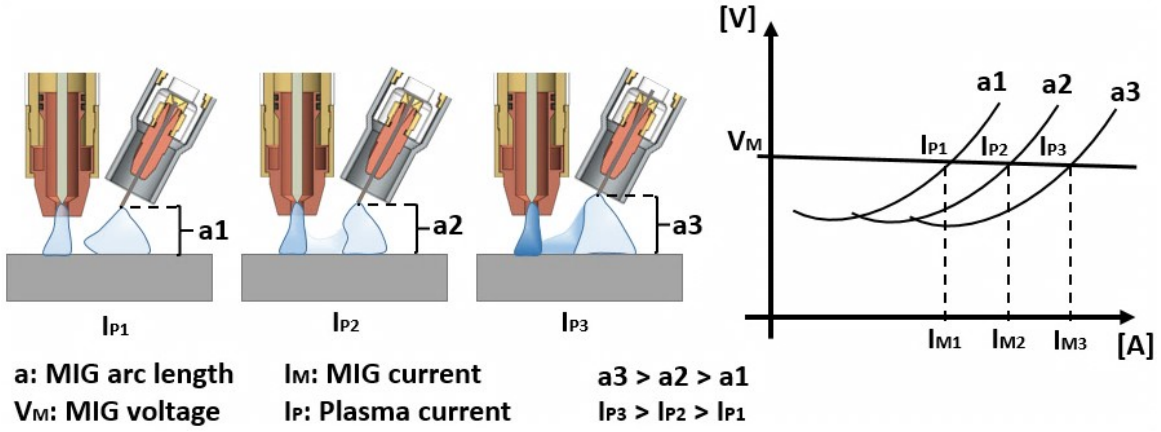

Figure 6.21 – Illustration of the phenomenon of internal control of MIG-Standard process during the paraxial hybrid plasma-MIG welding process.

Darstellung des Phänomens der internen Kontrolle des MSG-Standard-Prozesses während des paraxialen Plasma-MSG-Hybridschweißprozesses.

The Figure 6.22 shows the current-voltage characteristics curves of the MIG process, noticing that the MIG voltage does not change significantly when the plasma current increases, however, when both welding processes work with currents above 200 A, the excessive repulsion between the welding arcs causes strong instabilities in the hybrid welding processes. Furthermore, with higher current configured in both welding processes, more metal vapors are released in the shielding gas and, therefore, the MIG voltage has the tendency to decrease. In the simulation and experimental studies with the TIG-MIG hybrid process made by Kanemaru et al. [13, 14], it was demonstrated that during the interaction between the MIG and TIG arcs the current path is established, influencing the thermal efficiency of the hybrid welding process and inducing a voltage drop in the TIG process. However, no significant changes were evidenced in the MIG arc voltage, although, it is commented that it is not recommend working with high MIG currents values, due to the metal transfer tends to be unstable and will reach the rotating spray transfer [13, 14].

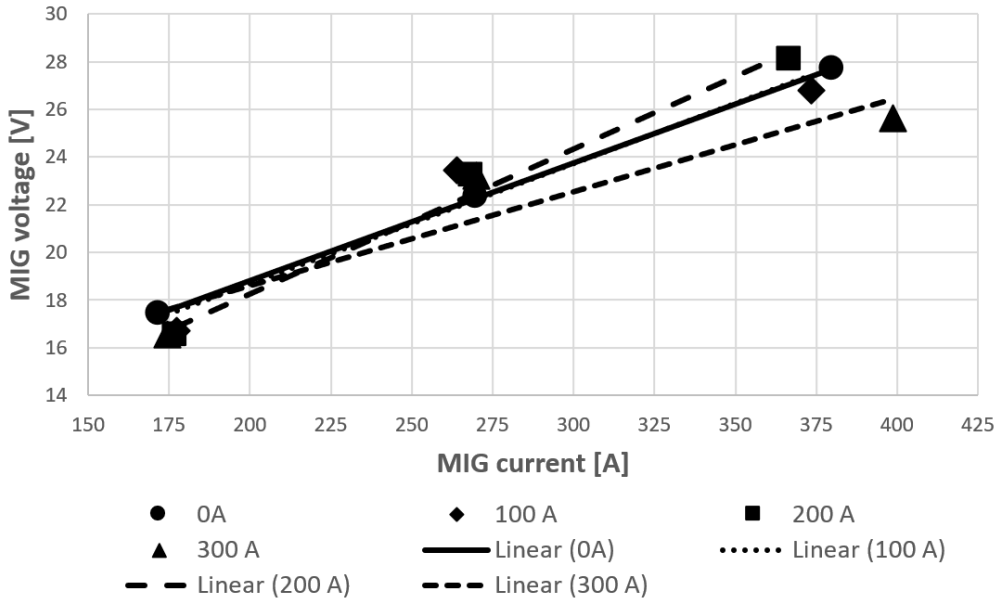

Figure 6.22 – Voltage-current characteristics of MIG process for different plasma currents. Torch distances: 20 mm.

Spannungs-Strom-Eigenschaften des MSG-Prozesses für unterschiedliche Plasma-Prozessströme. Brennerabstände: 20 mm.

Analyzing the behavior of the plasma process voltage for different wire feed speeds; a strong drop in voltage is observed (Figure 6.23). This drop in the plasma voltage

depends on the wire feed speed. Similar behavior was observed when the coupling between plasma and MIG process was studied. However, the voltage drop is diminished when the plasma current increases. The voltage drop is around 43% when a wire feed speed of 16 m/min is used, taking as reference the single plasma process with a current of 100 A (Figure 6.23). For wire feed speed of 8 m/min, the plasma voltage decreases by 23%. When plasma current is set up to 300 A, the plasma voltage drop decreases to 20%, with no large differences (standard deviation of 0.46 V) for different wire feed speeds. This behavior agrees with the explanation proposed by Kanemaru et al. [13][14], Han et al [9] and Guo et al. [11] where the main explanation is the increase in metal vapors, reducing the ionization potential and, therefore, the voltage required for maintaining the arc. The reduction of the differences in plasma voltage while the plasma current increases demonstrates that influence of the MIG process is lower while the plasma current intensity increases.

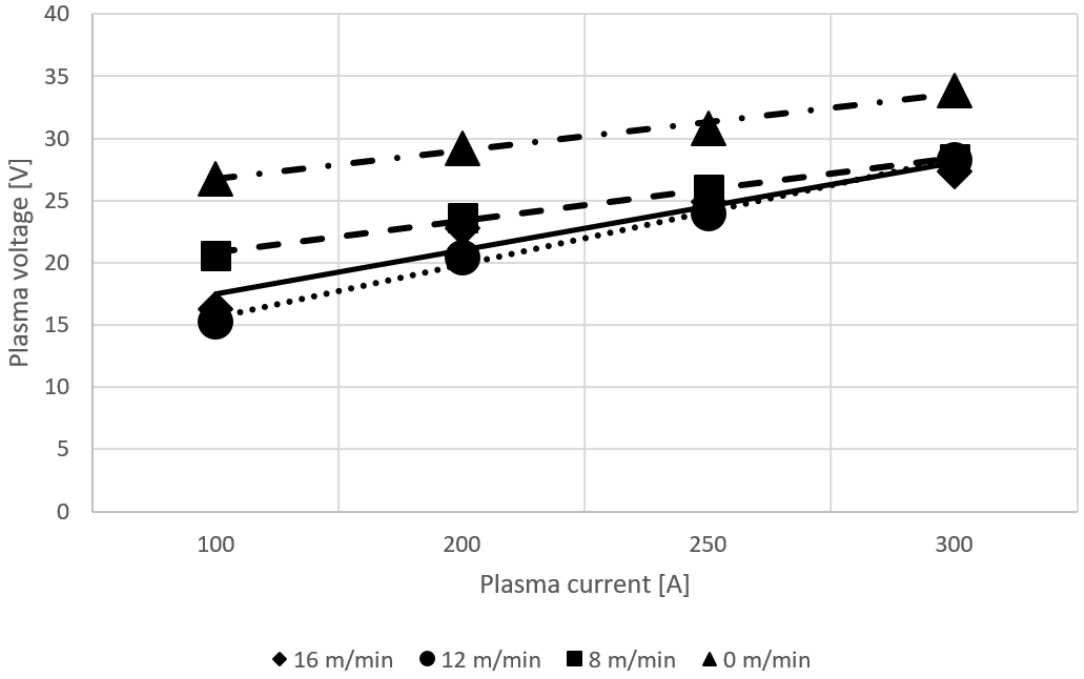

Figure 6.23 – Voltage-current curve of the plasma process for different wire feed speed with MIG-Standard.

Spannungs-Strom-Kurve des Plasmaprozesses für unterschiedliche Drahtvorschubgeschwindigkeiten mit MSG-

6.2.1.2 MIG-Pulsed process

When the plasma current is increased a similar behavior in the welding arc is observed on the MIG-pulsed and MIG-standard modes. Figure 6.24 shows voltage curves of the MIG-Pulsed process, noticing that for 300 A of plasma current the instability is significant. On the other hand, the MIG-Pulsed current signal presented some instabilities just for 300 A of plasma current, mainly because of the strong interaction between the arcs (Figure 9.8).

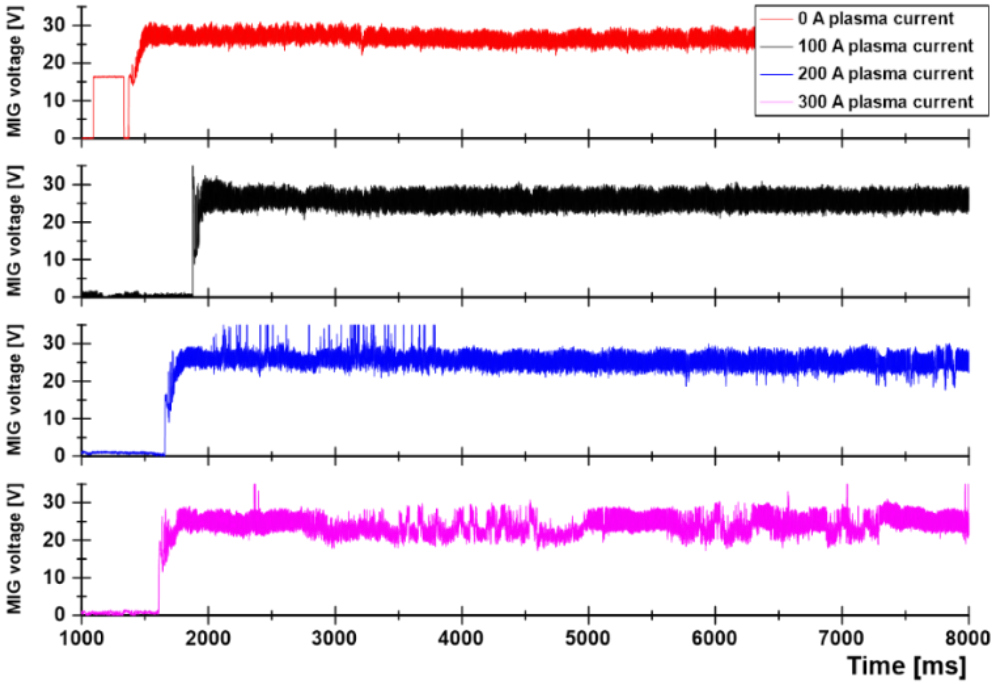

Figure 6.24 – MIG-Pulsed voltage for different plasma currents. MIG wire feed speed: 16 m/min.

MSG-Impuls Spannung für verschiedene Plasmastromintensitäten. MSG-Drahtvorschubgeschwindigkeit: 16 m/min.

The current signal histogram does not show a significant variation on its pulse and base periods when the plasma current increases, however, a defined base phase is not observed for 300 A of plasma current, indicating instability in the MIG process for that configuration (Figure 6.25b). On the other hand, the voltage histogram shows a significant variation for different plasma current, where the base period is the most influenced, with a tendency to decrease in value as the plasma current increases. This voltage behavior could mean that plasma current is influencing the arc length of the MIG process, especially in the base period, because MIG current is lower and susceptible to an arc deflection effect. Another possibility suggested, is

due to the quantity of metallic vapors produced by the hybrid process increases, influencing mainly the base period because the current is lower and, therefore, requiring less voltage to maintain the arc.

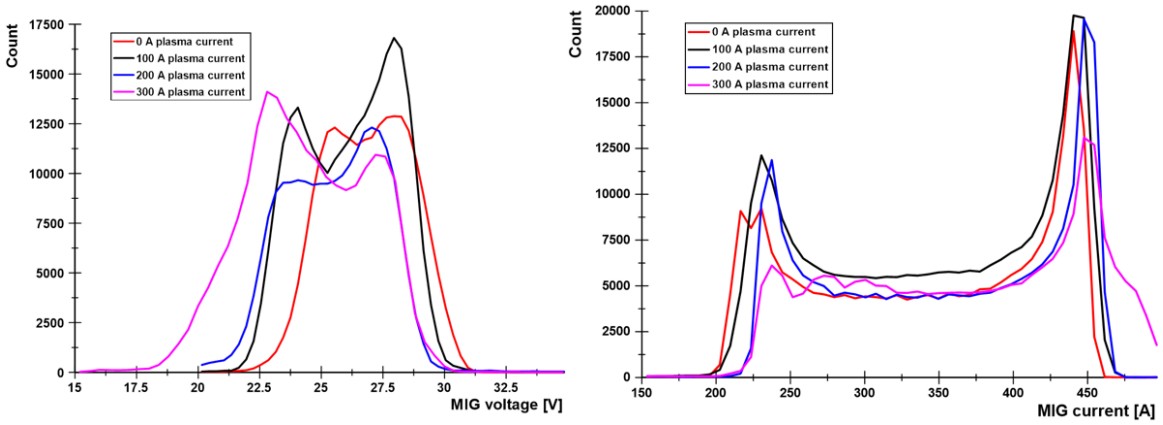

(a) (b)

Figure 6.25 – Histograms for (a) voltage and (b) current of the MIG-Pulsed for different plasma current. MIG wire feed speed: 16 m/min.

Histogramme für (a) Spannung und (b) Strom des MSG-Impuls für verschiedene Plasmastromintensitäten. MSG-Drahtvorschubgeschwindigkeit: 16 m/min.

The average voltage of the MIG-Pulsed process for different plasma currents is shown in Figure 6.26, observing a constant behavior, with standard deviations of 0.4 V (16 m/min) and 0.07 V (14 m/min). Similar pattern had the average current of the MIG-Pulsed process (Figure 6.27). This constant behavior may be due to the pulse period having a greater influence at the time of calculating the average values and, as was observed in the histograms, the pulse period had a more stable behavior than the base period. This suggests that the plasma process has no influence on the MIG-Pulsed process during the hybrid welding.

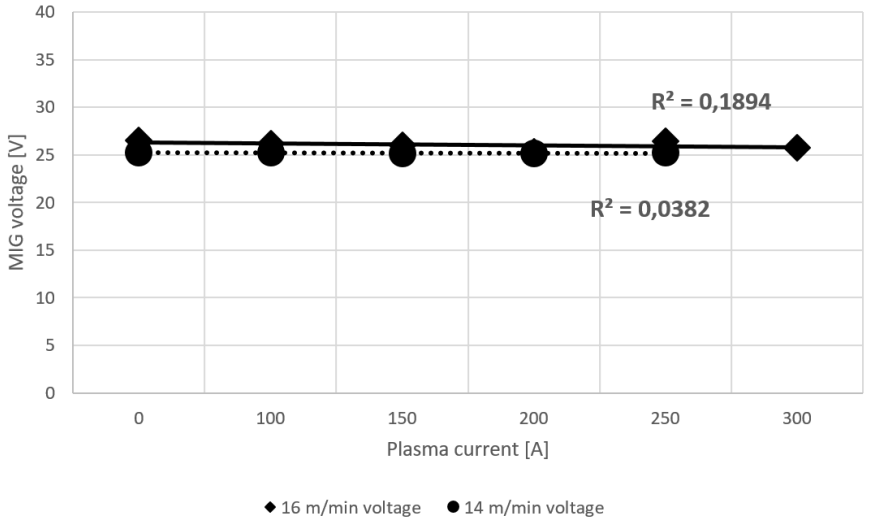

Figure 6.26 - Influence of the plasma current on MIG process voltage.

Einfluss des Plasmastroms auf die MSG-Prozessspannung.

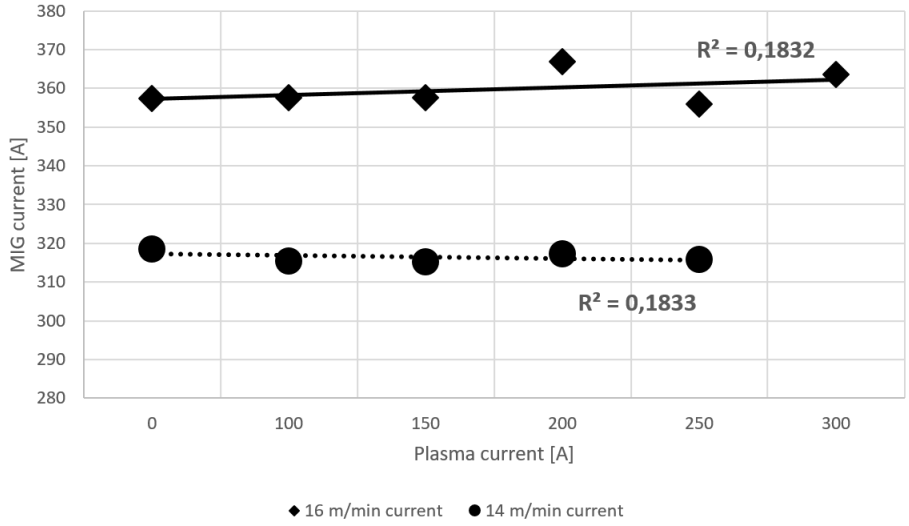

Figure 6.27 - Influence of the plasma current on MIG process current.

Einfluss des Plasmastroms auf den MSG-Prozessstrom.

Through the high-speed images presented in Figure 6.28, the establishment of the current path for all the plasma currents is observed. The repulsion between the welding arcs is visible, however, it weakens during the base periods of the MIG process, due to the lower current during this period. Figure 6.29 shows the arc length measurements for the MIG-Pulsed process, where there is no clear trend. This can be explained by the fact that during the base periods, the MIG process becomes unstable for high plasma currents, causing changes in the arc length and, therefore, influencing the final average length.

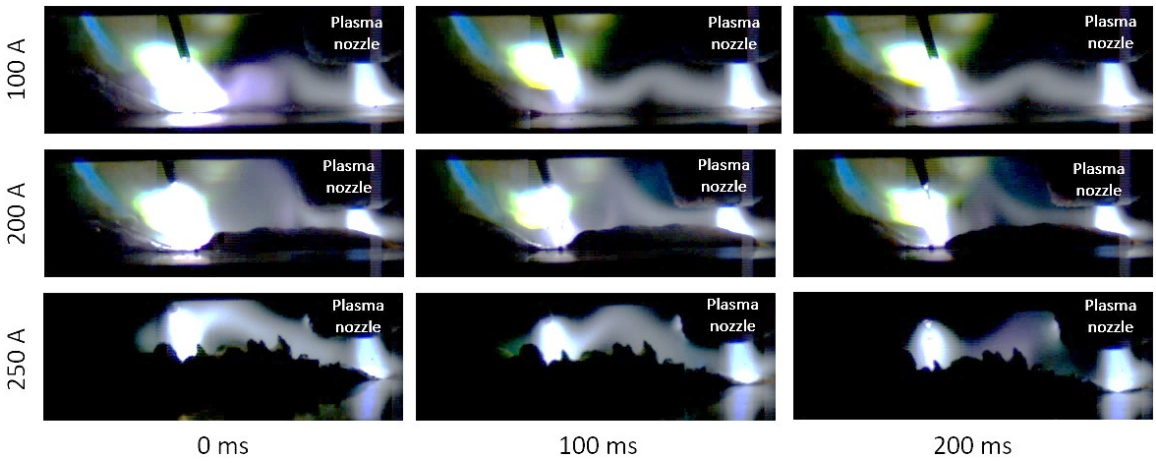

Figure 6.28 – MIG-Pulsed process behavior for different plasma currents. MIG wire feed speed: 14 m/min; torch distances: 20 mm.

MSG-Impuls Prozessverhalten für unterschiedliche Plasmastromintensitäten. MSG-Drahtvorschubgeschwindigkeit: 14 m/min; Brennerabstände: 20 mm.

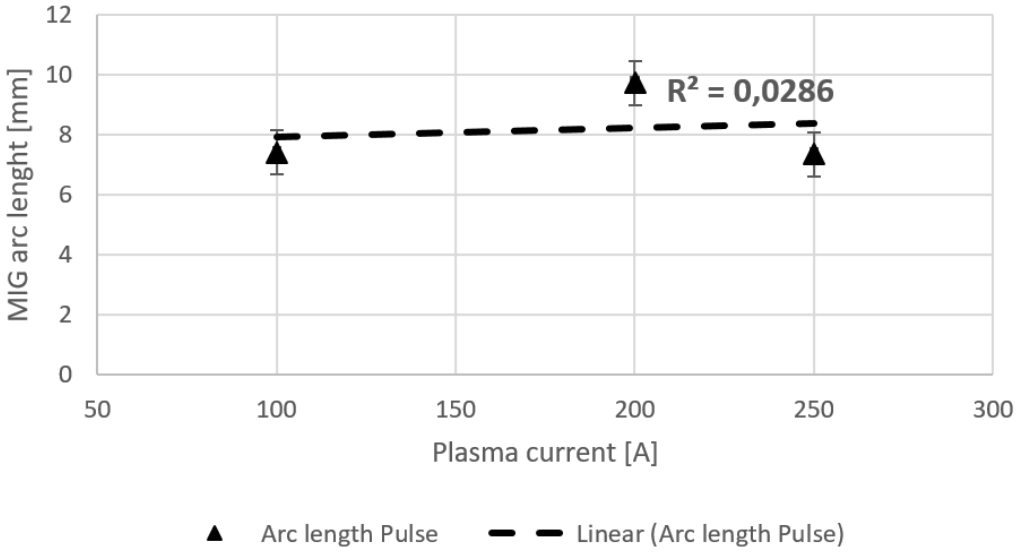

Figure 6.29 – MIG-Pulsed arc length for different plasma currents. MIG wire feed speed: 14 m/min; torch distances: 20 mm.

MSG-Impuls Lichtbogenlänge für unterschiedliche Plasmastromintensitäten. MSG-Drahtvorschubgeschwindigkeit: 14 m/min; Brennerabstände: 20 mm.

Figure 6.30 shows the cross sections for the paraxial hybrid plasma-MIG process when the plasma current increases and MIG-Pulsed is used. The penetration depth has no significant differences when the plasma current increases, the exception is for 300 A, where the penetration profile is irregular due to instability of the welding process. These instabilities appear when MIG current is configured with higher

levels than plasma process, thus, the advantages of the hybrid process are lost [7, 13]. Penetration measurements in Figure 6.31 show a maximum value of 14 mm with plasma current of 200 A. With higher plasma currents the penetration had the tendency to decrease, promoted by the instabilities between the arcs. Although the plasma current has a slight influence in the penetration with MIG-pulsed, the weld bead penetration is deeper than with MIG-Standard. This difference in penetration between pulsed and spray metal transfer is due to the high current reached in the pulse phase of the MIG-Pulsed, that is around 450 A, in comparison with the 367 A of the MIG-Standard. Although, the influence of plasma current was more significant with MIG-Standard.

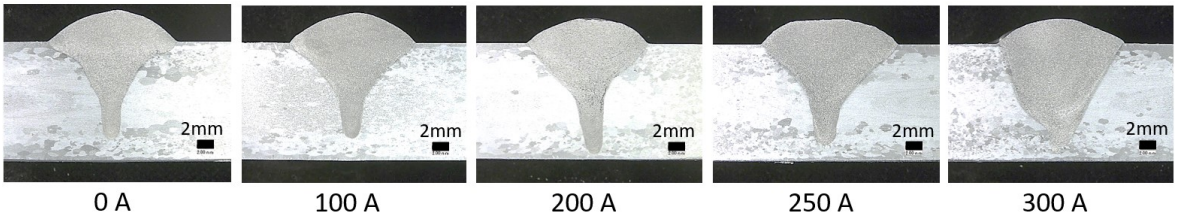

Figure 6.30 - Weld bead cross sections for different plasma currents with 16 m/min of wire feed speed with MIG-Pulsed.

Schweißraupenquerschnitte für unterschiedliche Plasmaströme mit 16 m/min Drahtvorschubgeschwindigkeit mit MSG-Impuls.

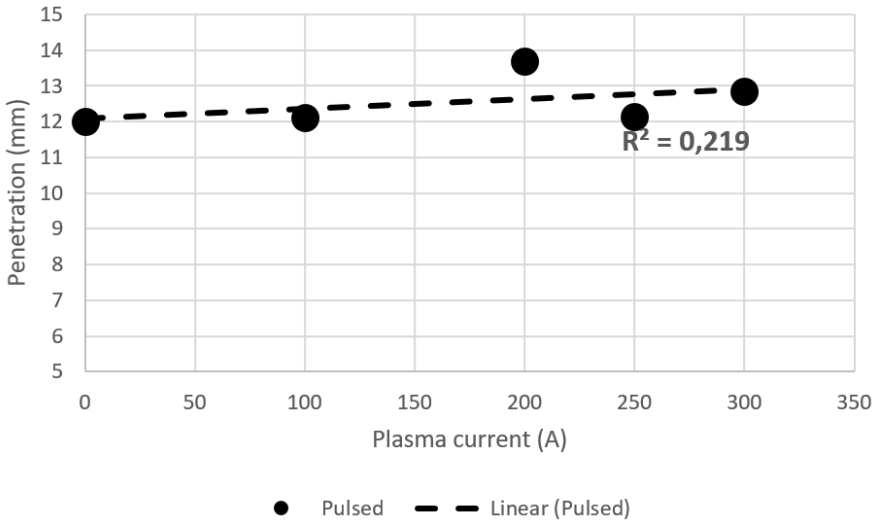

Figure 6.31 - Influence of the plasma current on the MIG-Pulsed process penetration with 16 m/min of wire feed speed.

Einfluss des Plasmastroms auf die Einbrand des MSG-Impuls-Prozesses auf 16 m/min Drahtvorschubgeschwindigkeit.

Weld beads width and reinforcement had a linear tendency without a significant influence of the plasma current, with a correlation coefficient of 0.35 and the

standard deviation is 1 mm (Figure 9.9). This behavior was similar as with MIG-Standard, where the plasma current just influences in the weld bead penetration and not in the width and reinforcement. In this case, the high current at the pulse phase has a higher effect on the penetration, however, the plasma process influence is still noticed.

Analyzing how the MIG-Pulsed process influences on the voltage-current curve of the plasma process, it is noticed that the maximum voltage drop is reached with 100 A of plasma current and the wire feed speed has no influence in the intensity of the plasma voltage drop (Figure 6.32). This behavior was expected from the previous analysis of the voltage and current, where no significant changes in the electrical signals were noticed. The voltage drop in the plasma process had the same behavior as with the MIG-Standard (Figure 6.23) and, as was explained, the drop is mainly caused by the great amount of metallic vapor, reducing the ionization potential of the shielding gas.

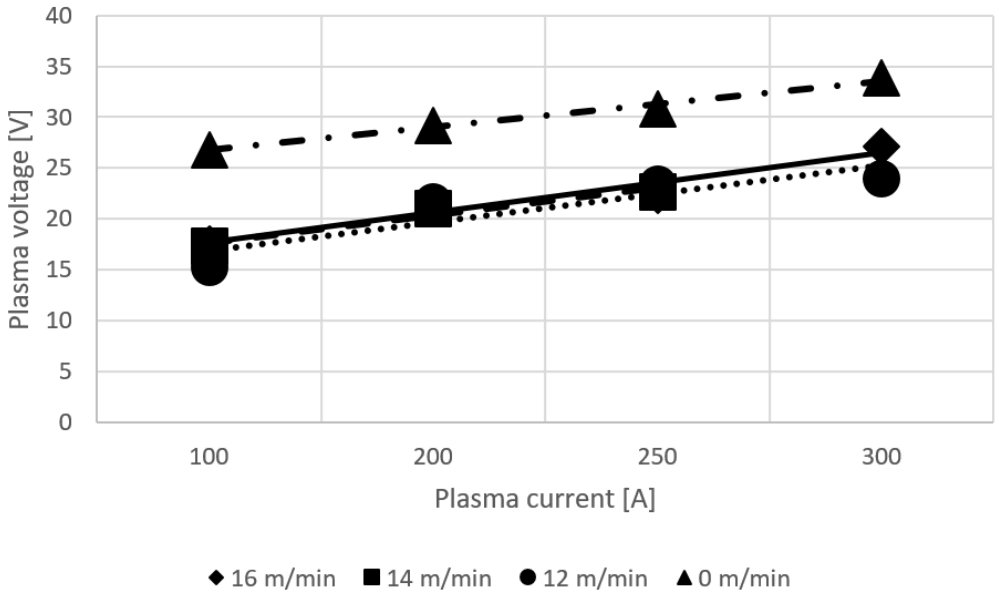

Figure 6.32 - Voltage-current curve of the plasma process for different wire feed speed with MIG-Pulsed.

Spannungs-Strom-Kurve des Plasmaprozesses für unterschiedliche Drahtvorschubgeschwindigkeiten mit MSG-

6.2.2 Plasma alternating current

6.2.2.1 MIG-Standard process

In the paraxial hybrid plasma-MIG process configured with alternating current in the plasma process is observed that the influence on penetration depth is not as strong as with direct current. Figure 6.33 shows the weld bead cross sections and porosities are observed just for the sample of single MIG process. Penetration increases with higher levels of plasma-AC, however, it is not deeper than plasma-DC. A comparison of the penetrations between plasma-AC and DC is presented in Figure 6.34, showing how the DC configuration achieves greater penetrations, although the tendency to decrease for high current plasma is the same for both.

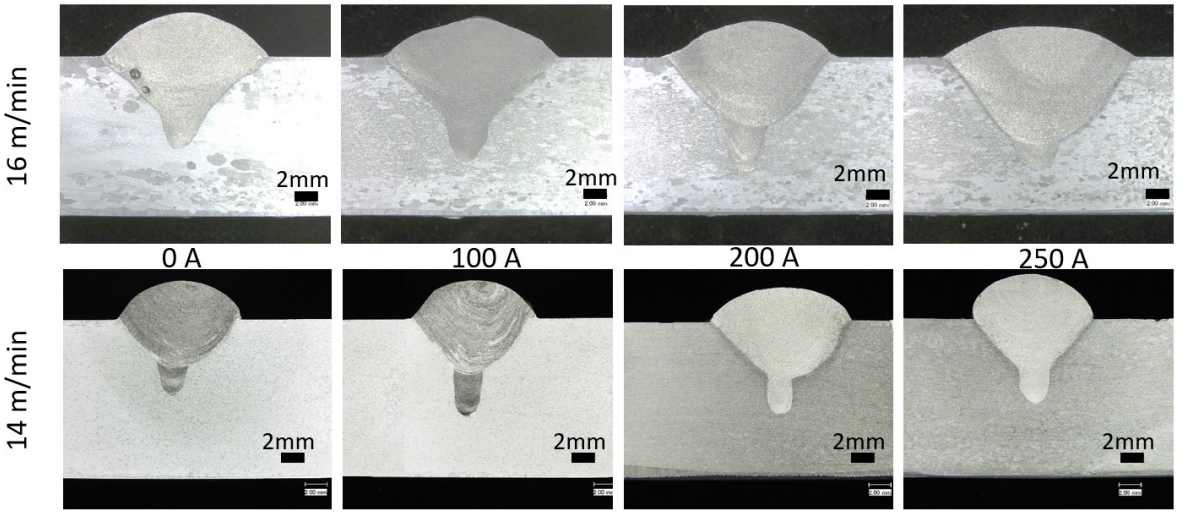

Figure 6.33 - Weld bead cross sections for different plasma alternating current intensities.

Schweißraupenquerschnitte für unterschiedliche Plasma-Wechselstromintensitäten.

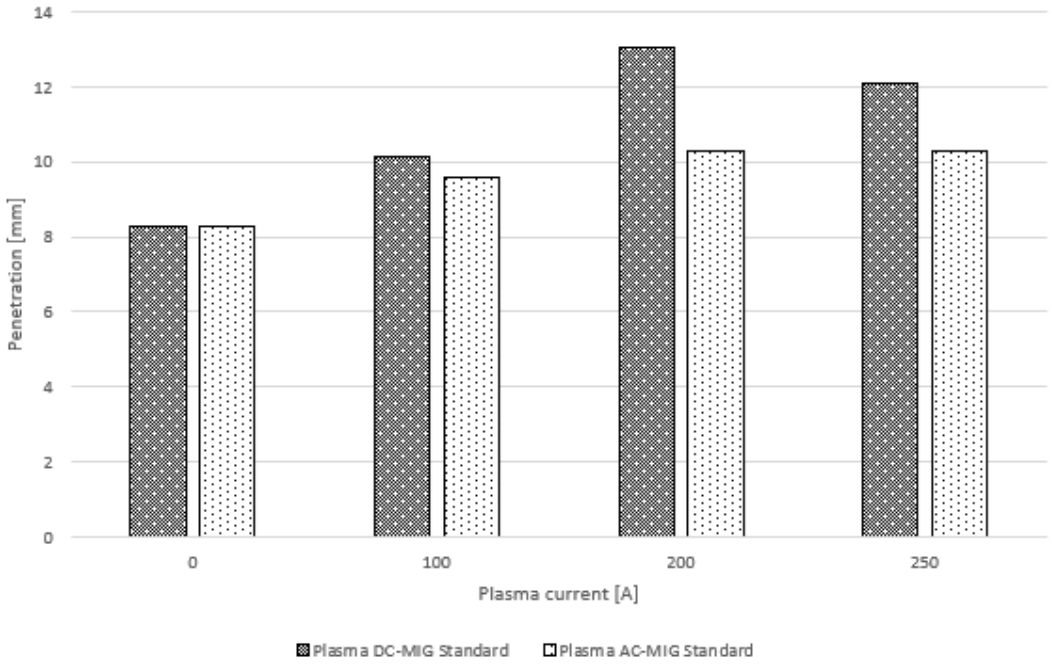

Figure 6.34 – Penetration comparison for paraxial hybrid plasma-MIG process with plasma-DC and plasma-AC. Wire feed speed: 16 m/min.
Vergleich der Einbrand für das paraxiale hybride Plasma-MIG-Verfahren mit Plasma-DC und Plasma-AC. Drahtvorschubgeschwindigkeit: 16m/min.

Comparing the penetration behavior between 16 m/min and 14 m/min wire feed speeds with plasma-AC (Figure 6.35), it observed that just for 16 m/min there is a trend towards increased penetration. With wire feed speed of 14 m/min, the penetration has not a clear tendency to increase due to the strong arc deflection, this influence in the arc pressure of the plasma arc and the metal transfer of the MIG process (Figure 6.35).

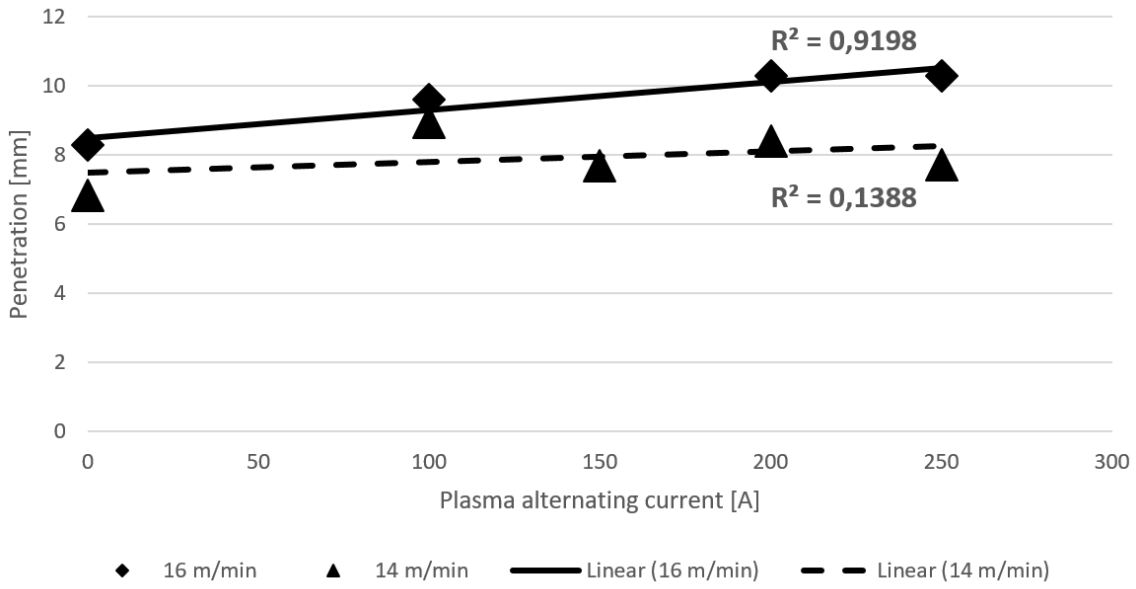

Figure 6.35 – Influence of the plasma-AC on the weld bead penetration for different wire feed speed.

Einfluss des Plasma-AC auf die Einbrand bei unterschiedlicher Drahtvorschubgeschwindigkeit.

Weld beads width for 16 m/min of wire feed speed have a direct correlation to increase with plasma-AC (Figure 6.36). With 14 m/min the weld beads width and reinforcement have not a clear tendency, mainly due to instabilities in the arc. For 16 m/min the reinforcement is reduced when the plasma-AC is raised, this behavior is explained with the increase of the weld beads width, which is due to the increase in arc length caused by the current flow permitted by the current path between the welding processes.

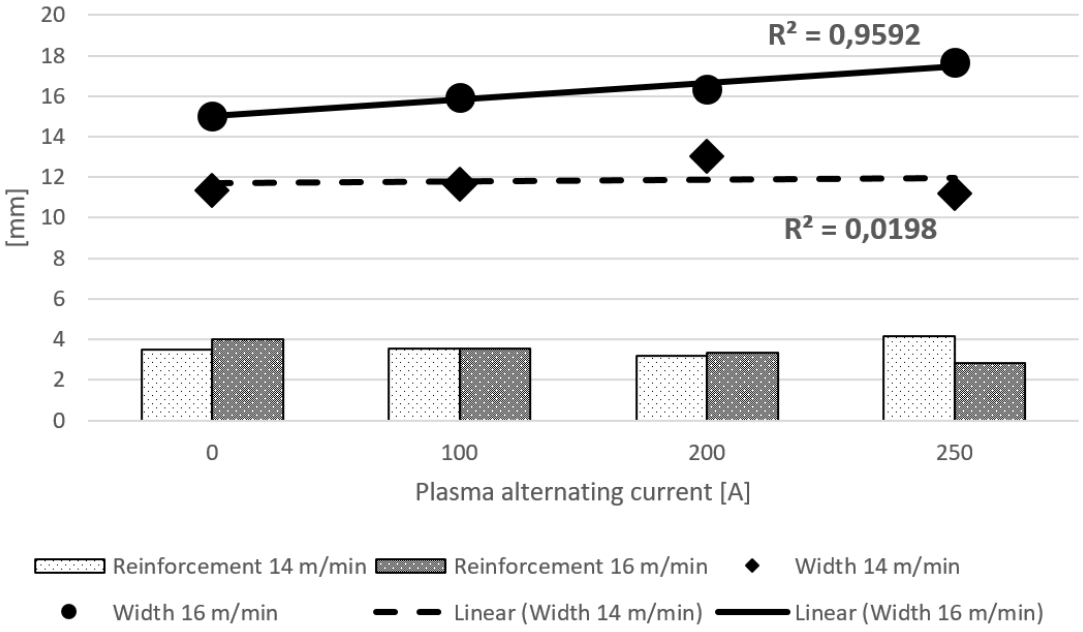

Figure 6.36 - Influence of the plasma-AC on the weld bead width and reinforcement for wire feed speed of 16 m/min and 14 m/min.

Einfluss des Plasma-Wechselstroms auf die Schweißraupenbreite und -überhöhung für Drahtvorschubgeschwindigkeiten von 16 m/min und 14 m/min.

Analyzing the images obtained from high-speed videos (Figure 6.37), it can be observed how the arc length of the MIG-Standard process increases as the plasma-AC rises. This behavior is the same as observed for plasma-DC. In addition, it is noticed how the current path during the polarity transition is practically extinguished, although due to the short period of time of this transition the effects on the arc continue (longer MIG arc length). The arc length measurements presented in Figure 6.38 show that the increase is linear while the plasma current was rising. It happened due to the wire melting speed being superior to the wire feed speed and, therefore, the autoregulation arc length of the MIG-Standard process cannot work properly. The wire melting speed increase promoted by the current that flows by the current path, established between the welding arcs.

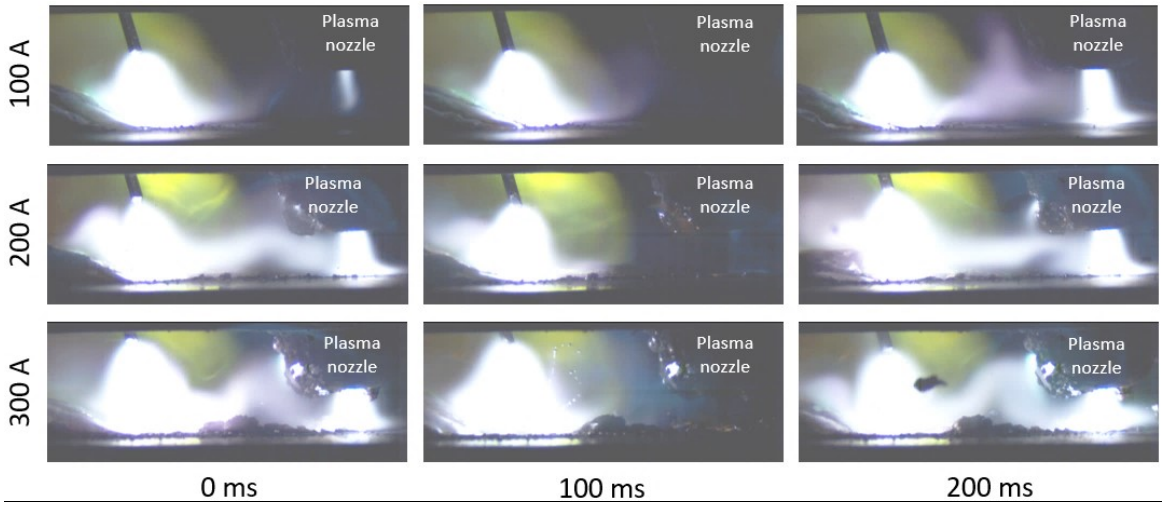

Figure 6.37 - MIG-Standard process behavior for different plasma-AC intensities. MIG wire feed speed: 16 m/min; torch distances: 20 mm.

MSG-Standard-Prozessverhalten für unterschiedliche Plasma-Wechselstromintensitäten. MSG-Drahtvorschubgeschwindigkeit: 16 m/min; Brennerabstände: 20 mm.

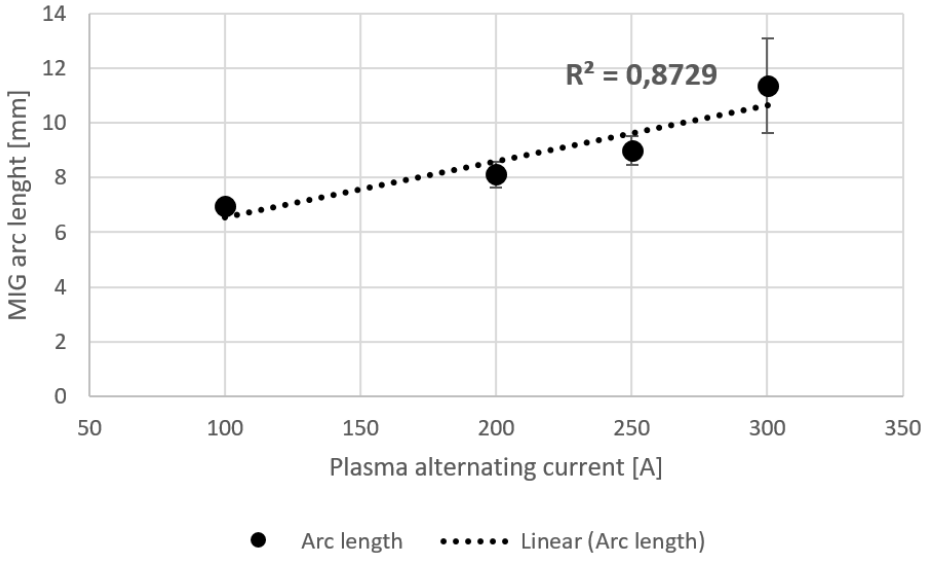

Figure 6.38 - MIG arc length for different plasma-AC intensities. MIG wire feed speed: 16 m/min; torch distances: 20 mm.

MSG-Lichtbogenlänge für unterschiedliche Plasma-Wechselstromintensitäten. MSG-Drahtvorschubgeschwindigkeit: 16 m/min; Brennerabstände: 20 mm.

Comparing the high speed videos in Figure 6.19 and Figure 6.37 is observed that the molten pool is different with plasma-AC, the material removed is less than with plasma-DC, suggesting an explanation to the lower penetration reached by AC. Figure 6.39 shows the oscillograms for plasma-AC in different levels and it is

observed that in positive polarity the current is maintained in 50 A, while in negative polarity the current is increased as require to achieve the RMS level configured in the power source. In simulations made by Kanemaru et al. [13] on hybrid TIG-MIG process, it was found that for low TIG currents in the range from 50 to 200 A, they are insufficient for melting the base material. Then most of the current becomes in the current path, which does not contribute to the heat input of the base metal. Thus, according with exposed by Kanemaru et al. [13], during the positive polarity it is not melting base material, the plasma current during this polarity is just contributing to the current path formation, therefore, the responsible for the penetration is the negative polarity with current levels over 200 A, however, it is not enough to reach the penetration obtained with plasma process using direct current.

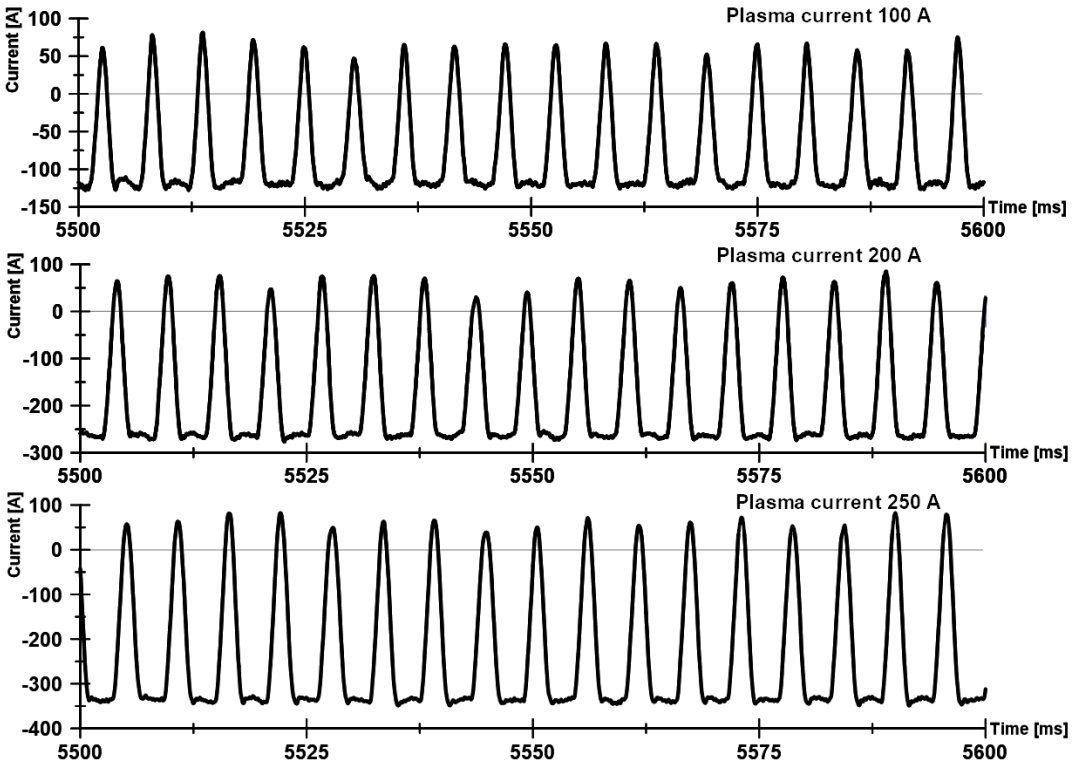

Figure 6.39 – Oscillograms for plasma-AC process during hybrid welding. Wire feed speed: 16 m/mim; Torch distances: 20 mm.

Oszillogramme für den Plasma-Wechselstromprozess beim Hybridschweißen. MSG-Drahtvorschubgeschwindigkeit: 16 m/min; Brennerabstände: 20 mm.

The current and voltage signals of the MIG process for different plasma-AC intensity did not present significant differences, although it was noticed noise in the acquired signals (Figure 9.10). With plasma current of 250 A, the hybrid process turned

unstable mainly due to the strong arc deflection promoted by the alternating polarities of the plasma process.

The Figure 6.40 shows the plasma-AC influencing the average MIG current, noticing a tendency to increase the MIG current for 16 m/min and 14 m/min, however, for this last wire feed speed the increase ratio is lower than for 16 m/min. The explanation for the lower influence of the plasma current on the average MIG current for wire feed speed of 14 m/min, is based on the low stability of the current path formation. With 14 m/min the increase in MIG current is around 8 A, while for 16 m/min is 20 A and, as was discussed in chapters before, with higher plasma and MIG current, stronger is the current path and quantity of metallic vapors that influence the MIG current and voltage, promoting the current flow between the welding processes.

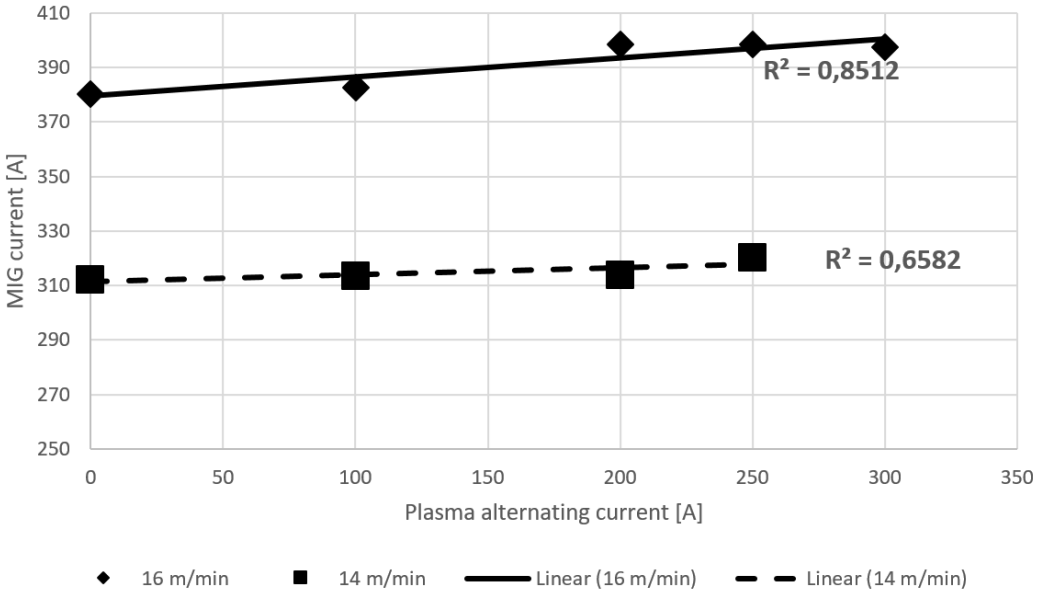

Figure 6.40 - Influence of the plasma-AC on MIG process current for different wire feed speeds.

Einfluss der Plasma-Wechselstromintensitäten auf den MSG-Prozessstrom auf unterschiedliche Drahtvorschubgeschwindigkeiten.

The MIG average voltage had a drop around 1.5 V for 16 m/min in comparison with the single MIG process voltage (Figure 6.41). Although, with 14 m/min no influences were noticed. The drop voltage was also noticed by Han et al. [7] in the paraxial plasma-MIG process with alternating current, describing that the charged particles in the coupled region spread to the MIG arc region, replenish the lost charged

particles and energy, and improve the electrical conductivity of the MIG arc. Therefore, the power supply compensation is correspondingly reduced and the MIG arc voltage is decreased. With increasing the plasma current, the temperature and metal vapor in the molten pool increases, which causes the MIG arc conductivity to improve and the arc voltage to decrease.

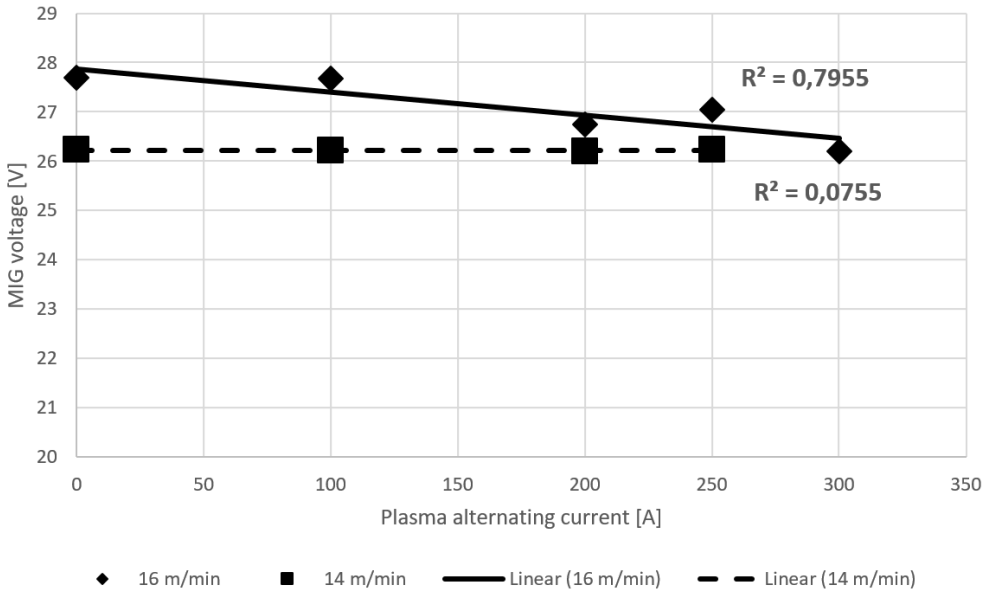

Figure 6.41 - Influence of the plasma-AC on MIG-Standard process voltage.

Einfluss des Plasma-Wechselstroms auf die MSG-Standard-Prozessspannung.

The voltage-current characteristic curves of the MIG process during the hybrid process are presented in Figure 6.42, showing that for the same MIG current the voltage in the hybrid process is lower than the single process. Figure 2.8 presented the voltage-current characteristics obtained by Han et al. [7], it is observed a similar behavior in MIG voltage as in Figure 6.42. The main influence on the MIG voltage is observed just for low MIG currents, thus, the plasma process has a stronger influence on the MIG process in these conditions. While how higher the MIG current is, the less influence on the plasma process on the MIG process. This also was observed for the hybrid TIG-MIG process in the work of Kanemaru et al. [13].

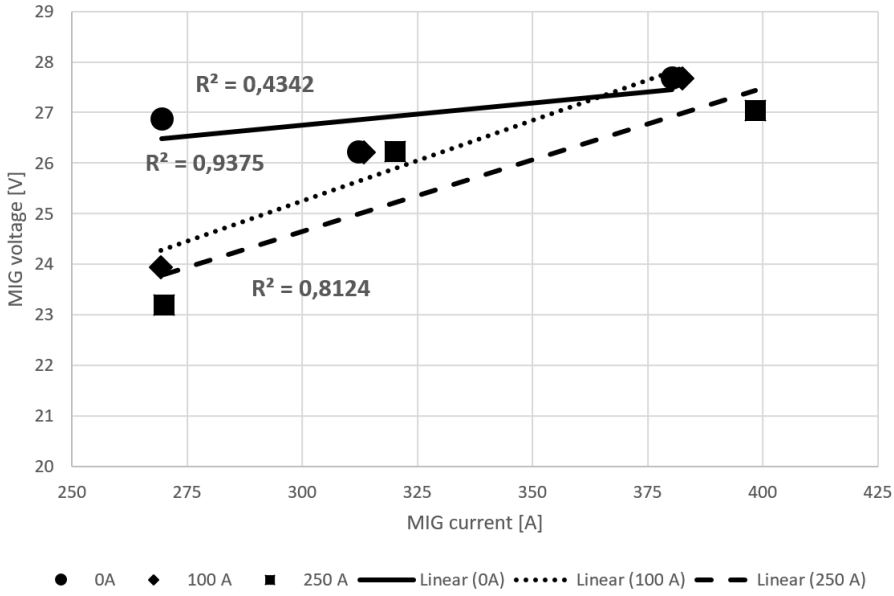

Figure 6.42 – Voltage-current characteristics of the MIG arc for different plasma-AC.

Spannungs-Strom-Eigenschaften des MSG-Lichtbogenschweißens für unterschiedliche Plasma-Wechselstromintensitäten.

Comparing the averages of the electrical signals of the MIG-Standard process for plasma-DC and AC, it is observed that with alternating current the tendency to increase the MIG current is constant, although, in both cases (DC and AC) the maximum current transferred to the MIG process is with 300 A of plasma current (Figure 6.43). On the other hand, the average voltage of the MIG process had a tendency to decrease while the plasma current (AC and DC) increased. Therefore, it is possible to conclude that the behavior of the electrical signals of the MIG-Standard process are independent of the type of current the plasma process uses (AC or DC).

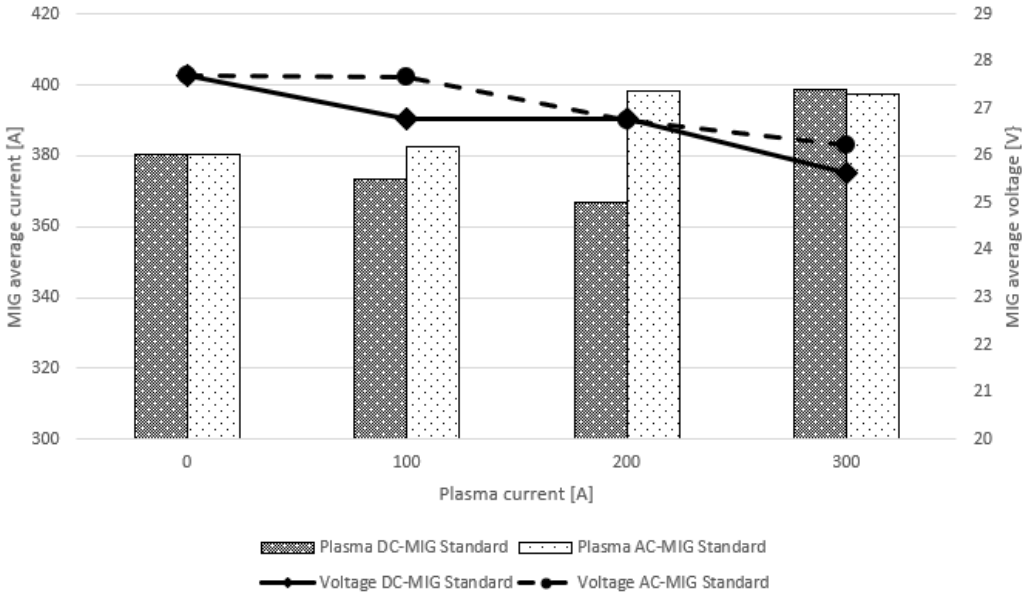

Figure 6.43 - Influence of the plasma process (AC/DC) on the MIG-Standard process electrical signals during the hybrid welding. Wire feed speed: 16 m/mim; Torch distances: 20 mm.

Einfluss des Plasmaprozesses (AC/DC) auf die elektrischen Signale des MSG-Prozesses (Standard) während des Hybridschweißens. MSG-Drahtvorschubgeschwindigkeit: 16 m/min; Brennerabstände: 20 mm.

6.2.2.2 MIG-Pulsed process

The paraxial hybrid plasma-MIG process with pulsed metal transfer behaved stably until the plasma current reached 200 A. After this current level the interaction between the arcs was unstable as observed from the voltage curves in Figure 6.44. The current measurements did not present instabilities for plasma currents greater than 200 A (Figure 9.11). The histograms of Figure 6.45 show an increase of MIG current in the base period about 20 A, while in the pulse period no significant changes are observed. In the case of voltage signal, for plasma currents of 200 A the MIG voltage decreased approximately 2 V, while for 250 A the voltage of the base and pulse periods are not distinguished, therefore, an unstable metal transfer in the MIG process is expected.

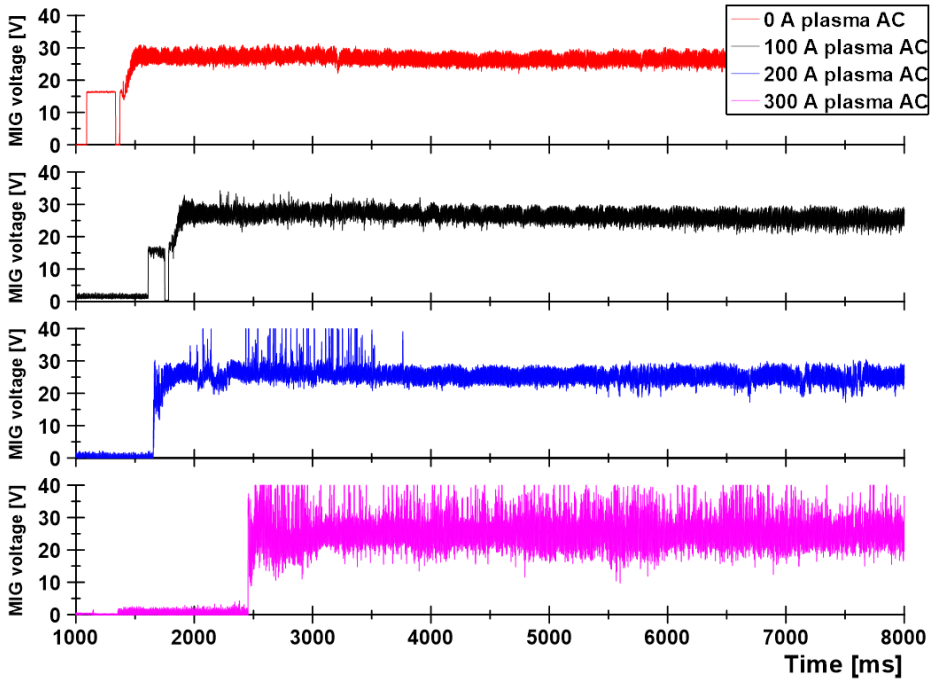

Figure 6.44 – MIG-Pulsed voltage for different plasma-AC. MIG wire feed speed: 16 m/min.

MSG-Impuls Spannung und Strom für verschiedene Plasma-Wechselstromintensitäten. MSG-Drahtvorschubgeschwindigkeit: 16 m/min.

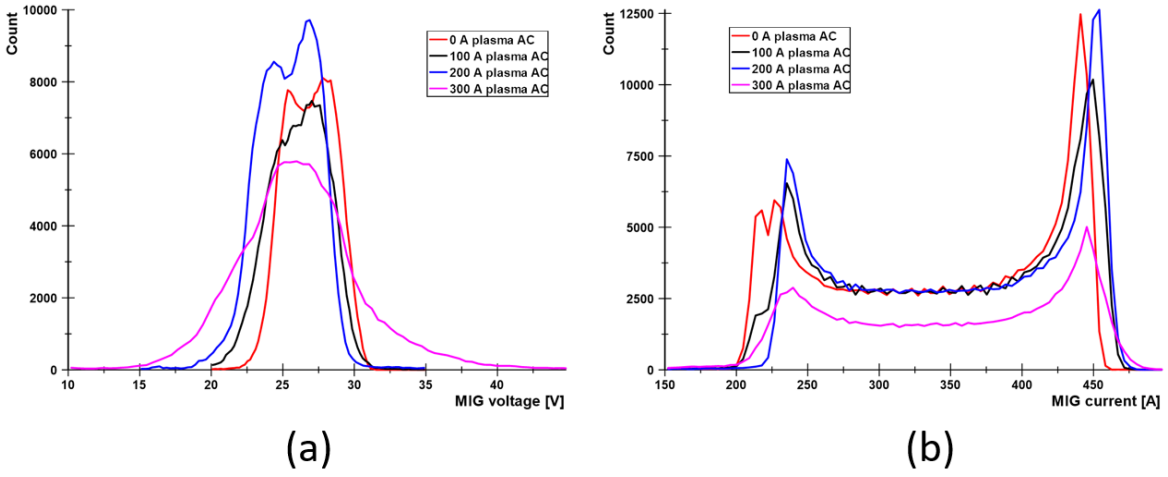

Figure 6.45 - Histograms for (a) voltage and (b) current of the MIG-Pulsed for different plasma-AC. MIG wire feed speed: 16 m/min.

Histogramme für (a) Spannung und (b) Strom des MSG-Impuls für verschiedene Plasma-Wechselstromintensitäten. MSG-Drahtvorschubgeschwindigkeit: 16 m/min.

The macro sections of the weld beads made by paraxial hybrid plasma-MIG process are presented in Figure 6.46 observing that plasma-AC had not a significant influence. Irregular profiles were noticed with 250 A due to the instability of the arcs

interaction. Figure 6.47 shows the weld bead penetration measurements, noticing that plasma-AC intensity had no influence on MIG-Pulsed as it was with MIG-Standard process (Figure 6.35). In addition, comparing with plasma-DC is observed that the penetration had no significant differences, mainly due to the low effect that plasma process has on the MIG-Pulsed process with AC configuration.

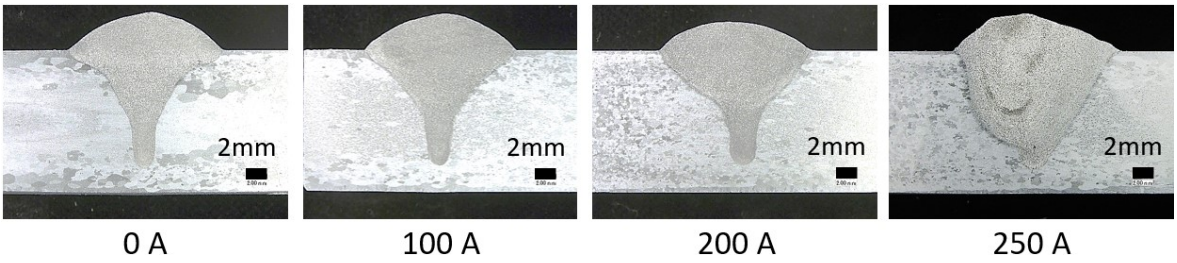

Figure 6.46 - Weld beads cross sections for different plasma-AC with 16 m/min of wire feed speed with MIG-Pulsed.

Schweißraupenquerschnitte für unterschiedliche Plasma-Wechselstromintensitäten mit 16 m/min Drahtvorschubgeschwindigkeit bei MSG-Impuls.

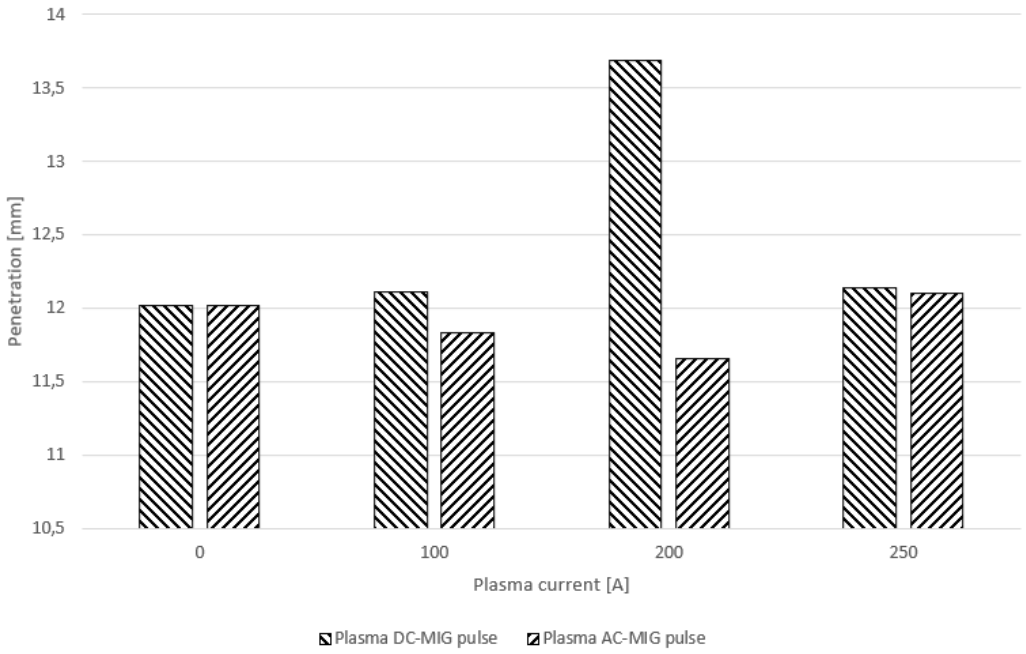

Figure 6.47 - Influence of the plasma-AC with MIG-Pulsed on the penetration to 16 m/min of wire feed speed.

Einfluss der Plasma-Wechselstromintensitäten mit MSG-Impuls auf das Einbrand auf 16 m/min Drahtvorschubgeschwindigkeit.

Weld beads width had a slight increase to 250 A (Figure 6.48), however, at high current level the weld bead geometry is influenced by the welding arc interactions

and stabilities, causing irregular geometries. The reinforcement had not a clear tendency, although the standard deviation was 0.4 mm. This behavior is strongly promoted by the arc deflection between arcs, provoking instabilities in the molten pool and influencing the weld bead geometry.

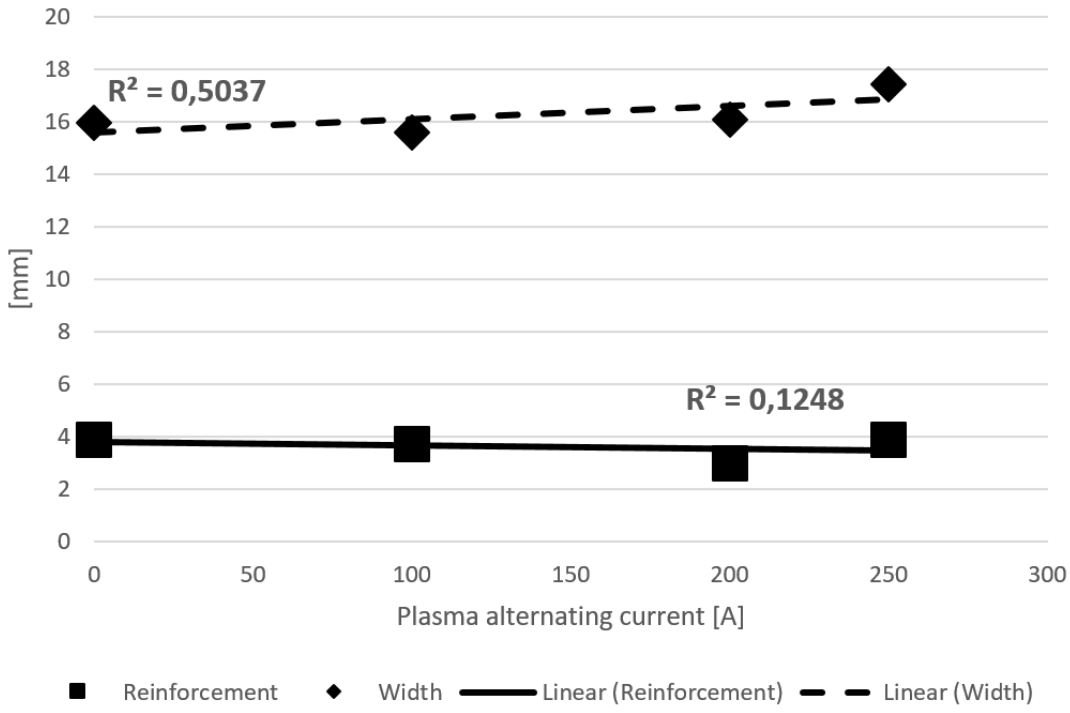

Figure 6.48 - Influence of the plasma-AC with MIG-Pulsed on weld beads width and reinforcement to 16 m/min of wire feed speed.

Einfluss des Plasma-AC mit MSG-Impuls auf die Schweißraupenbreite und -überhöhung auf 16 m/min Drahtvorschubgeschwindigkeit.

Analyzing the average current of MIG-Pulsed is noticed a gain of 12 A when the plasma-AC was 200 A (Figure 6.49). The average voltage had not a clear tendency, specially influenced by the instabilities with plasma current over 200 A, causing a dispersion of 1.6 V. Comparing the averages values of the electrical signals for plasma-AC and DC, MIG voltage had the tendency to reduce its value when the plasma process current increases, this behavior is the same independent of the type of current that plasma process uses (Figure 6.50). However, the drop voltage is higher with MIG-Pulsed (around 2 V), possibly due to the base period where the current and voltage are lower and, therefore, more susceptible to arc deflection effect and the reduction of the voltage by metallic vapors.

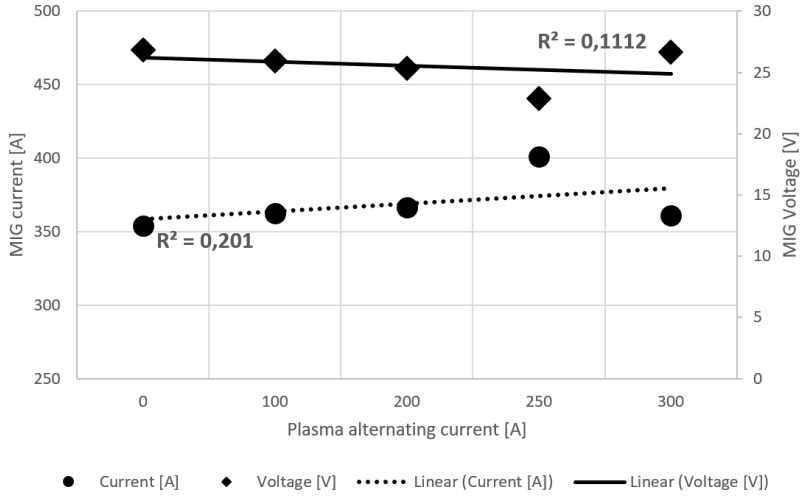

Figure 6.49 - Influence of the plasma-AC on MIG process current and voltage with 16 m/min of wire feed speed.

Einfluss der Plasma-Wechselstromintensitäten auf den Strom und die Spannung des MSG-Prozesses bei einer Drahtvorschubgeschwindigkeit von 16 m/min.

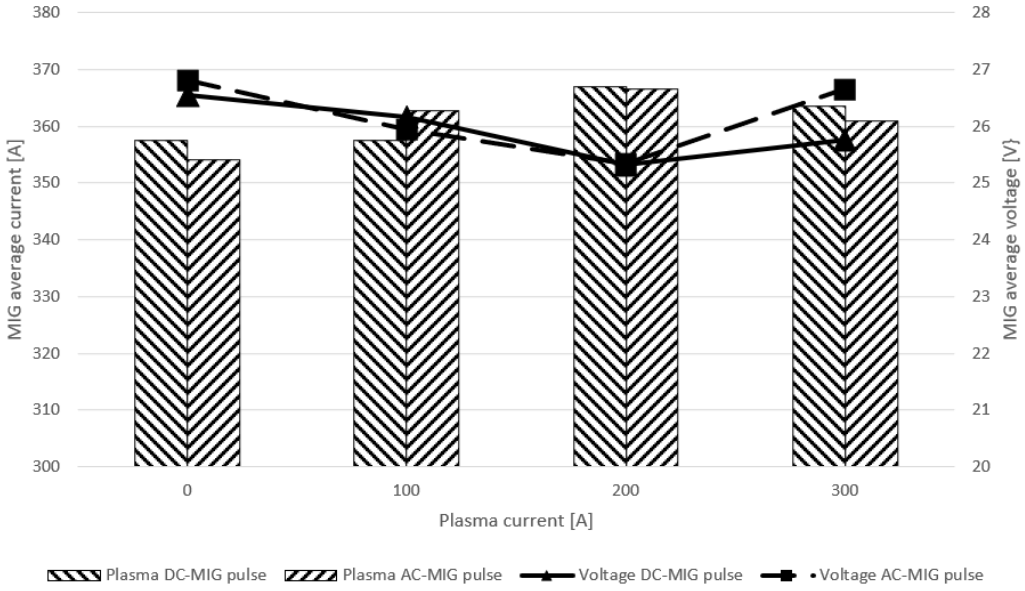

Figure 6.50 - Influence of the plasma process (AC/DC) on the MIG-Pulsed process electrical signals during the hybrid welding. Wire feed speed: 16 m/mim; Torch distances: 20 mm.

Einfluss des Plasmaprozesses (AC/DC) auf die elektrischen Signale des MSG-Prozesses (Impuls) während des Hybridschweißens. MSG-Drahtvorschubgeschwindigkeit: 16 m/min; Brennerabstände: 20 mm.

The images of Figure 6.51 obtained by means of a high-speed camera, show that current path is established between the two welding arcs, however, during the transition periods between negative and positive polarity of plasma process, the

current path is interrupted, influencing the behavior of the MIG-Pulsed process. Figure 6.52 shows the arc length measurements, observing a slight tendency to increase, although with a standard deviation of 0.7 mm. This behavior of the arc length is due to instability of the current path, which influenced the melting speed of the wire-electrode. The current path instability is due to the change of polarities on the plasma process, and the current flow between the welding processes is interrupted during the polarity transition, it provokes a non-constant melting speed of the wire-electrode and, therefore, an erratic change of the arc length in the MIG-Pulsed process. As also discussed during the analysis of the electrical signals, the low currents in the MIG process during the base period contribute to the destabilization of the current path and therefore of the arc length.

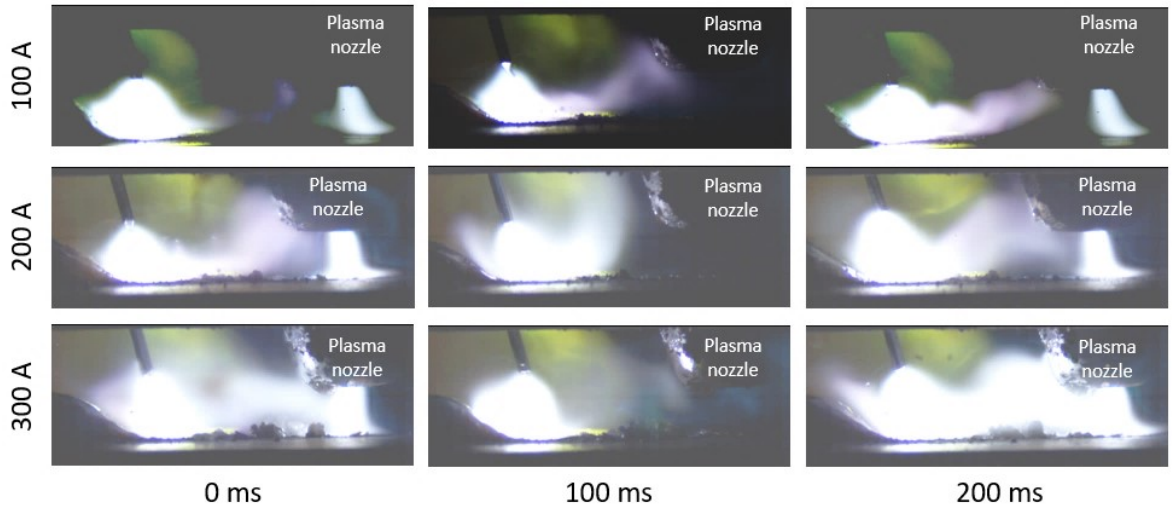

Figure 6.51 - MIG-Pulse process behavior for different plasma-AC. MIG wire feed speed: 16 m/min; torch distances: 20 mm.

MSG-Impuls-Prozessverhalten für unterschiedliche Plasma-Wechselstromintensitäten. MSG-Drahtvorschubgeschwindigkeit: 16 m/min; Brennerabstände: 20 mm.

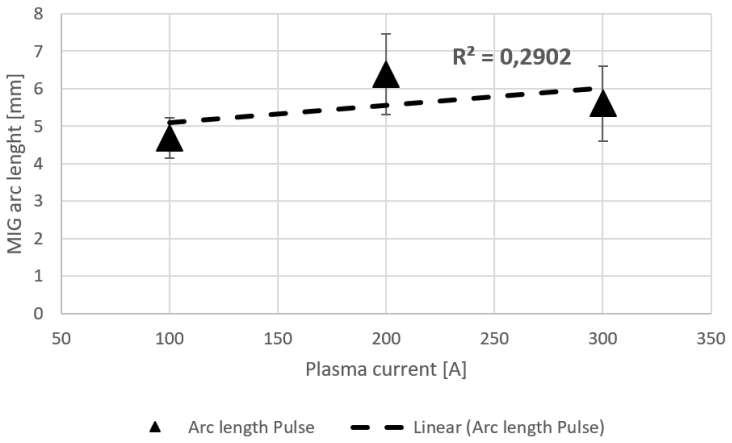

Figure 6.52 - Arc length of the MIG-Pulsed welding process for different plasma-AC.

Lichtbogenlänge des MSG-Impuls-Schweißprozesses für unterschiedliche Plasma-AC.

The Figure 6.53 shows the current-voltage curve for the plasma-AC process, noticing that the MIG-Pulsed caused a drop voltage about 5 V and the wire feed speed had not a significant influence. The behavior observed for 300 A of plasma current is a result of the strong instability between the welding arcs.

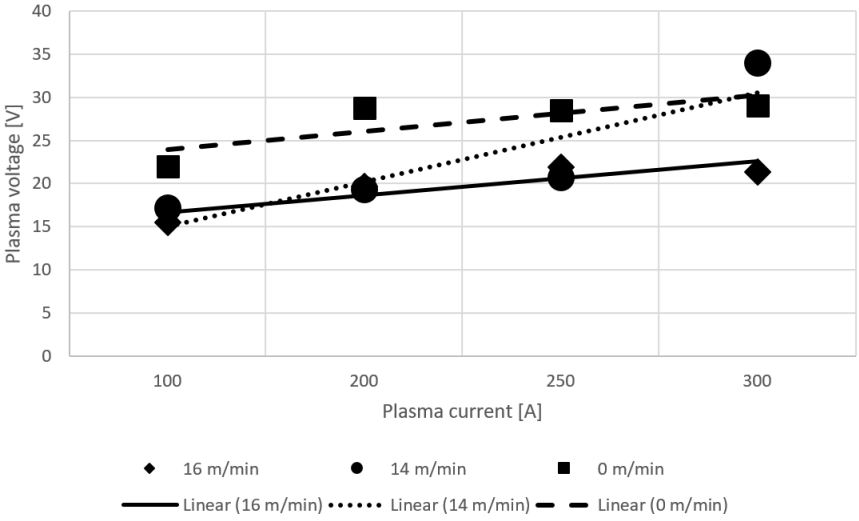

Figure 6.53 - Voltage-current curve of the plasma process AC for different wire feed speeds with MIG-Pulsed.

Spannungs-Strom-Kurve des Plasmaprozesses AC für unterschiedliche Drahtvorschubgeschwindigkeiten mit MSG-Impuls.

6.2.3 Conclusions

The paraxial hybrid plasma-MIG process demonstrates that it is capable to work with different metal transfer in the MIG process and with different polarities in the plasma process, achieving weld beads with low porosities and defects in general. The maximum penetration was obtained by the combination of plasma DC (200 A) and MIG-Pulsed process, however, single MIG process with the same configuration reached 12 mm of penetration, while paraxial hybrid plasma-MIG process reach 13.7 mm, it mean that hybrid process obtained just a 14% more of penetration in its best welding condition. Therefore the best configuration for the paraxial hybrid plasma-MIG process is with the MIG-Pulsed and Plasma-DC processes because the hybrid arc between both processes is more stable (low interaction between them) and the plasma constrictor nozzle is not damaged.

It is concluded that there is effectively an interaction between the welding arcs during coupling, which is intensified when one of them increases its energy. There is an increase in the current of the MIG-Standard process and a decrease in the voltage of the plasma process (with AC and DC configuration). In the case of the MIG-Pulse process there is no clear trend in the behavior of its electrical signals, which may be due to the low current level in its base period, which affects the formation and stability of the current path, the main medium for current flow between processes. This current flow influenced the wire melting rate of the MIG-Standard process, which increased the arc length in a linear manner as the plasma current (AC or DC) increased. In the case of the MIG-Pulsed process there was no clear tendency to increase.

6.3 Relevance of MIG and plasma processes on the penetration of the hybrid welding

The welding processes that compound the paraxial hybrid plasma-MIG process were studied separately in the last chapters, both showed an influence in the penetration and in the electrical signals of each other. However, it is relevant to know which one has the strongest influence in the penetration. The Figure 6.54 shows the comparison of the penetration reached by the paraxial plasma-MIG process in function of the arc power of both welding processes coupled. The first 2 curves on the left (dots and crosses) were obtained increasing the wire feed speed of the MIG

process and maintaining the plasma current constant in 100 A. On the right side of the same plot, it is observed 2 curves (square and triangle) that represent the penetration of the hybrid process when the plasma current (direct and alternating) is increased and the MIG wire feed speed is maintained constant in 16 m/min. From Figure 6.54 is concluded that changes in the wire feed speed has a stronger influence on the weld bead penetration than changes in the plasma current. Furthermore, it is observed that the hybrid process requires less energy when the plasma current is maintained low and the MIG process increases its current (curves with dots and crosses).

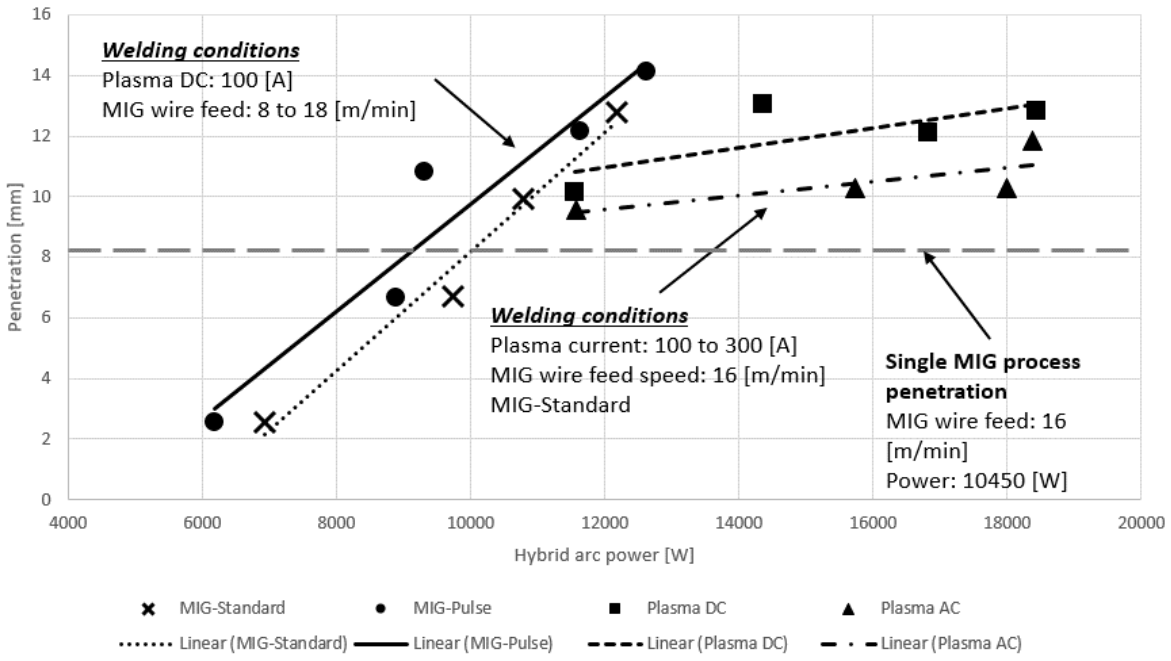

Figure 6.54 – Penetration comparison obtained by the paraxial hybrid plasma-MIG process with different arc power, depending on which welding process increases its current (MIG or plasma).

Vergleich der Einbrand durch den paraxialen Plasma-MSG-Hybridprozess mit unterschiedlichen Lichtbogenleistungsintensitäten, je nachdem welcher Schweißprozess seinen Strom erhöht (MSG oder Plasma).

Kanermaru et al. [13] studying the TIG-MIG hybrid process noticed that penetration depth was increased when TIG current was greater than MIG current. However, in the range of TIG current less than MIG current, the penetration depth was independent of TIG process, as was noticed with plasma process in Figure 6.54. The results obtained by Kanemaru et al. [13] suggest that plasma current needs to be greater than the MIG current for arc stability. Then, increased plasma current

increases the penetration depth. From the study of the TIG-MIG process it is possible to conclude that an energy balance is necessary between welding processes, deciding the specific task of each one. In the case of the paraxial hybrid plasma-MIG process, the penetration was mostly influenced by the MIG process, because its current was greater than plasma process, when the latter was maintained at 100 A. On the other hand, the plasma current is limited by the constrictor nozzle, which cannot work in currents greater than 300 A. Therefore, the plasma process cannot exceed the MIG process current, which with 16 m/min has a current of 380 A. Based on the results obtained in this study, it is suggested that in the paraxial hybrid plasma-MIG process, the plasma current should be low enough to maintain the stability of the hybrid process and provide a preheat on the base material, while the MIG process works with high current levels to reach deep penetrations.

The behavior observed in the penetration obtained by the paraxial hybrid plasma-MIG process in Figure 6.54, when plasma current increases, can be interpreted as a decrease in the efficiency of the process, which is caused by the formation of the current path, which is promoted mainly by the plasma process. As it was observed in Figure 6.19 when plasma current increases, the current path becomes more constant and stronger, which influences the melting rate of the wire-electrode, causing an increase in the MIG arc length, which in turn influences the final penetration achieved by the process [52]. Measurements of the efficiency of the TIG-MIG hybrid process show that it is 10% less efficient than its single versions [14], because part of the MIG current does not flow into the base metal due to the formation of the current path, which decreases the energy imposed on the base metal. Currently there is no bibliography on the efficiency of the plasma-MIG process, however, Figure 6.54 shows that by increasing the power of the hybrid process by increasing plasma current, penetration is not strongly influenced, turning the process inefficient in this term.

The penetration achieved by the paraxial hybrid plasma-MIG process was superior to the single MIG process, as seen in Figure 6.54. This increase in penetration was around 20%, compared with a single MIG process with 16 m/min of wire feed speed. This is a significant value, if it is compared to the results obtained by Kanemaru et

al [13] for the TIG-MIG process, where it reduced the welding time by 17 to 44% compared to the single TIG process. Therefore, it is possible to conclude that the paraxial hybrid plasma-MIG process achieves greater penetration than the single Plasma and MIG processes.

6.4 Commercial alternative: SuperMIG

The SuperMIG equipment, a commercial alternative to the paraxial hybrid plasma-MIG process, was tested according to conditions described in the sub-chapter 5.3. The analysis of the weld beads (Figure 9.12) and electrical signals (Figure 9.13 and Figure 9.14) show that there are no significant differences between the SuperMIG and the paraxial hybrid plasma-MIG process. The current path in the welding arcs was noticed in SuperMIG, following the same trend observed in the results observed in Chapter 6.2. Cross sections of the weld beads made by SuperMIG are presented in Figure 6.55, where it is noticed that increasing the plasma current increases the penetration, similar to the results obtained by the paraxial hybrid plasma-MIG process.

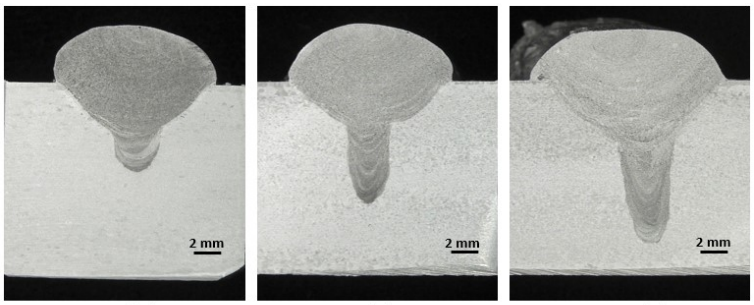

Figure 6.55 – Weld bead cross sections for different plasma currents (a) 100 A (b) 200 A (c) 300 A made by SuperMIG. MIG wire feed speed: 16 m/min; Magnetic level compensation: 40%.

Schweißraupenquerschnitte für unterschiedliche Plasmaströme (a) 100 A (b) 200 A (c) 300 A von SuperMIG. MSG-Drahtvorschubgeschwindigkeit: 16 m/min; Magnetpegelkompensation: 40%.

The absence of differences between the weld beads obtained by the commercial version SuperMIG and the experimental version of the paraxial hybrid plasma-MIG process was expected, because the configuration between the torches is the same. However, the behavior of the electrical signals and the current path was expected to be different. In the next sub-chapter the influence of the parameter called

“magnetic compensation level” will be studied, which aims to stabilize the interaction between the coupled arcs by applying an external magnetic field between them. This parameter is expected to influence especially the electrical signals of the welding processes, because it should mainly affect the deflection of the arcs and the formation of the current path.

6.4.1 Magnetic level compensation

The SuperMIG is characterized by special electromagnets placed on the shielding gas nozzle end (Figure 4.3), which are designed to apply the required magnetic force to push the plasma back to the impingement spot and hold it in place during the welding process. The electromagnets create 2 forces and the direction is based on the interaction of two magnetic fields, one force keeps plasma in center, and the other one “returns” the plasma to counteract the MIG forces [8]. The electromagnets are controlled by SuperMIG display by means of the parameter named “Magnetic level compensation” and it has no unit of measurement, the intensity of this parameter is measured in percentages, starting from 5% until 70%.

From the description given by Weldobot [8], it is possible to expect that the "Magnetic level compensation" induces in the plasma and MIG arcs a controlled deflection, which should increase when the intensity of the external magnetic fields exerted by the electromagnets increases. If the arcs approach each other it means a change in the length of the arcs, which would have a direct relation with the magnetic level compensation. Figure 6.56 shows the behavior of the SuperMIG arc when the external magnetic field intensity is increased, noticing that the current path is established between the arcs of the MIG and plasma processes. However, no significant changes were observed between the arcs for different intensities configured and the process stability was similar to the paraxial hybrid plasma-MIG process (Figure 6.19).

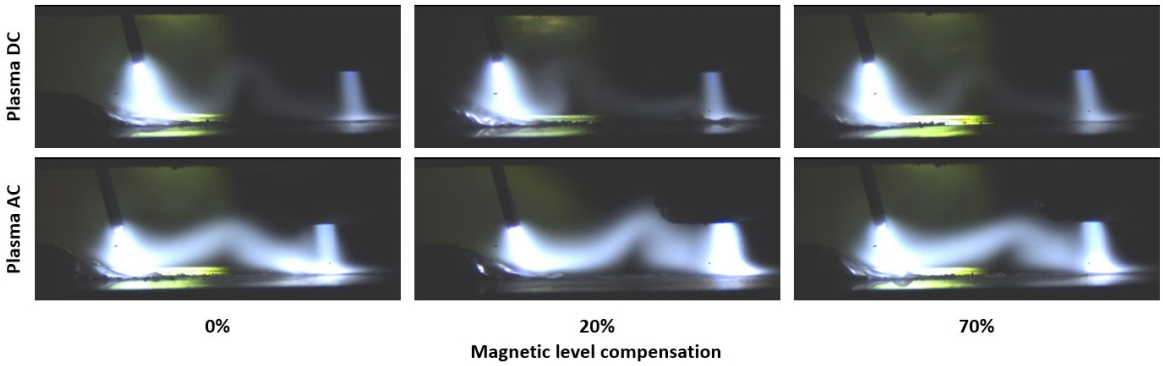

Figure 6.56 – Comparison of arcs behavior of the SuperMIG when the magnetic level compensation increases for different plasma current polarities. MIG wire feed speed: 14 m/min; plasma current: 100 A.

Vergleich des Lichtbogenverhaltens des SuperMIG bei zunehmender magnetischer Niveaukompensation für unterschiedliche Plasmastrompolaritäten. MSG-Drahtvorschubgeschwindigkeit: 14 m/min; Plasmastrom: 100 A.

The voltage and current measurements of the plasma and MIG processes in SuperMIG do not show significant changes when the magnetic level compensation is increased (Figure 9.15) and, as observed in Figure 6.56, no significant deflections (attraction) were noticed in the arcs of each welding process. The current path behavior was the same for each external magnetic field intensity tested. This suggests that magnetic level compensation would have no influence in the weld bead, due to power and stability of the arcs did not change.

The analysis of the weld beads made for different magnetic level compensation are presented in Figure 6.57, not observing significant differences between them. These observations are confirmed with the measurements made to the cross sections of the weld beads, not noticing differences in the penetration, width and reinforcement of the weld beads. Similar results were obtained by SLV München [3], where no influences were noticed on the weld bead appearance, quality and profile penetration with the same equipment on steel.

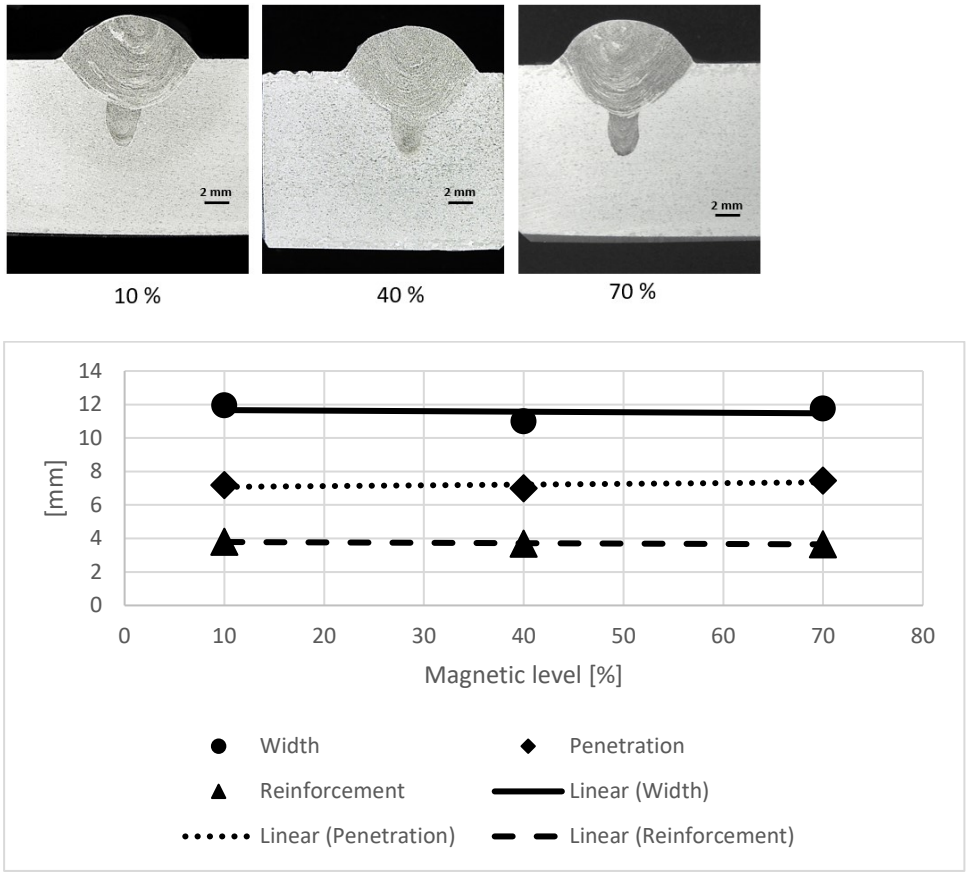

Figure 6.57 – Weld beads cross sections and its measurements for different magnetic level percentages. MIG wire feed speed: 14 m/min; plasma current: 100 A.

Schweißraupenquerschnitte und deren Messungen für unterschiedliche Prozentsätze des Magnetpegels. MSG-Drahtvorschubgeschwindigkeit: 14 m/min; Plasmastrom: 100 A.

The measurements of the current and voltage of the electromagnets for different intensities of the magnetic level compensation are presented in Figure 6.58 and no significant changes are noticed in the electrical signals. The values of the voltage and current are considerably lower in comparison with the welding processes, in addition, there are no specifications about the coils in the electromagnet, therefore, it is not possible to estimate the intensity of the magnetic field produced by the currents and voltages measured. Simulations made by SLV München [3] on the influence of the external magnetic fields of 0 mT, 5 mT and 10 mT on the plasma and MIG arcs behavior, concluding that only a strong external magnetic field (superior than 5 mT) can significant influence the welding arcs. The model calculations cast doubt on whether a sufficiently strong magnetic field can be

generated with the installed coils in the electromagnets of the SuperMIG, in order to be able to influence the arcs of each process [3].

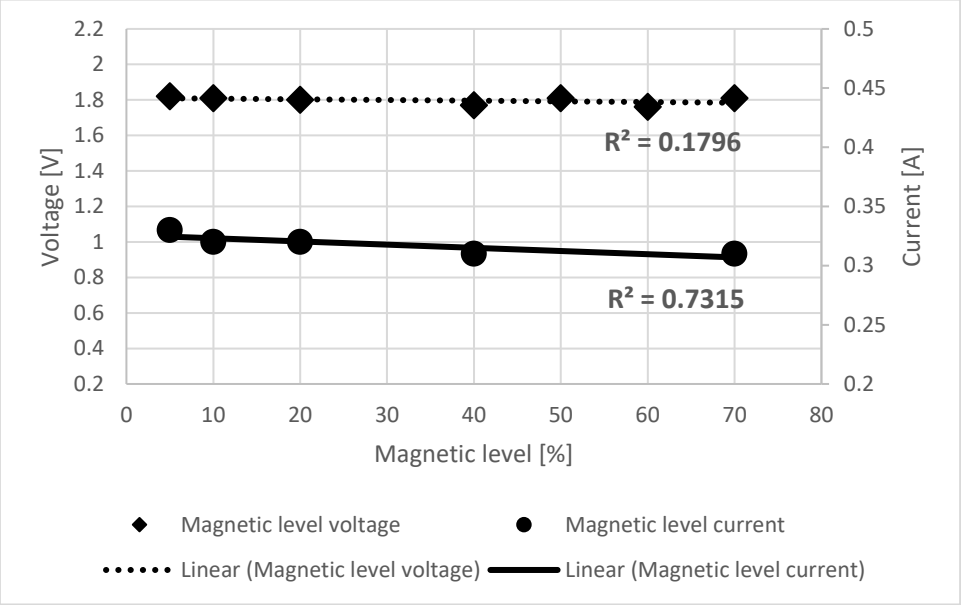

Figure 6.58 – Characterization of the magnetic level compensation intensities in RMS current and voltage. MIG wire feed speed: 14 m/min; plasma current: 100 A.

Charakterisierung der Magnetpegelkompensationsintensitäten in Effektivstrom und -spannung. MSG-Drahtvorschubgeschwindigkeit: 14 m/min; Plasmastrom: 100 A.

A Fast Fourier transform (FFT) analysis was made in the current signal of the electromagnet (Figure 9.16), with the objective to know if there is a patron or change in the frequency of the signals and no differences were noticed. All the curves have the same behavior in frequency and current intensity (Figure 9.17). Therefore, it is possible to conclude that there are no differences in set intensity of 10% or 70%.

The electrical signals of the electromagnets were measured when the plasma current and the wire feed speed were increased, each parameter separately, in order to know if the SuperMIG equipment has a capacity to adapt changes in the intensity of the magnetic fields generated by the welding processes. Figure 6.59 shows that there are no differences in the current and voltage of the electromagnets when the plasma current increases, which discarded the option of a self-adjustment of the magnetic field generated by the electromagnets. Furthermore, an increase in the voltage and current in the electromagnets is observed for plasma currents greater than 200 A, which coincides with the unstable behavior of the welding arcs

studied in the previous chapters. This increase in current and voltage may be due to an induced current from the MIG and plasma arcs in the electromagnets. In the case of increasing the wire feed speed, there is a tendency to increase the intensity of the electric signals in the electromagnets, however, the variation is low, approximately 0.3 V and 0.06 A (Figure 6.60). In contrast, increasing the plasma current the variation of the voltage and current in the electromagnets was superior than for high levels of wire feed speed, this may be due to the position of the plasma process with respect to the electromagnets, which would increase the induction of current on them in comparison with MIG process (Figure 4.3).

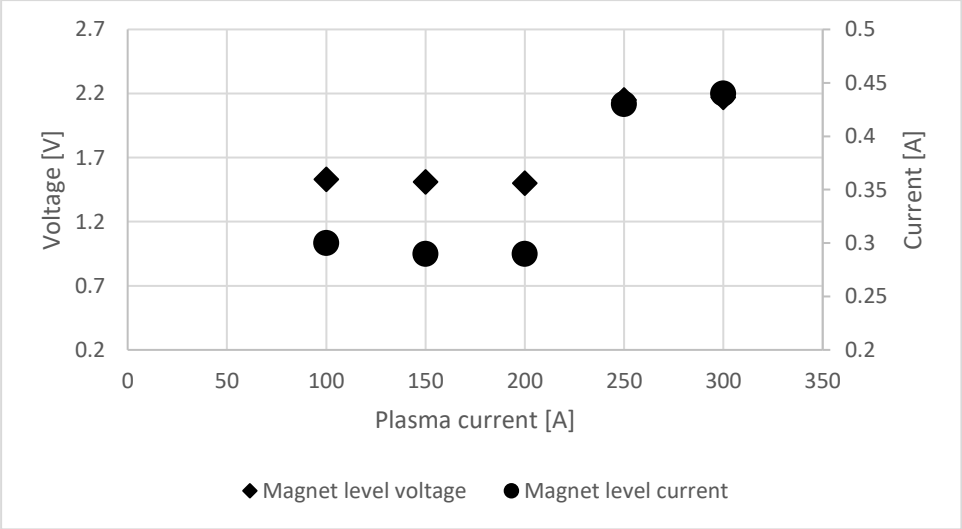

Figure 6.59 – Influence of the plasma process on the electrical signals of the electromagnets. MIG wire feed speed: 14 m/min; magnetic level compensation: 40%.

Einfluss des Plasmaprozesses auf die elektrischen Signale der Elektromagnete. MSG-Drahtvorschubgeschwindigkeit: 14 m / min; Magnetpegelkompensation: 40%.

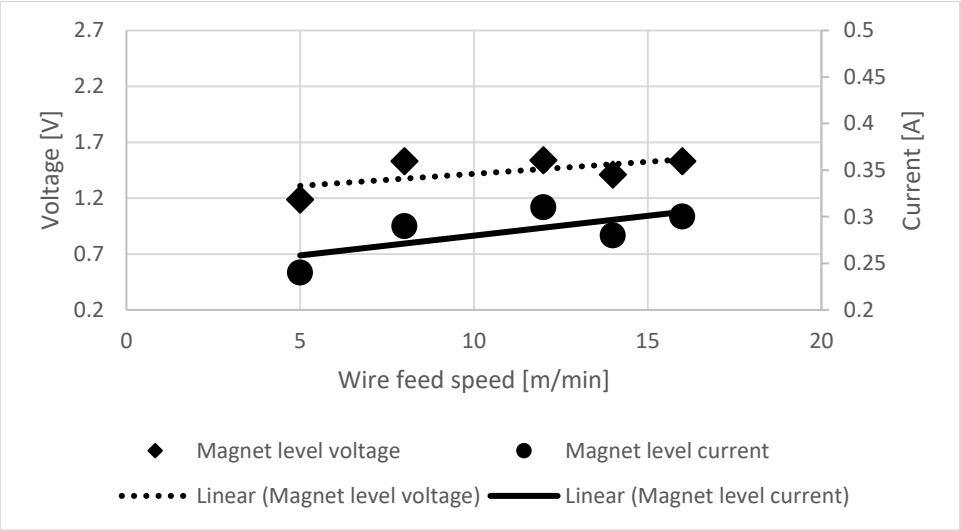

Figure 6.60 – Influence of the wire feed speed on the electrical signals of the electromagnets. MIG wire feed speed: 14 m/min; magnetic level compensation: 40%.

Einfluss der Drahtvorschubgeschwindigkeit auf die elektrischen Signale der Elektromagnete. MSG-Drahtvorschubgeschwindigkeit: 14 m/min; Magnetpegelkompensation: 40%

6.4.2 Conclusions

Analyzing the interaction between the arcs in the SuperMIG and their electrical signals, in addition to measuring the voltage and current of the electromagnets, it is not possible to conclude that the external magnetic field generated by the electromagnets is influential in the stability or behavior of the MIG and plasma arcs coupled. Other studies that used the SuperMIG equipment do not mention the magnetic level compensation in their studies, or the requirement of an external magnetic field to stabilize the interaction between the welding arcs [7, 11, 56]. Simulations and experiments made on the SuperMIG for steel as base material and wire-electrode demonstrate that the external magnetic field has not an influence in the quality, appearance and profile penetration of the weld beads [3]. Furthermore, the simulation concluded that coils in the SuperMIG torch would not have the capacity to generate a strong magnetic field to influence the arcs of each welding process. On the other hand, the studies made on the TIG-MIG hybrid welding process did not use external magnetic fields to achieve good stability and interaction between the arcs [13, 14, 53–55]. The interaction between the welding arcs observed in these studies were similar to obtained by SuperMIG or plasma-MIG paraxial process, specially the establishment of the current path between the arcs.

Comparing the results obtained by the paraxial hybrid plasma-MIG process with the SuperMIG, it is noticed that the quality of the weld bead and the stability of the arcs coupling do not depends on an external magnetic field.

6.5 Application: Aluminum joints EN AW6060-T66

The application of the paraxial hybrid plasma-MIG process on aluminum joints was done in two manners: in the first analysis 10 mm joints were compared using plasma-DC and AC; the second analysis is done on 15 mm thick joints where the paraxial hybrid process is compared with the single MIG process (Standard mode) and the SuperMIG. The goal of the study on 10 mm thick plates is to observe if there are differences in mechanical properties when using AC or DC in the plasma process when it is working coupled with the MIG process. While the study on 15 mm thick joints, the objective is to observe the limits of the hybrid process in comparison to a single process.

The conditions to make the joints are described in Chapter 5. The parameters used were sought with the aim of achieving the highest possible welding speed, while the stability of the welding process was not compromised.

6.5.1 Microstructures

Tests on 10 mm joints show that there are no significant differences in the quality of joints made with plasma-DC or AC. Superficially no defects or undercuts are observed. The weld bead made with DC presents a smoother surface than the joint made with AC (Figure 9.18). In case of the joint roots there are no significant differences between both types of current, with total penetration (Figure 9.19). Analyzing the weld bead cross sections, total penetration without lack of fusion in the roots for both current types is observed (Figure 6.61). Large internal porosities or cracks are not observed.

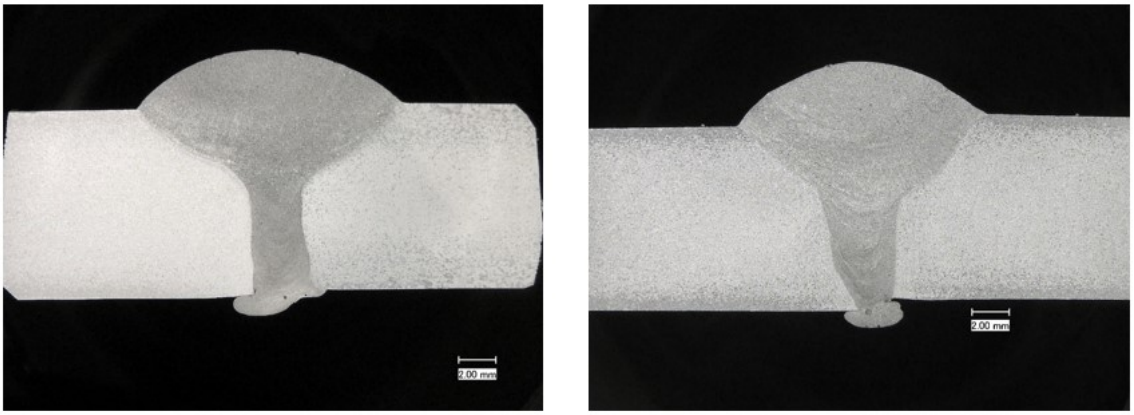

Figure 6.61 – Joint comparison made by paraxial hybrid plasma-MIG process between plasma direct and alternating current. Butt joint 10 mm thickness without gap and 100 A as plasma current with 15 m/min of wire feed speed.

Gemeinsamer Vergleich durch Plasma-MIG-Hybridverfahren zwischen Plasma-Gleich- und Wechselstrom. Stoßverbindung 10 mm Dicke ohne Spalt und 100 A als Plasmastrom mit 15 m/min Drahtvorschubgeschwindigkeit.

The 15 mm thick joints without edge preparations (I-joint) and 2 mm gap were tested, total penetration was reached. Figure 6.62 shows a comparison between single MIG, SuperMIG and paraxial plasma-MIG process where all of them reach total penetration, however, the profile of the single MIG process was narrower than the other welding processes. The superficial appearance of the weld beads made by a single MIG process had an irregular surface (Figure 9.20), caused by the unstable metal transfer (rotative spray) due to high current used (around 400 A). The different penetration shape is due to the short arc of the single MIG process, causing an arc constriction and a reduction of the weld bead width. Furthermore, the high wire feed speed made the molten pool size bigger due to the excessive molten material coming from the wire-electrode and base material. It caused changes in the arc length by accumulation and lack of material in some areas of the weld bead (Figure 9.20c). In contrast, the hybrid processes had smooth superficial appearance and good penetration shape due to the MIG arc length being higher, caused by the current path between the arcs. In addition, the extra power from the plasma process increases the molten pool temperature causing a reduction of the superficial tension of the liquid metal and, therefore, increases the weld bead width.

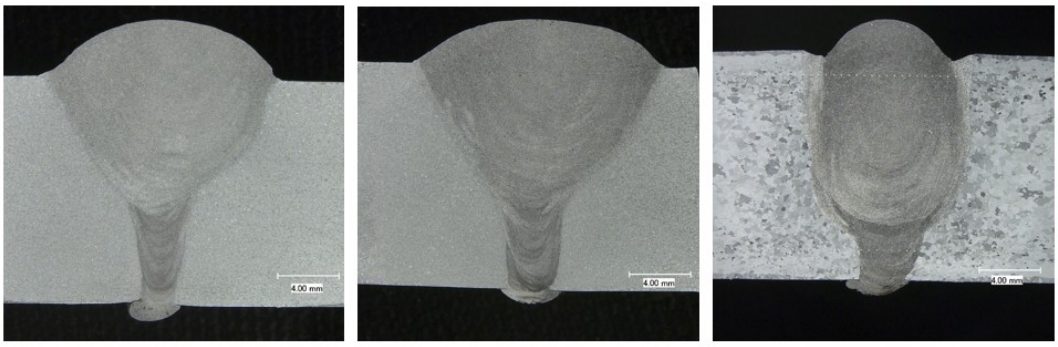

Figure 6.62 - Welding joints with 2 mm gap and without bevels (I-Joint) made by (a) paraxial plasma-MIG (b) SuperMIG (c) MIG. Aluminum joints 15 mm thick. Plasma-DC.

Schweißverbindungen mit 2 mm Spalt und I-Stoß aus (a) Plasma-MSG paraxial (b) SuperMIG (c) MSG. Aluminiumverbindung 15 mm dick. Plasma-DC.

Joints made with plasma-AC resulted in less oxygen content, especially in the face region of the weld bead (Figure 6.63). This result agrees with the study made by Cho et al. [57], where it was proved that a single plasma-AC process reduces the amount of oxygen in the weld bead, compared with welds made with DC. This reduction in the oxygen suggests a minor quantity of oxides inside of the weld beads. Magnesium and silicon have no significant changes in their amounts, discarding an influence of the plasma polarity in the diffusion of these alloys.

Analyzing the microstructure of the joints of 10 mm thick, the weld metal (WM) is composed mainly by dendrites, where the joint made by plasma-AC shows a minor dendrite arm spacing (Figure 6.64a) in comparison with plasma-DC (Figure 6.65a). In Figure 6.66 is shown the SEM images of the WM and it is noticed the presences of micro-pores or interdendritic pores [25], who have two main formation mechanisms. One is the solidification shrinkage of liquid metal, and the other is due to gas formation. However, it is difficult to tell that those pores are caused by which mechanism. On the other hand, in Figure 6.66 is also noticed Al-Si structures in the interdendritic spaces of eutectic structures in the α-Al matrix, described by Liang et al. [53] and Nikseresh et al. [58]. In addition, the wire filler ER4043 enriched the Al-Si structures found in the interdendritic spaces of the WM, due to the around 5% of silicon content.

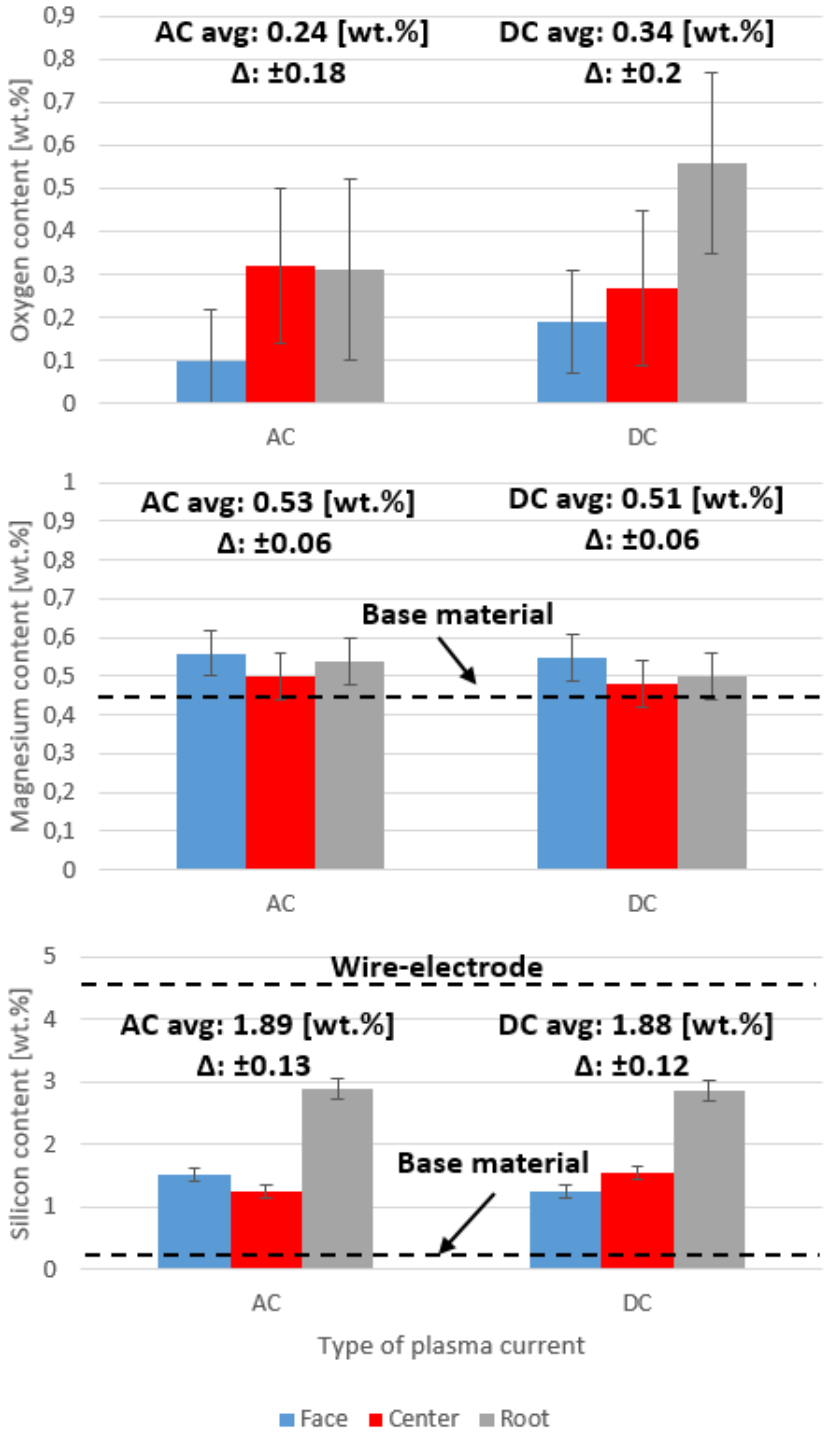

Figure 6.63 - Distribution of oxygen, magnesium and silicon in the weld beads made by paraxial plasma-MIG process with different plasma polarity in joints of 10 mm thick.

Verteilung von Sauerstoff, Magnesium und Silizium in den Schweißraupe, hergestellt durch ein paraxiales Plasma-MSG-Verfahren mit unterschiedlicher Plasmapolarität in Verbindungen mit einer Dicke von 10 mm.

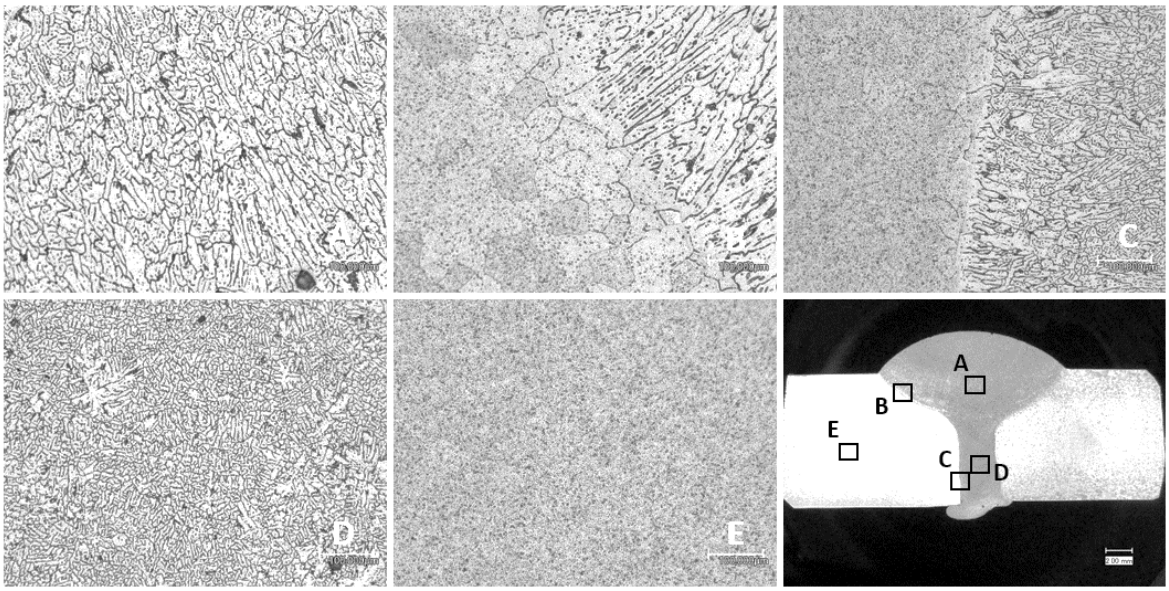

Figure 6.64 – Microstructures of weld beads made by paraxial plasma-MIG process with plasma AC. MIG wire feed: 15 m/min; plasma AC: 100 A. Aluminum joint 10 mm thick.

Mikrostrukturen von Schweißraupen hergestellt im paraxialen Plasma-MSG-Verfahren mit Plasma-AC. MSG-Drahtvorschub: 15 m/min; Plasma-AC: 100 A. Aluminiumverbindung 10 mm dick.

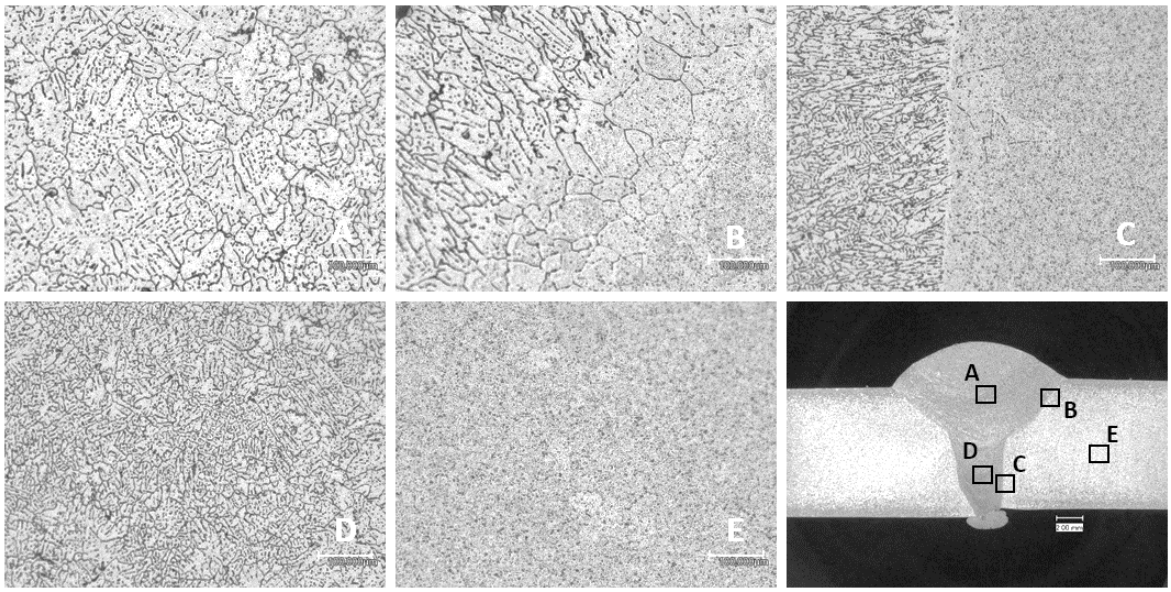

Figure 6.65 - Microstructures of weld beads made by paraxial plasma-MIG process with plasma DC. MIG wire feed: 15 m/min; plasma DC: 100 A. Aluminum joint 10 mm thick

Mikrostrukturen von Schweißraupen hergestellt in einem Plasma-MSG-Paraxialprozess mit Plasma-DC. MSG-Drahtvorschub: 15 m/min; Plasma DC: 100 A. Aluminiumverbindung 10 mm dick.

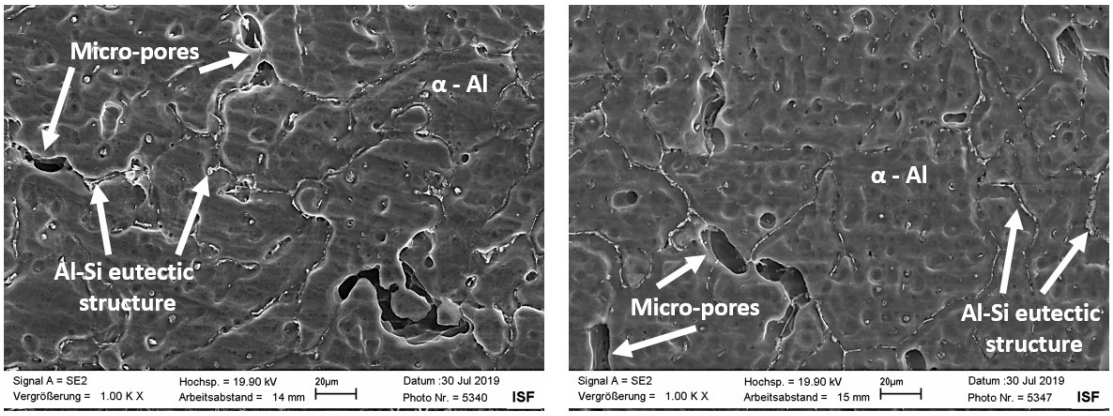

(a) (b)

Figure 6.66 – SEM of weld metal made by paraxial hybrid Plasma-MIG process with (a) Plasma-AC (b) Plasma-DC. Aluminum joints 10 mm thick.

REM von Schweißgut hergestellt durch ein Plasma-MSG-Paraxialverfahren mit (a) Plasma-AC (b) Plasma-DC. Aluminiumverbindung 10 mm dick.

The region of the WM near to partially melted zone (PMZ) consist mainly of columnar dendrites and there were no significant differences observed between plasma-AC (Figure 6.64b) and plasma-DC (Figure 6.65b). The columnar dendrites grow perpendicularly from PMZ to the center of the WM, due to the high temperature gradient. The next microstructure observed is the PMZ, characterized by refined grains due to the cooling rate is fast, finer grains structure are obtained in this area than in the HAZ. While comparing the PMZ obtained by plasma-AC (Figure 6.64b) and DC (Figure 6.65b) it is difficult to tell which one is finer, however, it is noticed that the PMZ of the plasma-DC is wider. This behavior in the PMZ width is due to higher power of the hybrid process with plasma-DC, who increase the heat input, which results in longer high temperature period and slower cooling rate. Thus, the grains suffer considerable coarsening and the area of recrystallization increases. On the other hand, the HAZ for both types of current did not show significant differences.

Comparing the microstructure of the face and root areas in the WM, regions A and D, it is noticed that grains in the root are finer, not observing differences between plasma-AC (Figure 6.64d) and plasma-DC (Figure 6.65d). The differences in grain size for same weld beads is due to the cooling rate being faster in the root than in the face region, mainly because the copper bar used as a backing increases the

cooling rate, in comparison with the face region where the hybrid arc is ignited and provides constant heat input. This behavior in the cooling rate also influences the PMZ in the root area, observing that there is not a clear definition of this zone, just noticing the WM and HAZ. Furthermore, no differences were observed in the PMZ in the root area for plasma-AC (Figure 6.64c) and plasma-DC (Figure 6.65c).

As the aluminum alloy for the 15 mm thick joints is the same as for the previously analyzed 10 mm thick joints, the microstructure in the joints is the same (Figure 9.21 and Figure 9.22). The main difference lies in the higher cooling rate due to the greater thickness of the 15 mm joints. Therefore, the microstructure is more refined. In addition, it was observed that the single MIG process (Figure 9.22) has more internal porosities than the hybrid processes (Figure 9.21), this because the single MIG process has less energy.

6.5.2 Mechanical properties

Microhardness tests were performed for the joints with 10 mm thickness, extracting 3 samples for each joint. In Figure 6.67 the microhardness profile in the upper region of the joint is compared, 1 mm below the surface. The characteristically microhardness profile of the aluminum with a wide heat affected zone (HAZ) is observed. The behavior of the microhardness is similar for AC and DC, however, the joints made with plasma-DC are softer than AC, due to the higher power reached with plasma-DC. With higher power means higher heat input and, therefore, the width of the HAZ increases. Gürel et al. [24] mention that this behavior is especially true for the precipitation-hardenable aluminum alloys. On the other hand, it is observed that in the weld metal (WM) there is a slight difference in the microhardness being harder the WM made by plasma-AC due to finer grains in comparison with the obtained by plasma-DC (Figure 6.64). The PMZ is well defined and for plasma-DC has a lower value than for AC, as observed for the HAZ. The PMZ is a transition area between the WM and HAZ. Normally, a part of grains in PMZ are finer than those in HAZ and the other part of grains are similar to the grains of HAZ. However, the values of microhardness in PMZ decreases rapidly from a higher value to a lower value. Another reason is that the temperature in a part of PMZ (finer grains) is high enough to achieve the solution temperature, which causes the precipitates strengthening phase (Mg_2Si) dissolving into the solid solution and

becoming a supersaturated solid solution. Then the re-precipitation does not occur due to the insufficient cooling time.

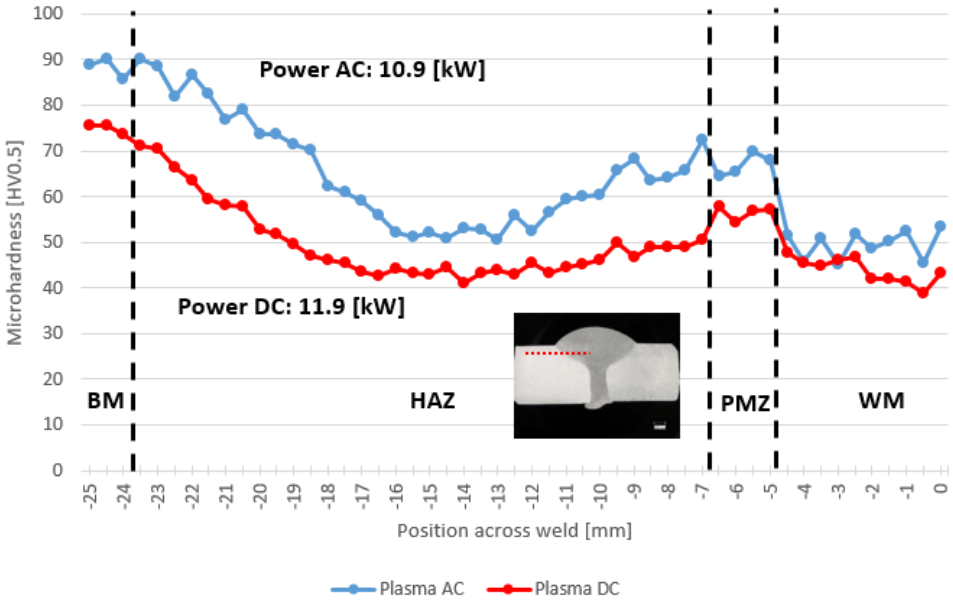

Figure 6.67 - Microhardness profiles of the weld beads made by the paraxial hybrid plasma-MIG process with plasma AC and DC. Aluminum joint 10 mm thick.

Mikrohärteprofile der Schweißraupen hergestellt nach dem paraxialen Plasma-MSG-Hybridverfahren mit Plasma-AC und DC. Aluminiumverbindung 10 mm dick.

The microhardness in the root region was also measured and the behavior of the profile has no significant differences between both types of currents (Figure 6.68). However, the PMZ is not well defined as in the face region mainly because the cooling rate in the root region is higher, influenced by the copper backing bar.

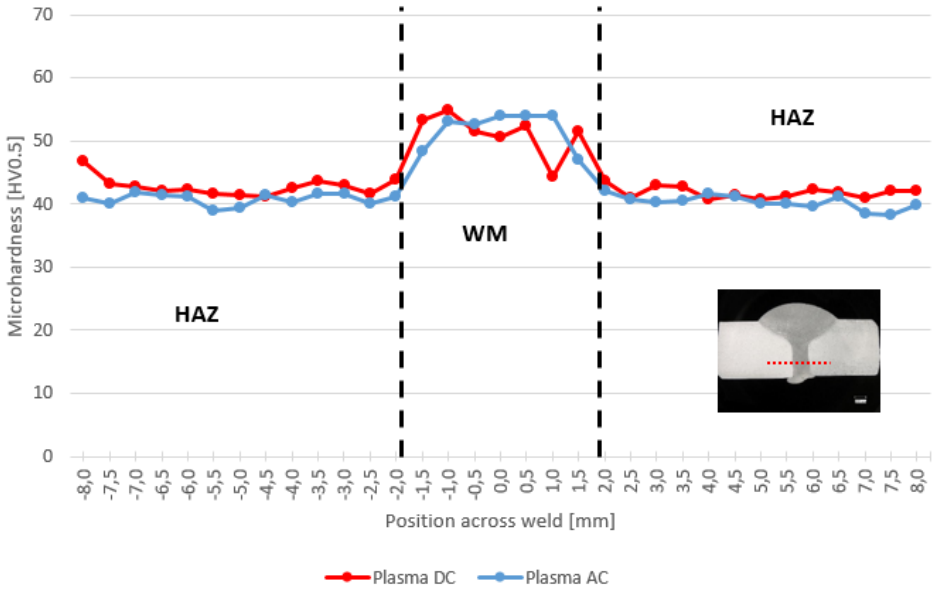

Figure 6.68 - Microhardness profiles across the root weld beads made by the paraxial hybrid plasma-MIG process with alternating and direct current. Aluminum joints 10 mm thick.

Mikrohärteprofile über den Schweißraupen, hergestellt nach dem Plasma-MSG-Paraxialverfahren mit Wechsel- und Gleichstrom. Aluminiumverbindung 10 mm dick.

The average microhardness for each region demonstrates that the hybrid process with plasma-AC is slightly harder than with plasma-DC, especially in the PMZ (Figure 6.69). Furthermore, the HAZ did not present significant differences for each type of current. On the other hand, it is observed that in the root area, the microhardness is greater in comparison to the face of the joint, which is due to the rapid cooling to which this zone is subjected, promoting grains finer and, therefore, increasing the microhardness of the area.

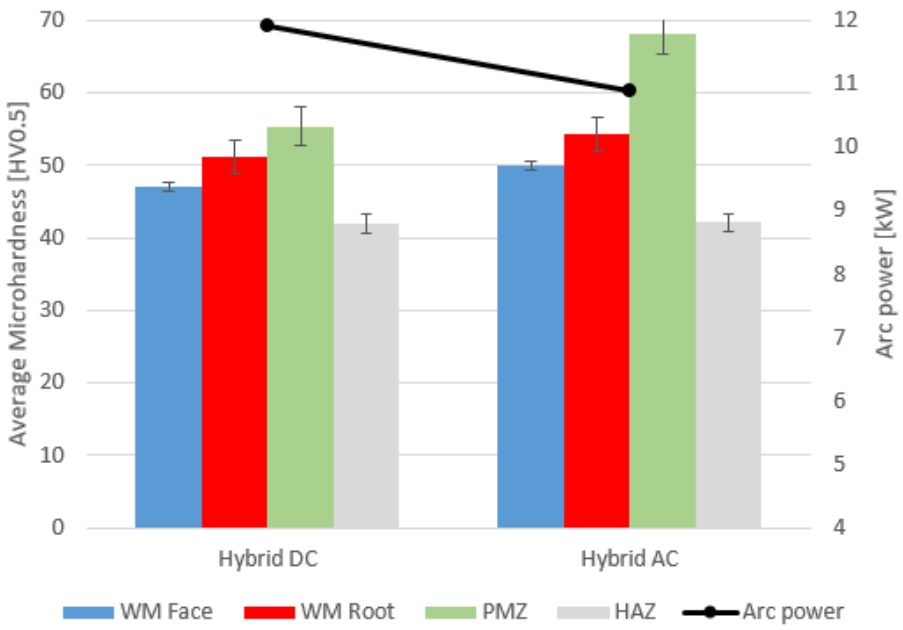

Figure 6.69 - Average microhardness and arc power for paraxial plasma-MIG process with plasma-DC and AC. Aluminum joint 10 mm thick.

Durchschnittliche Mikrohärte und Lichtbogenleistung für den paraxialen Plasma-MSG-Prozess mit Plasma-DC und AC. Aluminiumverbindung 10 mm dick.

Figure 6.70 compares the microhardness profiles for joints of 15 mm thick in the upper region of the joints and 1 mm below the surface. The weld beads made by the SuperMIG have the lowest microhardness, while the single MIG process and the plasma-MIG had similar microhardness values, however, the HAZ of the hybrid processes were wider than the single MIG process. The arc power of the SuperMIG arc was 16.2 kW, while the paraxial hybrid plasma-MIG process was 15.4 kW and the single MIG process was 9.5 kW. The arc power in the SuperMIG explains the lowest microhardness observed in the Figure 6.70, while the lowest arc power in the MIG process explains the narrower HAZ and higher microhardness. The PMZ is not noticed in the measurements, it suggests that temperature in the PMZ was not high enough to achieve the solution temperature and then to be strengthened by precipitation phases (Mg_2Si).

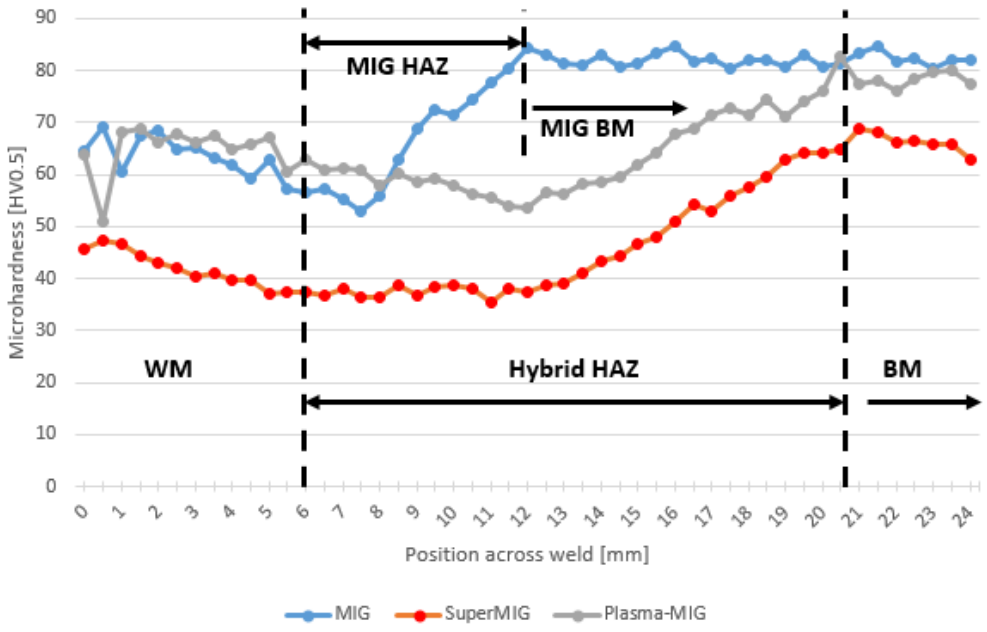

Figure 6.70 - Microhardness profiles for joints with 15 mm thick. Plasma-DC.

Mikrohärteprofile für Fugen mit 15 mm Dicke. Plasma-DC.

The average microhardness for the different regions in the weld bead cross section show that WM in the root region is slightly harder than in the face area, this is due to finer grains obtained by the higher cooling speed (Figure 6.71). Comparing the welding processes, MIG single process has the higher microhardness, mainly because the low arc power promotes higher cooling speeds.

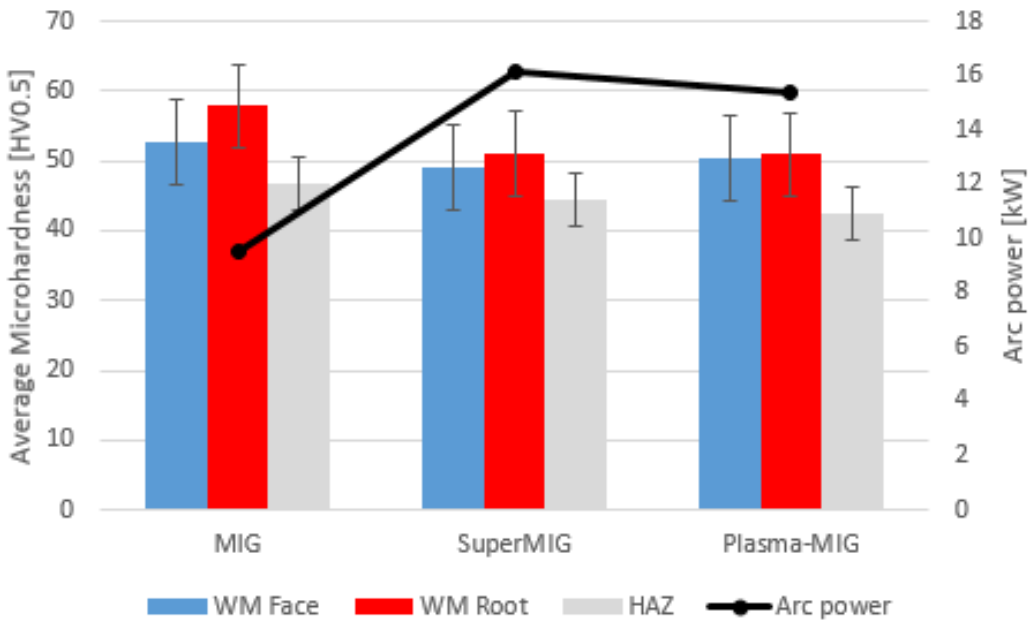

Figure 6.71 – Average microhardness and welding arc power comparison between different welding processes for a joint of 15 mm thickness. Plasma-DC.

Vergleich der durchschnittlichen Mikrohärte und der Lichtbogenleistung zwischen verschiedenen Schweißprozessen für eine Verbindung mit einer Dicke von 15 mm. Plasma-DC.

Tensile stress and elongation of the joints with 10 mm thick did not present significant differences as observed in the Figure 6.72, discarding an influence of the type of plasma current on the mechanical resistance of the joints. Figure 9.23 shows the samples after the tensile stress test. It can be seen that the joints are deformed and necking occurred before fracture. The fracture area is in HAZ, roughly 15-20 mm from the center of the WM. The joint demonstrated relatively good deformation capability before fracture. Comparing the fracture position of the Figure 9.23 and the microhardness profile of the Figure 6.67 is noticed that the fracture occurs in the most softener area of the HAZ. This behavior was also noticed by Liang et al. [54] with the TIG-MIG hybrid process in the alloy 6061-T6.

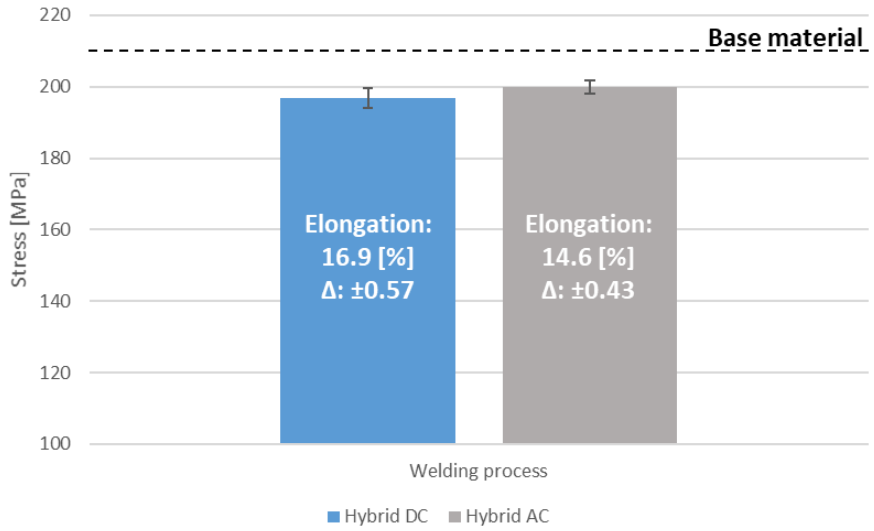

Figure 6.72 - Stress of the welding joints for plasma-MIG paraxial hybrid process with plasma DC and AC. Aluminum joints 10 mm thick.

Spannung der Schweißverbindungen für den paraxialen Plasma-MSG-Hybridprozess mit Plasma-DC und -AC. Aluminiumverbindung 10 mm dick.

Tensile stress tests for joints with 15 mm thick show that a single MIG process has around 20 MPa more of mechanical strength (Figure 6.73), while the elongation is lower in comparison with the joints made by hybrid processes. On the other hand, the SuperMIG process has the lowest strength resistance, mainly promoted by the higher arc power that produced the softener HAZ. Figure 9.24 shows the failure region of the tensile samples, noticing that fractures are located in the HAZ for all welding processes.

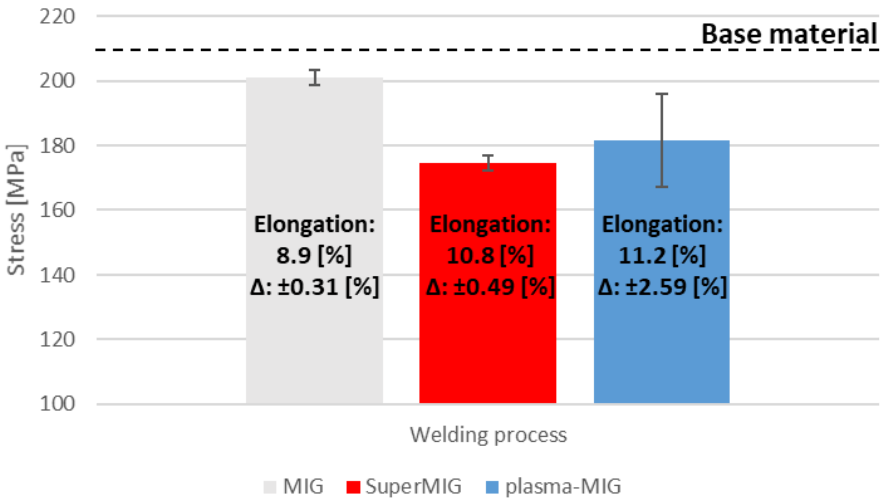

Figure 6.73 – Average tensile stress of 15 mm joints made by different welding processes. Plasma-DC.

Durchschnittliche Zugspannung von 15 mm dicken Verbindungen, die durch unterschiedliche Schweißverfahren hergestellt wurden. Plasma-DC.

6.5.3 Hydrogen measurements

Measurements of the amount of hydrogen in the face and in the root area were made as presented in Figure 6.74, showing that plasma-DC had a lower amount of hydrogen compared to AC. In addition, the highest concentrations of hydrogen were in the face region of the weld beads. The higher power of the hybrid process with plasma-DC could explain the lower amount of hydrogen in its joints, giving more time to the hydrogen to diffuse outside of the weld bead. Furthermore, the stability of the hybrid process with plasma DC would reduce the disturbance in the shielding gas, diminishing the quantity of air in contact with the molten pool. The face area had the highest concentration of hydrogen because is where the gases enter and exit from the molten pool. In addition, the hydrogen that diffuse from the root region, also diffuse towards the face region, making this area the most prone to gas concentrations. When the hydrogen amounts of the base material and the wire-electrode are compared with the total amount in the weld beads, it is observed that the hydrogen increases in about 5 times.

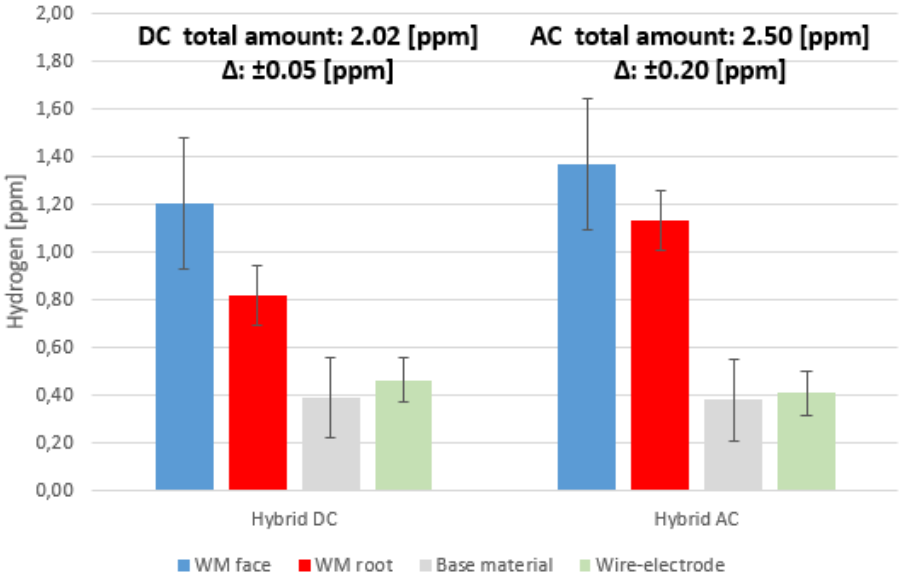

Figure 6.74 - Average hydrogen content in the joints, base material and wire-electrode for paraxial hybrid plasma-MIG process with plasma-DC and AC.

Durchschnittlicher Wasserstoffgehalt in den Verbindungen, im Grundmaterial und in der Drahtelektrode für den paraxialen Plasma-MSG-Hybridprozess mit Plasma-DC und -AC.

The X-ray images in the Figure 9.25 show internal porosities in the joint made with hybrid AC process, however, it is not possible to discard the presence of pores in the joint made with plasma-DC. Gürel et al. [24] mentioned that big pores are bubbles formed when during the cooling and solidification decreases the hydrogen solubility, specially a sharp drop at the solidification temperature between liquid and solid. Thus, if the bubbles cannot float out from the weld pool before solidification, they will form pores in the weld bead (Figure 9.25b).

The Figure 6.75 shows the hydrogen amount in the joints of 15 mm thick, noticing that the paraxial plasma-MIG process had the higher amount, especially in the root region. Comparing the hydrogen distribution with the joints of 10 mm thickness, it is noticed that 15 mm thickness concentrated it mainly in the root region. This behavior could be promoted by the higher cooling rates, this cause that molten pool cool down faster and then the hydrogen bubbles have no time to diffuse from the root to the face of the weld bead. However, as observed in the cross sections in the Figure 6.62, internal porosities are not noticed and mechanical properties were not influenced by the hydrogen content.

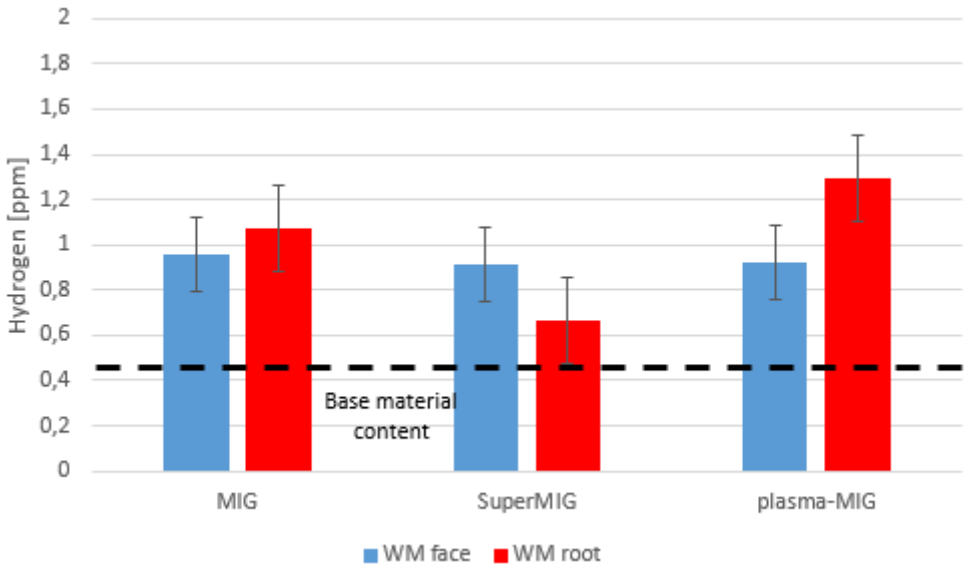

Figure 6.75 – Hydrogen content in 15 mm thickness joints. Plasma-DC.

Wasserstoffgehalt in 15 mm dicken Fugen. Plasma-DC.

6.5.4 Conclusions

All joints made of 10 mm aluminum plates without joint preparation had total penetration, independent of the type of current in the plasma process. Although, the joints made with alternating current had a higher amount of hydrogen than those made with direct current. The tensile tests did not show significant differences, being able to conclude that there is no significant influence in the tensile stress when the hybrid process is configured with plasma-AC or DC. However, the hybrid process becomes more stable when working with plasma-DC. Furthermore, the tungsten electrode has a longer useful life with direct current, positively influencing the productivity of the welding process.

The results also demonstrate that it is possible to make joints of 15 mm thickness in one pass with all the welding processes tested, however, the hybrid processes demonstrated are superior in weld bead appearance and arc stability. Furthermore, the differences between the SuperMIG and paraxial plasma-MIG process were not significant. The higher arc power of the hybrid process made the difference to reach a good penetration profile and contact angle in the reinforcement. Joints without gaps were not possible to make due to large amount of material provided to the molten pool by the higher wire feed speed, reducing the penetration and influencing the arc stability.

7 Conclusions and Outlook

This work presented the complex interaction between MIG and plasma processes when they are coupled in a tandem configuration to form a hybrid welding process, with the main objective to take advantage of the key characteristics of each one and in a synergic way to increase the productivity in the task of making welded joints. Furthermore, a direct comparison of both welding arcs with different types of static welding source characteristics was presented for the first time, which directly influences the behavior and stability of the hybrid welding process.

The gradual hybridization between the plasma and MIG processes showed that there is a strong interaction between them from the 25 mm distance between the welding torches. From this distance both welding arcs establish a plasma or current path, which allows them to exchange electrically charged particles that affect the normal behavior of the electrical signals of the welding process. This interaction is reflected in a strong voltage drop in the plasma process and an increase in current in the MIG process. In addition, the stability of the MIG process is strongly affected and the welding parameters must be adjusted to establish a new point of stability between the two processes.

Once the current path is established no significant differences in weld beads penetration were found for torch distances less than 25 mm. However, it was observed that the interaction of the welding arcs tends to be unstable when they are closer to each other. This instability is improved when the welding parameters are adapted, i.e. when an energy balance between them is established. This energy balance does not follow any particular criteria and only one study has proposed this parameter as an indicator of the stability of the hybrid process. However, it is recommended that one of the welding processes be the one with the highest energy. In the specific case of this study, it is recommended that the MIG process be the most energetic.

The use of a MIG process with different metallic transfer (Spray and Pulsed) had a direct influence on the arc length behavior of the MIG process. The current path transfers current to the MIG process from the plasma process, which increases the melting rate of the wire-electrode and affects the self-regulation system of the arc length for welding sources with static characteristics of constant voltage. This

phenomenon intensifies as the plasma current increases, reaching a point where the contact tip of the MIG torch is melted. On the other hand, with a Pulsed metal transfer configured this does not happen, because the arc length is regulated by an internal control system of the welding source, therefore, the arc length tends to be constant as the plasma current increases.

The use of alternating current in the plasma process to ensure cathodic cleaning in the aluminum joints proved not to be necessary. The MIG process performs the function of filling the joint and at the same time performing cathodic cleaning, while the plasma process establishes a keyhole or preheats the base material (depending on the configured current). In addition, the hybrid process proved to be more stable with direct current in the plasma process.

Studying the commercial version of the hybrid plasma-MIG process (SuperMIG) no significant differences were found when compared to the results obtained by joining the torches of each welding process independently. This also rules out the need for an external magnetic field to stabilize the welding arcs. The results of the joints made by each welding process do not show significant differences in the tensile strength and hydrogen content inside the joints. From this application the single MIG process still proves to be competitive compared to the hybrid option, where for 15 mm joints plasma-MIG proves to have a slight advantage compared to the MIG process.

Despite the acquired results and research in the hybrid processes, open tasks and unanswered questions remain. These are: determine the physical properties of the current path, measure metal vapors (by spectrometry) to estimate the minimum amount needed for current exchange, all this with the main objective of establishing a model of the current path. Also a study focusing on the deposition rate of the MIG process when influenced by the current path is recommended, as this would affect aspects such as vapor recoil pressure and the Marangoni effect in the molten pool. Based on the results obtained in this work, it is recommended to continue the research by changing the plasma process to the TIG process, because the latter can work with currents higher than 300 A, which would help to increase the productivity of the hybrid process in welding joint applications, reaching higher energy balances from those used in this work.

8 References

1. Scotti A, Ponomarev V (2008) Soldagem MIG/MAG: Melhor entendimento, melhor desempenho. Artliber, São Paulo
2. Essers WG, Willems GAM, Buelens JJC et al. (1981) Plasma-MIG welding – a new torch and arc starting method. Metal Construction: 36–42
3. GSI SLV München (2013) Entwicklung einer seriellen Kopplung des Plasma - und MSG- Prozesses zur Erhöhung der Wirtschaftlichkeit und Prozesssicherheit beim Schweißen im Anlagen- und Behälterbau: Schlussbericht: IBS 3621b/175/2-IGF 0811-0002 (5158)
4. Cunha TV, Dutra JC (2007) Processo Plasma-MIG – Contribuição do Arco Plasma na Capacidade de Fusão do Arame. Soldag. insp. 12(2): 89–96
5. Oliveira MA, Dutra JC (2007) Electrical model for the plasma-MIG hybrid welding process. Welding and Cutting 6(6): 324–328
6. Wu D, Tashiro S, WU Z et al. (2020) Interactive Phenomena in Hybrid KPAW–GMAW-P. WJ 99(5): 146–155. doi: 10.29391/2020.99.014
7. Han Y, Tong J, Hong H et al. (2018) The influence of hybrid arc coupling mechanism on GMAW arc in VPPA-GMAW hybrid welding of aluminum alloys. Int J Adv Manuf Technol 18: 679. doi: 10.1007/s00170-018-3007-5
8. WeldObot (2019) Hybrid Plasma-GMAW (SuperMIG®). https://weldobot.com/technology-1. Accessed 02 Oct 2019
9. Hong H, Han Y, Tong J et al. (2016) Study of arc shape and voltage-current characteristics in variable polarity plasma arc-MIG hybrid welding of aluminum alloys 37: 65–69
10. Huber M, Müller M, Cramer H (2015) Serial coupling of the plasma and GMA processes in order to increase the economic viability and process reliability of welding in installation engineering and tank construction. Welding and Cutting 14(3): 168–172
11. Guo Y, Pan H, Ren L et al. (2018) An investigation on plasma-MIG hybrid welding of 5083 aluminum alloy. Int J Adv Manuf Technol 98(5-8): 1433–1440. doi: 10.1007/s00170-018-2206-4
12. Welding Solutions I (2007) Hybrid welding: an alternative to SAW. Welding Journal 10: 42–45

13. Kanemaru S, Sasaki T, Sato T et al. (2014) Study for TIG–MIG hybrid welding process. Weld World 58(1): 11–18. doi: 10.1007/s40194-013-0090-y
14. Kanemaru S, Sasaki T, Sato T et al. (2015) Study for the mechanism of TIG-MIG hybrid welding process. Weld World 59(2): 261–268. doi: 10.1007/s40194-014-0205-0
15. Salonitis K, Pandremenos J, Paralikas J et al. (2009) Multifunctional Materials Used in Automotive Industry: A Critical Review. In: Pantelakis S, Rodopoulos C (eds) Engineering Against Fracture, vol 20. Springer Netherlands, Dordrecht, pp 59–70
16. Miller WS, Zhuang L, Bottema J et al. (2000) Recent development in aluminium alloys for the automotive industry. Materials Science and Engineering: A 280(1): 37–49. doi: 10.1016/S0921-5093(99)00653-X
17. Carle D, Blount G (1999) The suitability of aluminium as an alternative material for car bodies. Materials & Design 20(5): 267–272. doi: 10.1016/S0261-3069(99)00003-5
18. The Aluminium Association (2001) Aluminium: The Corrosion Resistant Automotive Material
19. Löveborn D, Larsson JK, Persson K-A (2017) Weldability of Aluminium Alloys for Automotive Applications. Physics Procedia 89: 89–99. doi: 10.1016/j.phpro.2017.08.011
20. IEA (2020) Energy intensity of passenger transport modes, 2018. https://www.iea.org/data-and-statistics/charts/energy-intensity-of-passenger-transport-modes-2018. Accessed 17 Apr 2020
21. Santos MC, Machado AR, Sales WF et al. (2016) Machining of aluminum alloys: a review. Int J Adv Manuf Technol 86(9-12): 3067–3080. doi: 10.1007/s00170-016-8431-9
22. Europäischen Komitees für Normung (2005) Aluminium und Aluminiumlegierungen - Chemische Zusammensetzung und Form von Halbzeug: DIN EN 573: 1–10
23. Europäischen Komitees für Normung (2016) Aluminium und Aluminiumlegierungen – Halbzeug – Bezeichnungen der Werkstoffzustände: DIN EN 515: 1–24

24. Çam G, İpekoğlu G (2017) Recent developments in joining of aluminum alloys. Int J Adv Manuf Technol 91(5-8): 1851–1866. doi: 10.1007/s00170-016-9861-0
25. Kou S (2003) Welding metallurgy, 2nd ed. Wiley-Interscience, Hoboken N.J.
26. International Institute of Welding (1984) The Physics of Welding, J. F. Lancaster. Robert Maxwell, M.C.
27. Kiyohara M, Yamamoto H, Harada S (1979) Melting characteristics of a wire electrode in the MIG-welding of aluminum. Arc Physics and Weld Pool Behaviour: 165–175
28. Dutra JC, Quites AM (1979) Tecnologia da Soldagem a Arco Voltaico, Florianópolis
29. Mathers G (2005) The welding of aluminium and its alloys. CRC Press/Woodhead Pub, Boca Raton FL
30. Rose S, Zähr M, Schnick M et al. (2011) Arc attachments on aluminium during tungsten electrode positive polarity in TIG welding of aluminium. Weld World 55: 91–99
31. Sarrafi R, Kovacevic R Cathodic cleaning of oxides from aluminum surface by variable-polarity arc
32. da Silva CLM, Scotti A (2006) The influence of double pulse on porosity formation in aluminum GMAW. Journal of Materials Processing Technology 171(3): 366–372. doi: 10.1016/j.jmatprotec.2005.07.008
33. Resigen U, Willms K, Wieland S The aging effects of aluminum magnesium alloy welding wires. Welding Journal 1(97): 26s-34s
34. Cirino LM, Dutra JC (2009) A influência do tempo de atuação da polaridade positiva na soldagem TIG CA do alumínio. Soldag. insp. 14(2): 131–139. doi: 10.1590/S0104-92242009000200005
35. Coe FR (1968) The quality assessment of gas metal arc welding wire. Welding Journal 47(8): 355s-363s
36. N.N. (1963) The Arc Welding of Aluminium. Aluminium Federation Information Bulletin 19
37. Woods RA (1974) Porosity and Hydrogen Absorption in Aluminum Welds: WJ_1974_03_s97(03): 97s-108s

38. Reisgen U, Stein L (2015) Grundlagen der Fügetechnik - Schweißen, Löten und Kleben, 1. Aufl. Fachbuchreihe Schweißtechnik, Band 161. DVS Media GmbH, Düsseldorf
39. Shore RJ, McCauley RB (1970) Effects of Porosity on High Strength Aluminum 7039: WJ_1970_07_s311. Welding Journal 49(10): 311s-321s
40. Fuji H, Aoki Y, Nogi K (2001) Electron Beam, Gas tungsten arc welding under microgravity. Trans. JWRI 30(1): 105–109
41. Guo G, Zhang M, Chen H et al. (2015) Effect of humidity on porosity, microstructure and fatigue strength of A7N01S-T5 aluminum alloy welded joints in high-speed trains. Mater. Des. 85: 309–317
42. Reisgen U, Willms K, Wieland S (2017) Influence of storage conditions on aluminum 4043A welding wires. Welding Journal 96(6): 220s-227s
43. Morais FC (2001) Influence of operational factors on porosity formation in aluminum MIG welding. MSc. Thesis, Federal University of Uberlandia
44. Canaby JL, Blazy F, Fries JF (1991) Effects of high temperature surface reaction of aluminum-lithium alloy on the porosity of welded areas. Mater. Sci. Eng. A. 136: 131–139
45. Pickens JR (1985) The weldability of lithium-containing aluminum-alloys. J. matter. Sci. 20: 4247–4258
46. Xiao RS, Yang WX, Chen K (2007) Porosity characterization in laser welds of Al-Li alloy 1420. Appl. Laser 27: 13–17
47. Çam G, Ventzke V, Dos Santos JF et al. (2000) Characterization of laser and electron beam welded Al-alloys. Prakt. Metallogr. 37(2): 59–89
48. Chen K, Yang WX, Xiao RS (2012) Direct laser welding for Al-Li alloy plate without prior surface cleaning. Laser Eng. 23: 361–369
49. Xiao R, Zhang X (2014) Problems and issues in laser beam welding of aluminum-lithium alloys. J Manuf Process 16: 166–175
50. (2014) Methode zur Bestimmung des Wasserstoffgehaltes von Massivdrähten und -stäben aus Aluminiumlegierungen für das Lichtbogen- oder Strahlschweißen
51. ASTM Standard Test Method for Determination of Hydrogen in Aluminum and Aluminum Alloys by Inert Gas Fusion(E2792 - 13)

52. e Silva RHG, dos Santos Paes LE, Barbosa RC et al. (2018) Assessing the effects of solid wire electrode extension (stick out) increase in MIG/MAG welding. J Braz. Soc. Mech. Sci. Eng. 40(1): 12. doi: 10.1007/s40430-017-0948-9
53. Liang Y, Hu S, Shen J et al. (2017) Geometrical and microstructural characteristics of the TIG-CMT hybrid welding in 6061 aluminum alloy cladding. Journal of Materials Processing Technology 239: 18–30. doi: 10.1016/j.jmatprotec.2016.08.005
54. Liang Y, Shen J, Hu S et al. (2018) Effect of TIG current on microstructural and mechanical properties of 6061-T6 aluminium alloy joints by TIG–CMT hybrid welding. Journal of Materials Processing Technology 255: 161–174. doi: 10.1016/j.jmatprotec.2017.12.006
55. Hong H, Han Y, Du M et al. (2016) Investigation on droplet momentum in VPPA-GMAW hybrid welding of aluminum alloys. Int J Adv Manuf Technol 86(5-8): 2301–2308. doi: 10.1007/s00170-016-8381-2
56. Sun Z, Han Y, Du M et al. (2019) An improved simulation of temperature field in VPPA–GMAW of Al–Cu–Mg alloy. Journal of Materials Processing Technology 263: 366–373. doi: 10.1016/j.jmatprotec.2018.08.017
57. Cho J, Lee J-J, Bae S-H (2015) Heat input analysis of variable polarity arc welding of aluminum. Int J Adv Manuf Technol 81(5-8): 1273–1280. doi: 10.1007/s00170-015-7292-y
58. Nikseresht Z, Karimzadeh F, Golozar MA et al. (2010) Effect of heat treatment on microstructure and corrosion behavior of Al6061 alloy weldment. Materials & Design 31(5): 2643–2648. doi: 10.1016/j.matdes.2009.12.001

9 Appendix

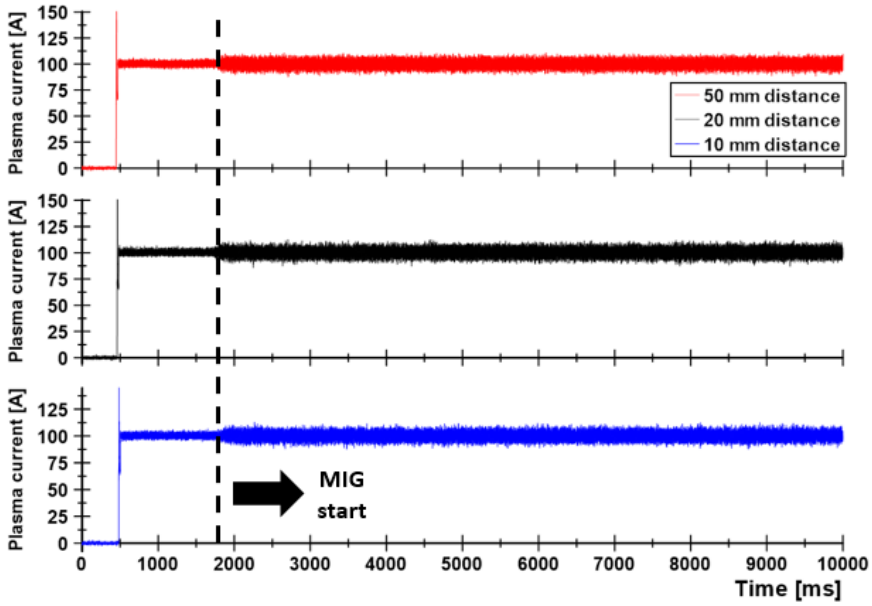

Figure 9.1 - Plasma current for different distances between torches. Plasma DC: 100 A; MIG wire feed speed: 16 m/min.

Plasmastrom für unterschiedliche Brennerabstände. Plasma DC: 100 A; MIG-Drahtvorschubgeschwindigkeit: 16 m/min.

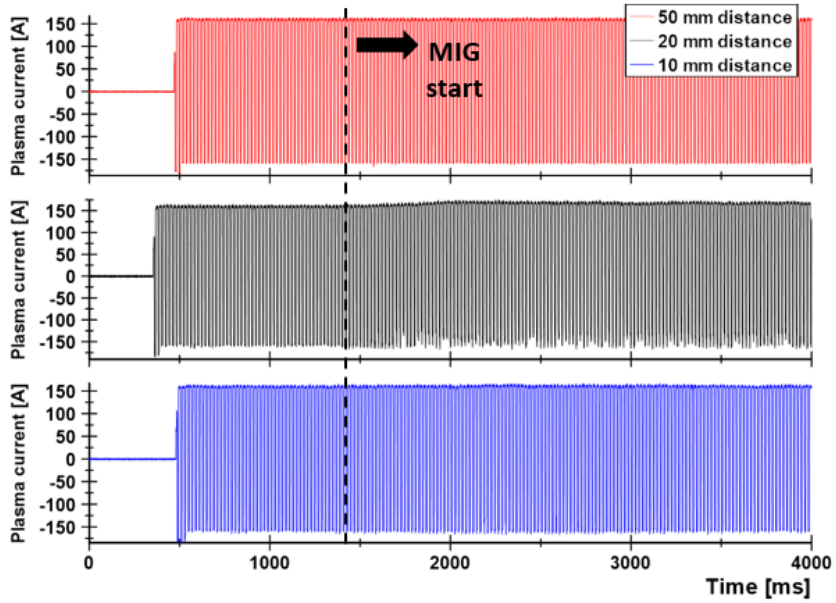

Figure 9.2 - Plasma alternating current for different distances between torches. Plasma AC: 150 A; MIG wire feed speed: 12 m/min.

Plasma-Wechselstrom für unterschiedliche Brennerabstände. Plasma-Wechselstrom: 150 A; MIG-Drahtvorschubgeschwindigkeit: 12 m/min.

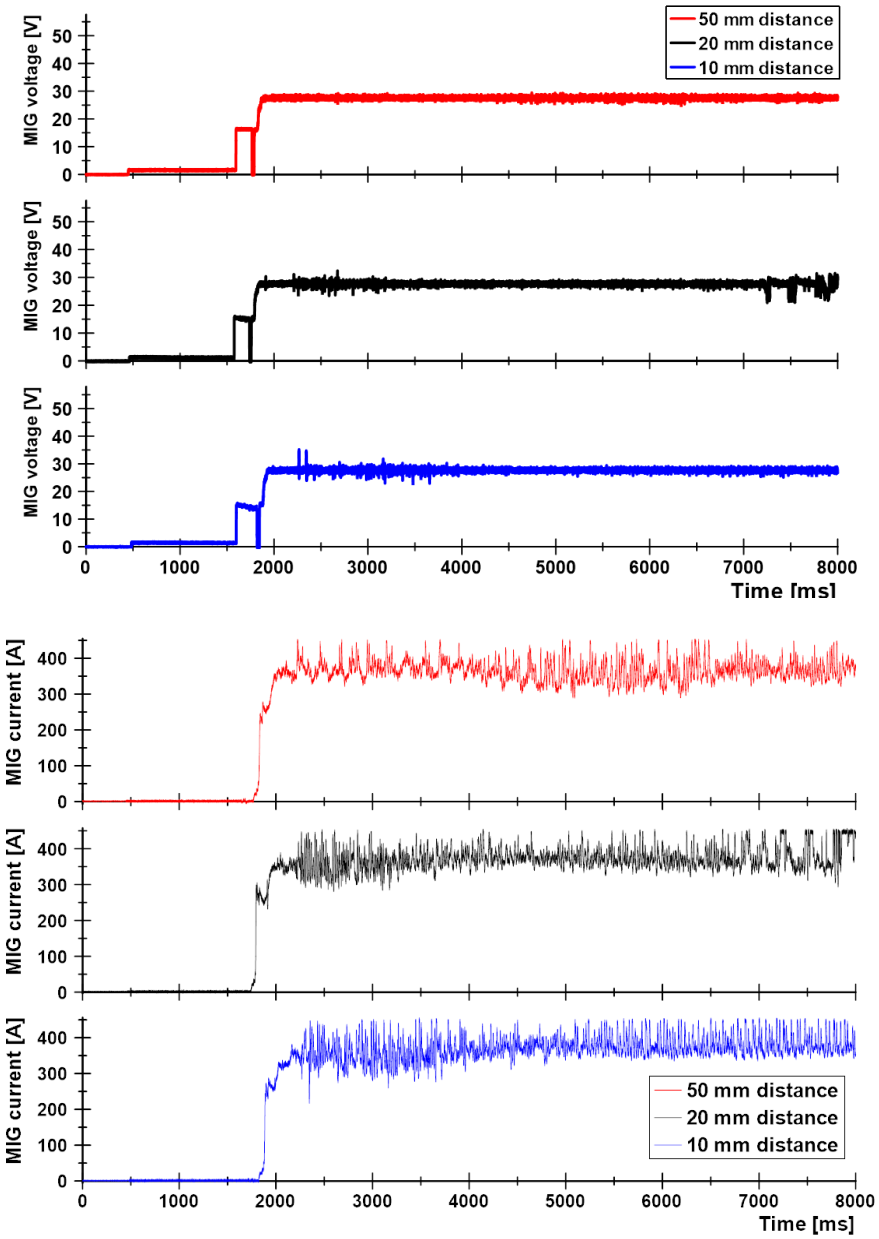

Figure 9.3 - MIG voltage and current for different distances between torches. Plasma DC: 100 A; MIG wire feed speed: 16 m/min.

MSG-Spannung und -Strom für unterschiedliche Abstände zwischen Brennern. Plasma DC: 100 A; MSG-Drahtvorschubgeschwindigkeit: 16 m/min.

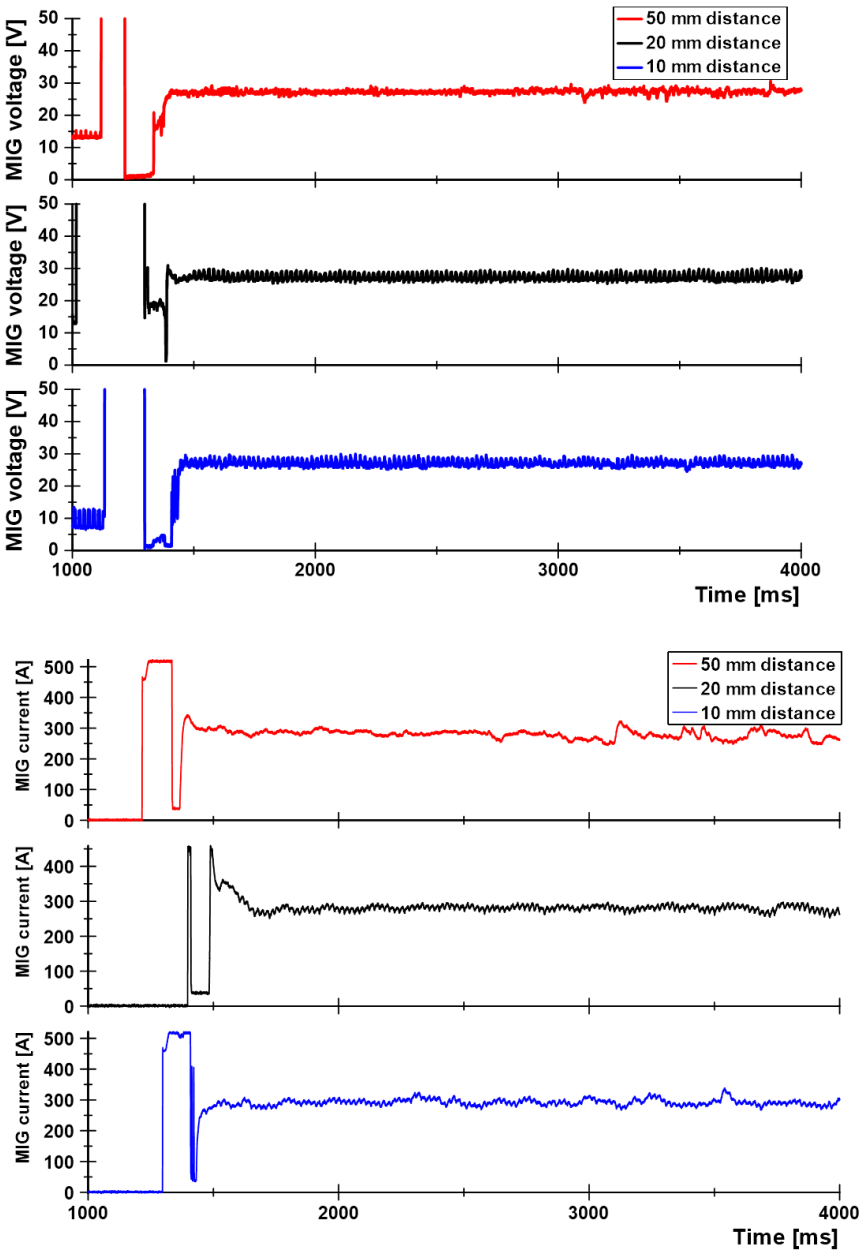

Figure 9.4 - MIG voltage and current for different distances between torches. Plasma AC: 150 A; MIG wire feed speed: 12 m/min.

MSG-Spannung und -Strom für unterschiedliche Abstände zwischen Brennern. Plasma-AC: 150 A; MSG-Drahtvorschubgeschwindigkeit: 12 m/min.

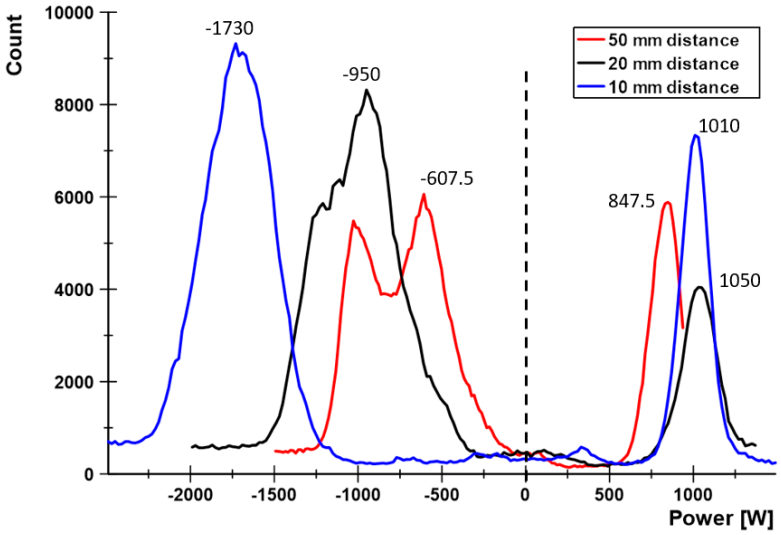

Figure 9.5 - Comparative histogram between plasma-AC powers for different distances between welding torches. Plasma-AC: 150 A; MIG wire feed speed: 12 m/min.

Vergleichendes Histogramm zwischen Plasma-Wechselstromleistungen für unterschiedliche Abstände zwischen Schweißbrennern. Plasma-AC: 150 A; MSG-Drahtvorschubgeschwindigkeit: 12 m/min.

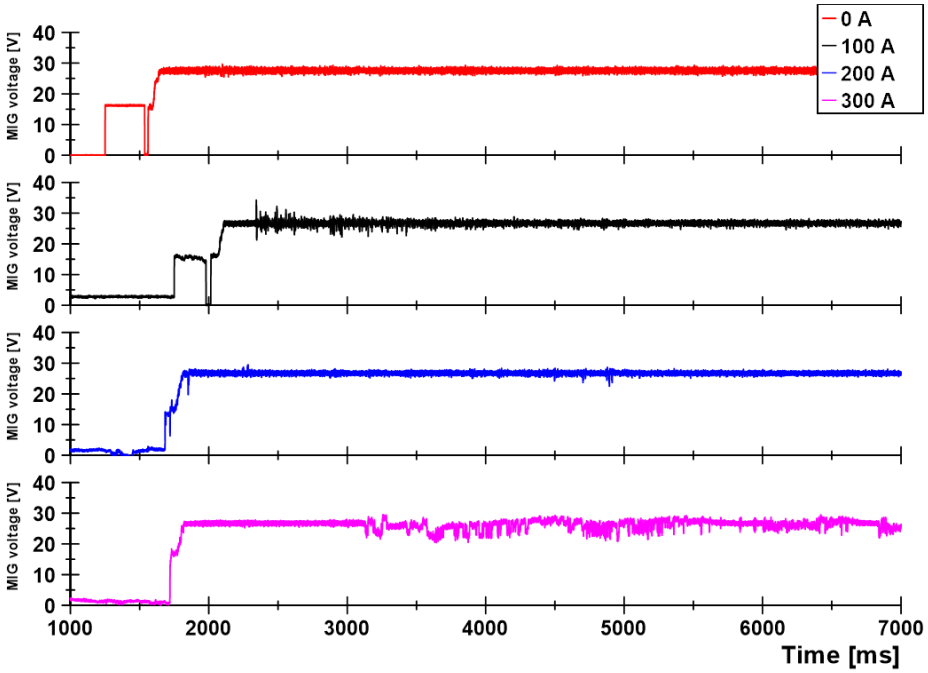

Figure 9.6 - MIG voltage for different plasma currents. MIG wire feed speed: 16 m/min.

MSG-Spannung für verschiedene Plasmaströme. MSG-Drahtvorschubgeschwindigkeit: 16 m/min.

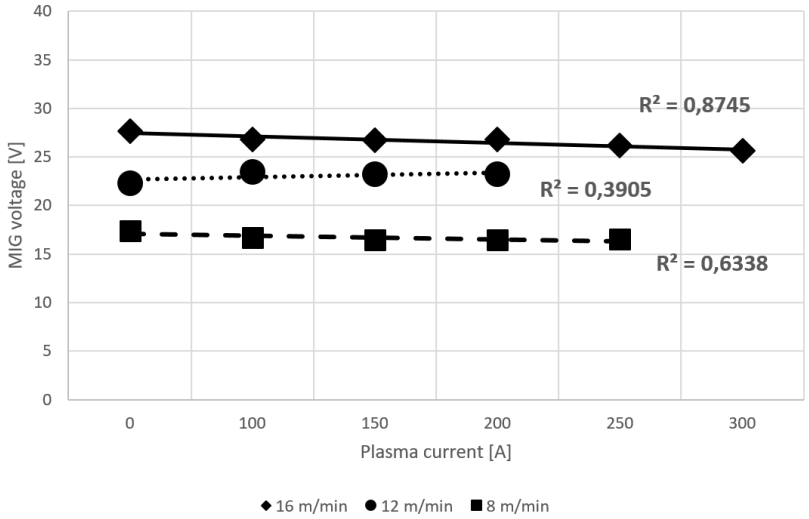

Figure 9.7 – Influence of the plasma current on MIG process voltage.

Einfluss des Plasmastroms auf die MSG-Prozessspannung.

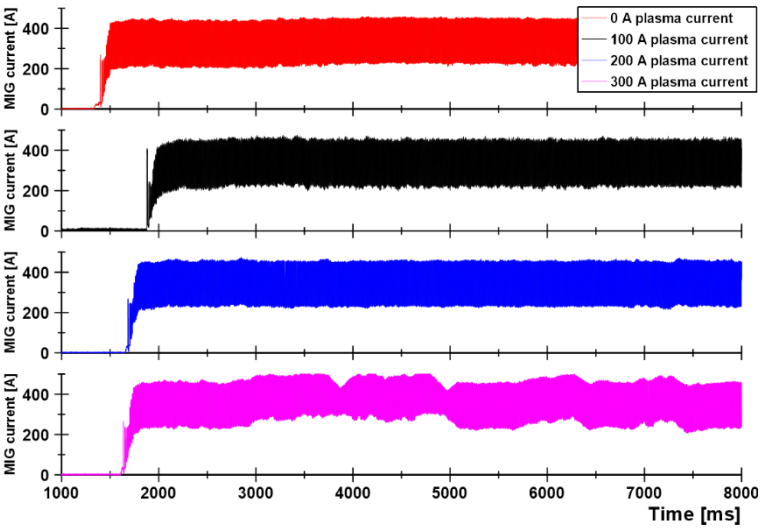

Figure 9.8 - MIG-Pulsed current for different plasma current intensities. MIG wire feed speed: 16 m/min.

MSG-Impuls Strom für verschiedene Plasmastromintensitäten. MSG-Drahtvorschubgeschwindigkeit: 16 m/min.

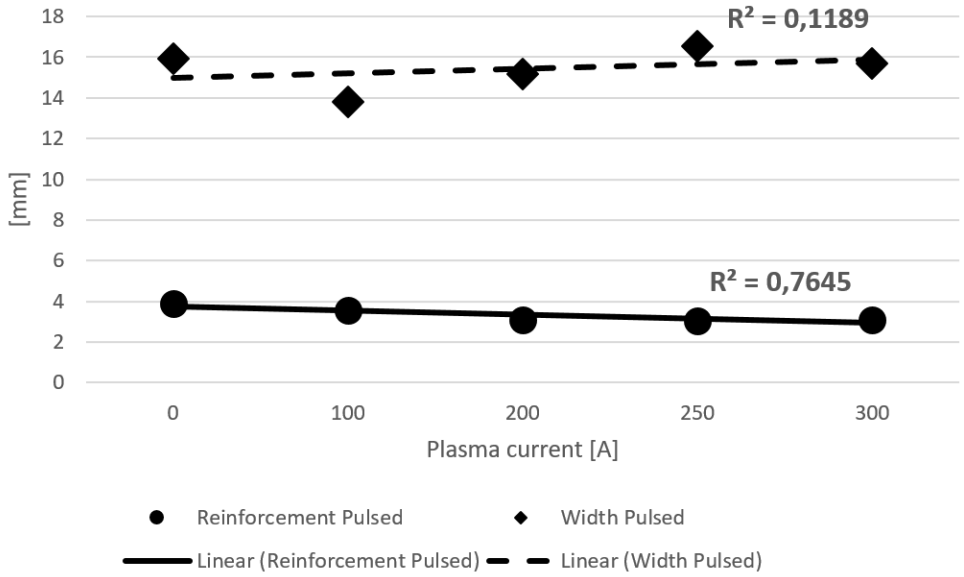

Figure 9.9 - Influence of the plasma current with MIG-Pulsed process in the width and reinforcement of the weld beads to 16 m/min of wire feed speed.

Einfluss des Plasmastroms beim MSG-Impuls-Verfahren auf die Breite und Überhöhung der Schweißraupen auf 16 m/min Drahtvorschubgeschwindigkeit.

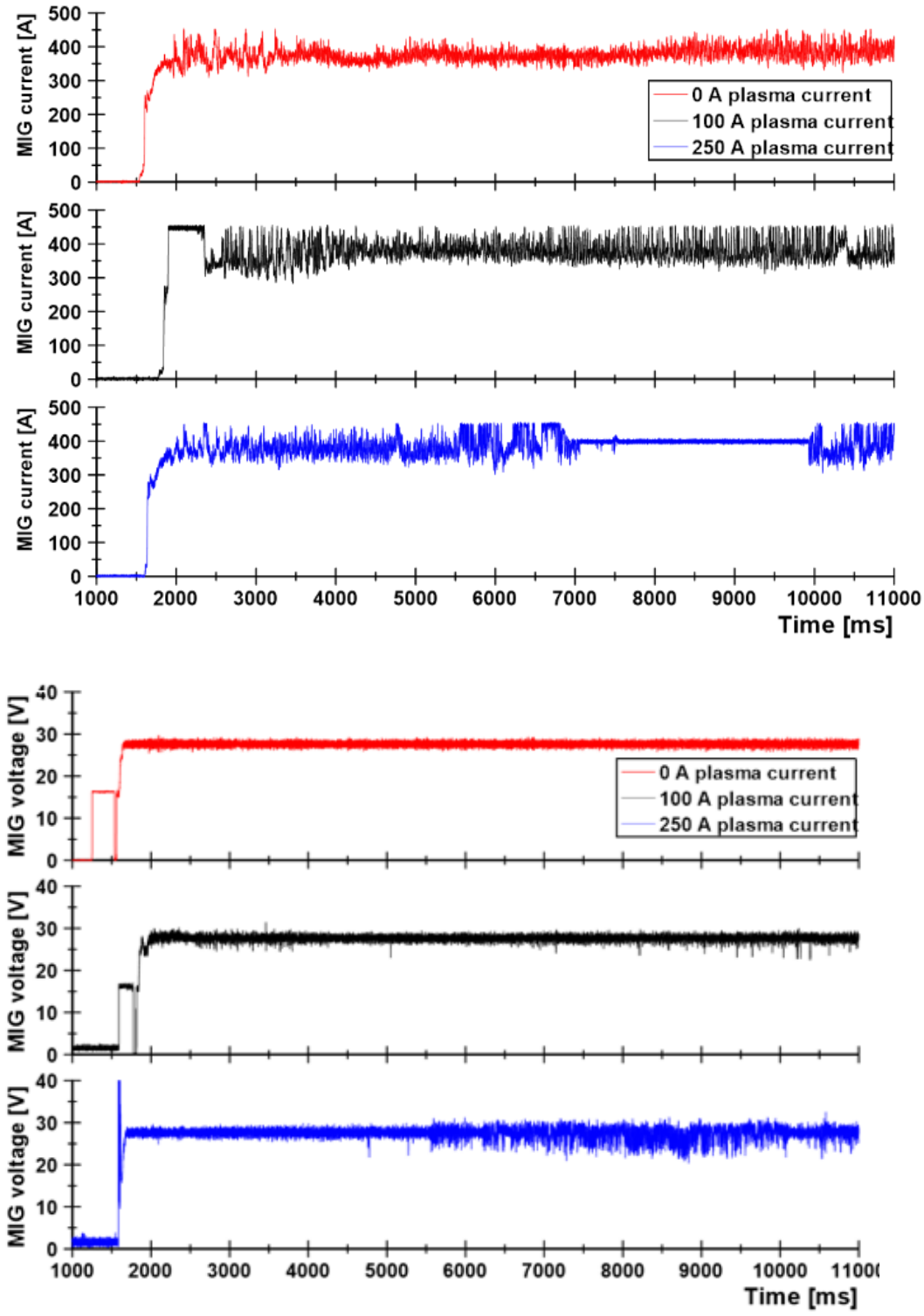

Figure 9.10 - MIG voltage and current for different plasma-AC intensities. MIG wire feed speed: 16 m/min.

MSG-Spannung und -Strom für verschiedene Plasma-Wechselstromintensitäten. MSG-Drahtvorschubgeschwindigkeit: 16 m/min.

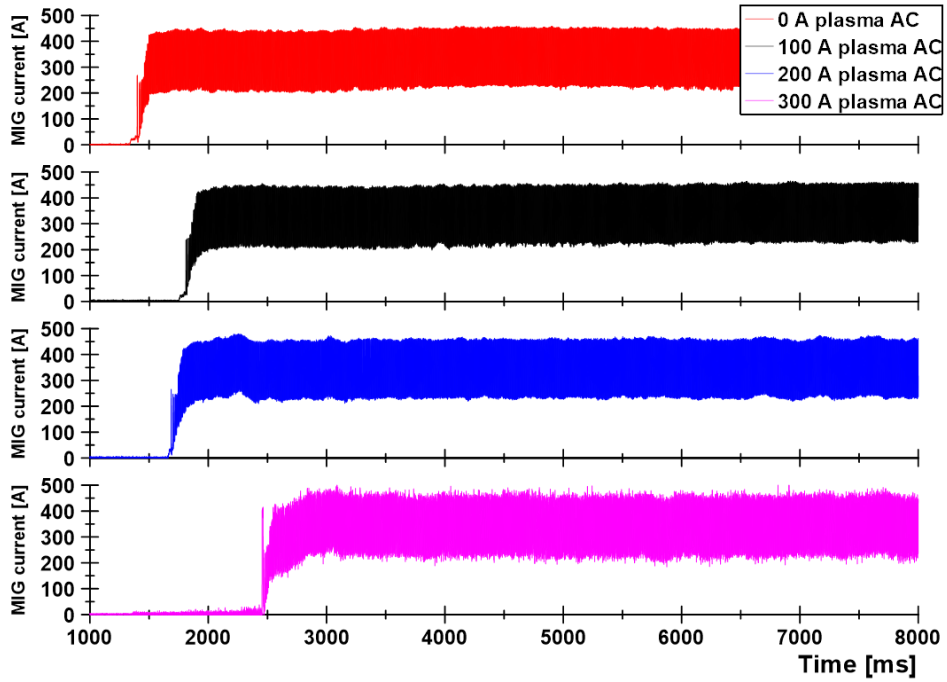

Figure 9.11 - MIG-Pulsed current for different plasma-AC. MIG wire feed speed: 16 m/min.

MSG-Impuls Strom für verschiedene Plasma-Wechselstromintensitäten. MSG-Drahtvorschubgeschwindigkeit: 16 m/min.

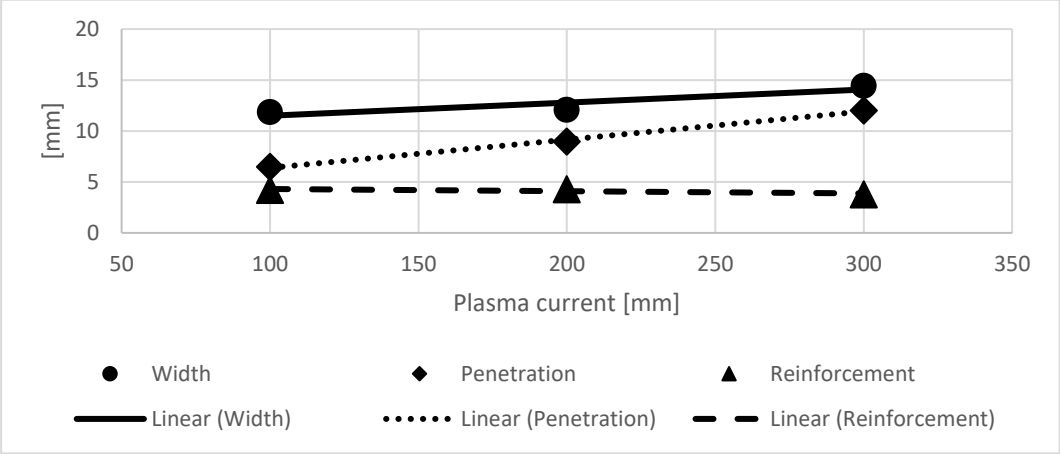

Figure 9.12 - Penetration, width and reinforcement of the weld bead cross sections made by SuperMIG with different plasma currents. MIG wire feed speed: 16 m/min; Magnetic level compensation: 40%.

Einbrand, Breite und Verstärkung der Schweißraupenquerschnitte von SuperMIG mit unterschiedlichen Plasmastromintensitäten. MSG-Drahtvorschubgeschwindigkeit: 16 m/min; Magnetpegelkompensation: 40%.

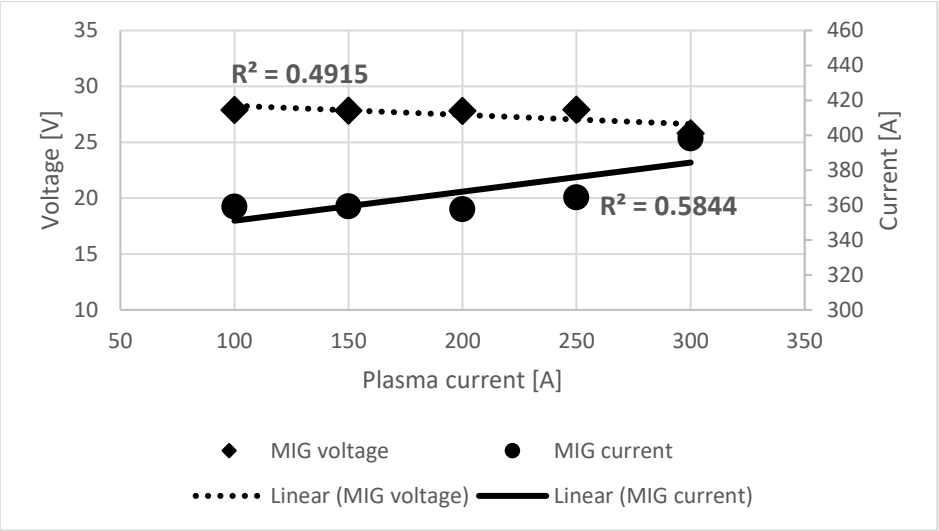

Figure 9.13 - Average voltage and current of the MIG process when the plasma current is increased. SuperMIG equipment; MIG wire feed: 16 m/min; Magnetic level compensation: 40%.

Durchschnittliche Spannung und Stromstärke des MSG-Prozesses, wenn der Plasmastrom erhöht wird. SuperMIG-Ausrüstung; MSG-Drahtvorschub: 16 m/min; Magnetpegelkompensation: 40%.

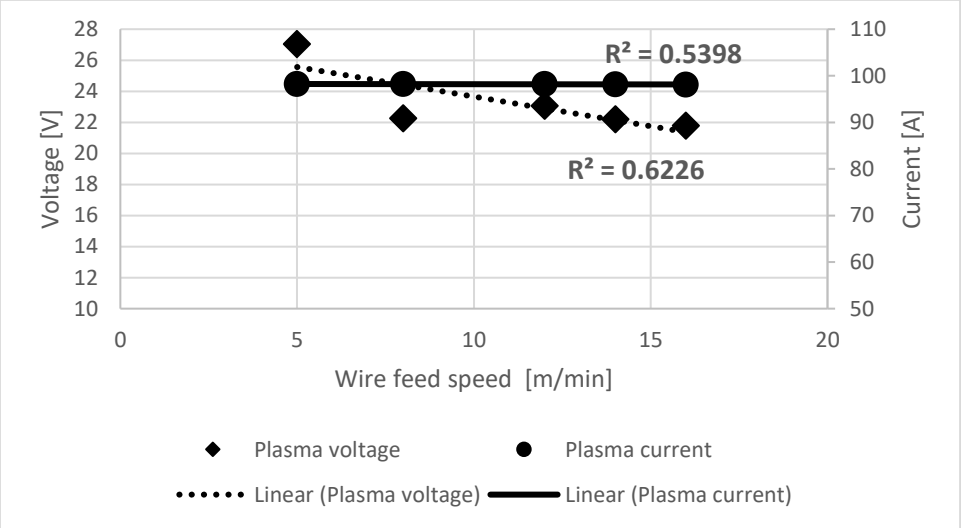

Figure 9.14 - Average voltage and current of the plasma process when the wire feed speed is increased. SuperMIG equipment; plasma current: 100 A; Magnetic level compensation: 40%.

Durchschnittliche Spannung und Stromstärke des Plasmaprozesses bei Erhöhung der Drahtvorschubgeschwindigkeit. SuperMIG-Ausrüstung; Plasmastrom: 100 A; Magnetpegelkompensation: 40%.

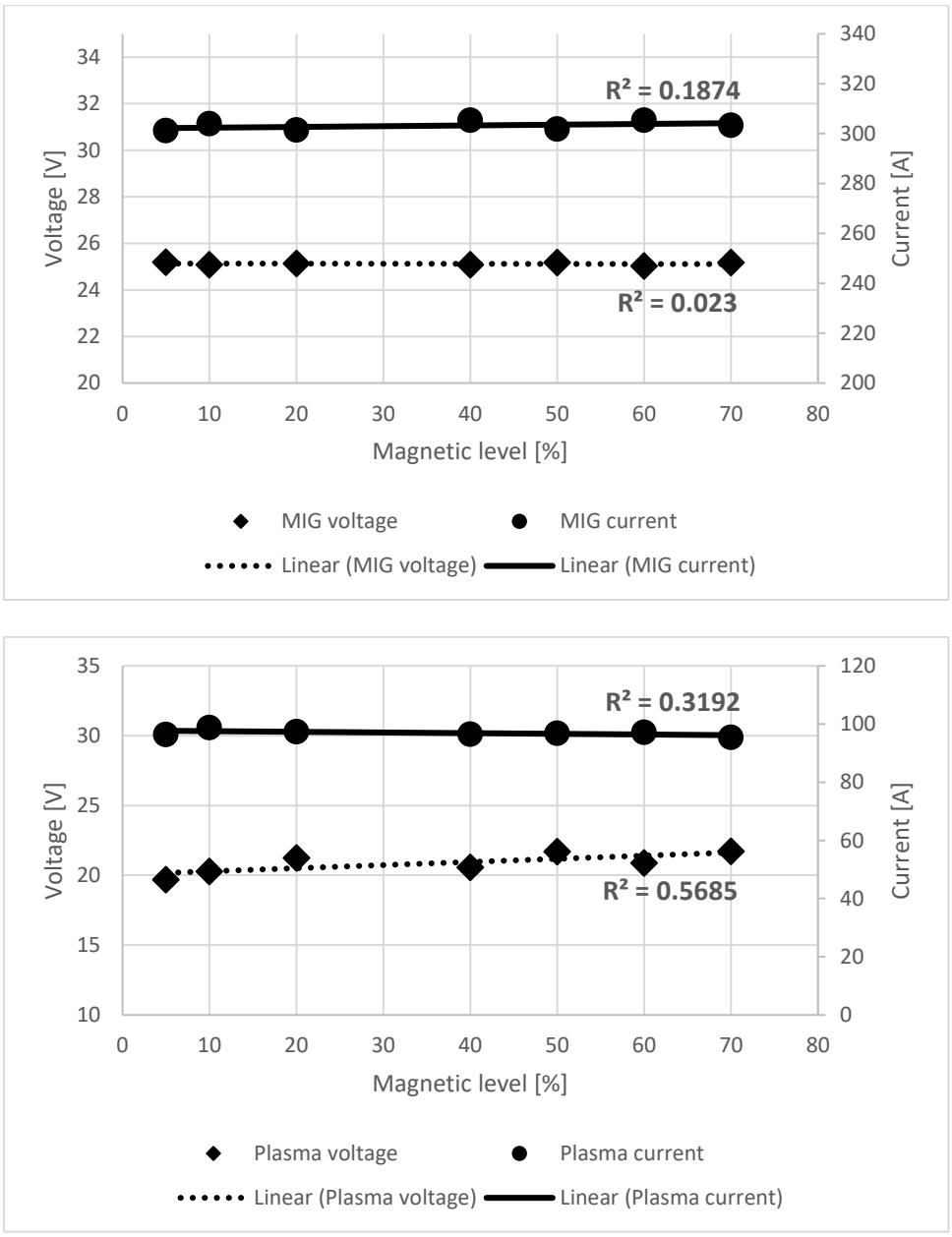

Figure 9.15 - Average current and voltage of MIG and plasma processes for different magnetic level intensities. MIG wire feed speed: 14 m/min; plasma current: 100 A.

Durchschnittlicher Strom und Spannung von MSG- und Plasmaprozessen für unterschiedliche Intensitäten des Magnetpegels. MSG-Drahtvorschubgeschwindigkeit: 14 m/min; Plasmastrom: 100 A.

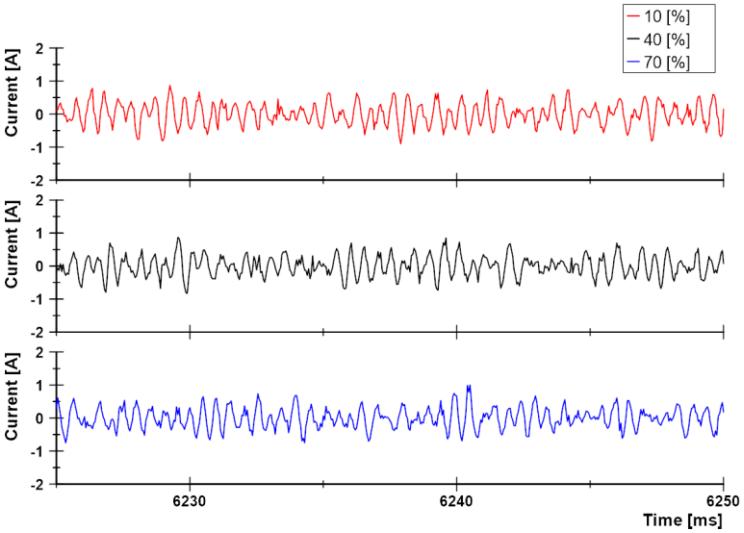

Figure 9.16 - Current signals of the electromagnets for different magnetic level compensations. MIG wire feed speed: 14 m/min; plasma current: 100 A.

Stromsignale der Elektromagnete für unterschiedliche Magnetpegelkompensationen. MSG-Drahtvorschubgeschwindigkeit: 14 m/min; Plasmastrom: 100 A.

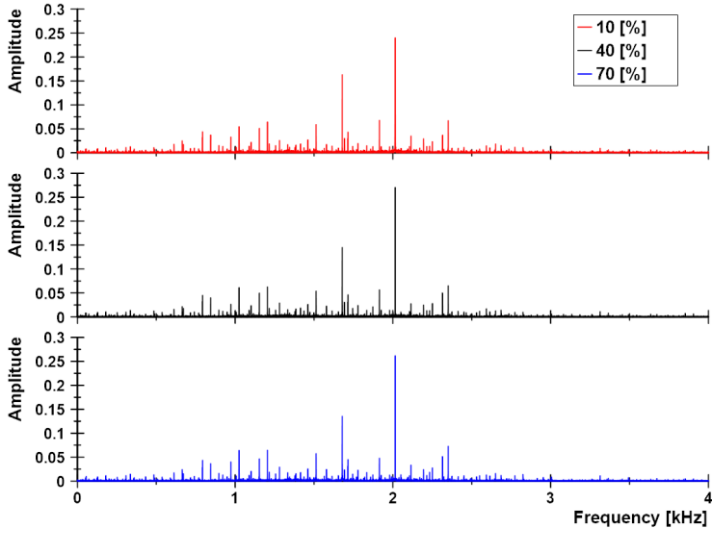

Figure 9.17 - Fast Fourier transform (FFT) of the current signal in the electromagnets for different magnetic level compensation. MIG wire feed speed: 14 m/min; plasma current: 100 A.

Schnelle Fourier-Transformation (FFT) des Stromsignals in den Elektromagneten für unterschiedliche Magnetpegelkompensationen. MSG-Drahtvorschubgeschwindigkeit: 14 m/min; Plasmastrom: 100 A.

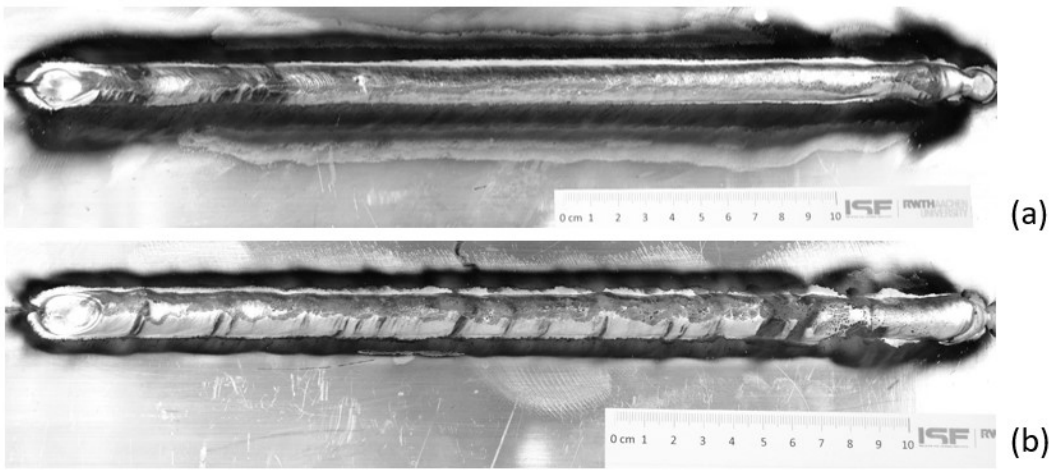

Figure 9.18 - Superficial appearance of the welding joints of 10 mm thickness aluminum AW6060-T66 with paraxial hybrid plasma-MIG process with (a) plasma-DC (b) plasma-AC.

Oberflächliches Erscheinungsbild der Schweißverbindungen aus 10 mm dickem Aluminium AW6060-T66 mit paraxialem Plasma-MSG-Hybridverfahren (a) Plasma DC (b) Plasma AC.

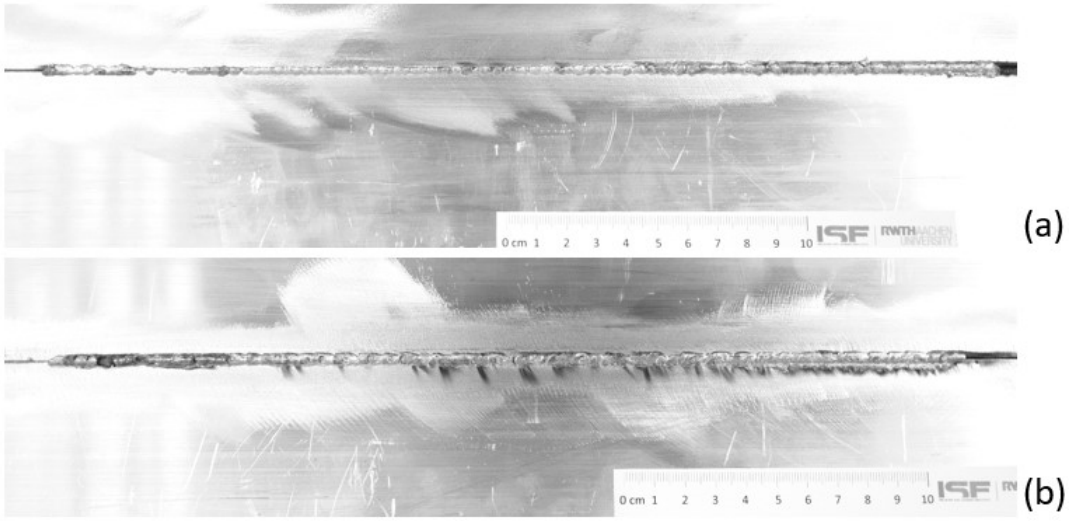

Figure 9.19 - Root appearance of the welding joints of 10 mm thickness aluminum AW6060-T66 with paraxial hybrid plasma-MIG process (a) plasma-DC (b) plasma-AC.

Wurzel der Schweißverbindungen aus 10 mm dickem Aluminium AW6060-T66 mit paraxialem Plasma-MSG-Hybridverfahren (a) Plasma DC (b) Plasma AC.

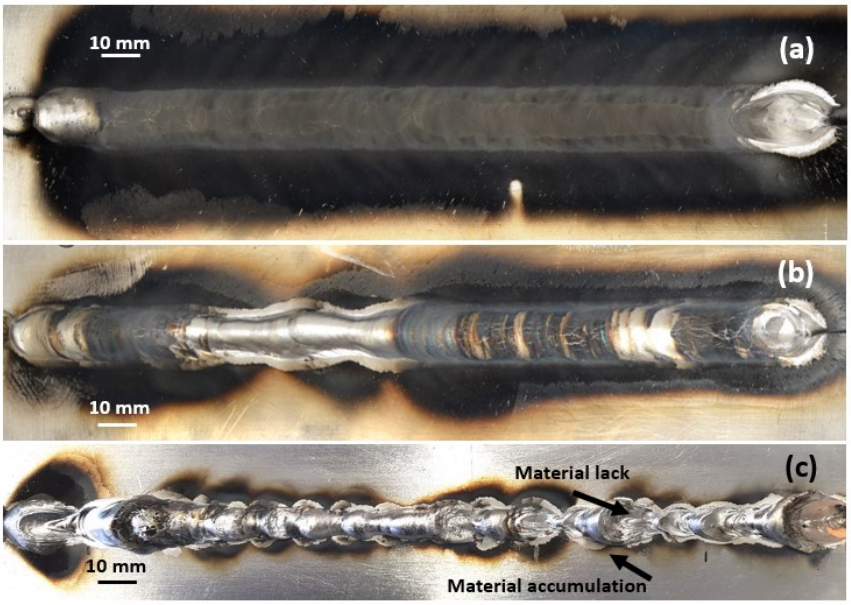

Figure 9.20 - Superficial appearance of the 15 mm joint without edge preparation (I-joint) made by (a) SuperMIG (b) paraxial plasma-MIG (c) MIG.

Oberflächliches Erscheinungsbild der 15-mm-Verbindung I-Stoß hergestellt durch (a) SuperMIG (b) Plasma-MSG-Paraxial (c) MSG.

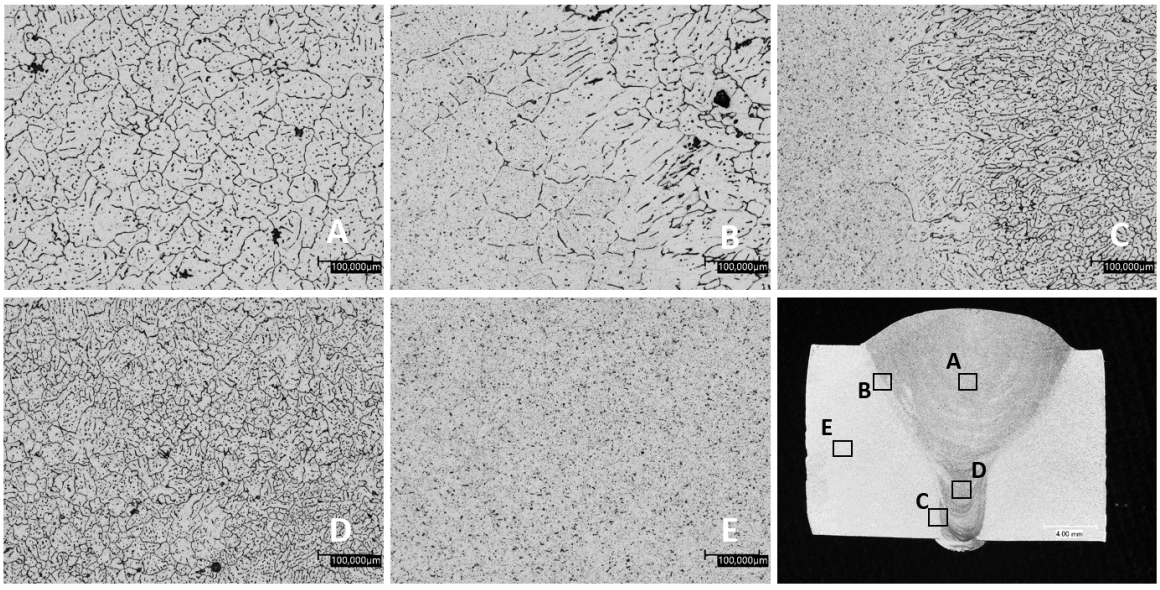

Figure 9.21 - Microstructures of weld beads made by SuperMIG. MIG wire feed: 18 m/min; plasma-DC: 200 A. Aluminum joints 15 mm thick.

Mikrostrukturen von Schweißraupen von SuperMIG. MSG-Drahtvorschub: 18 m/min; Plasma DC: 200 A. Aluminiumverbindung 15 mm dick.

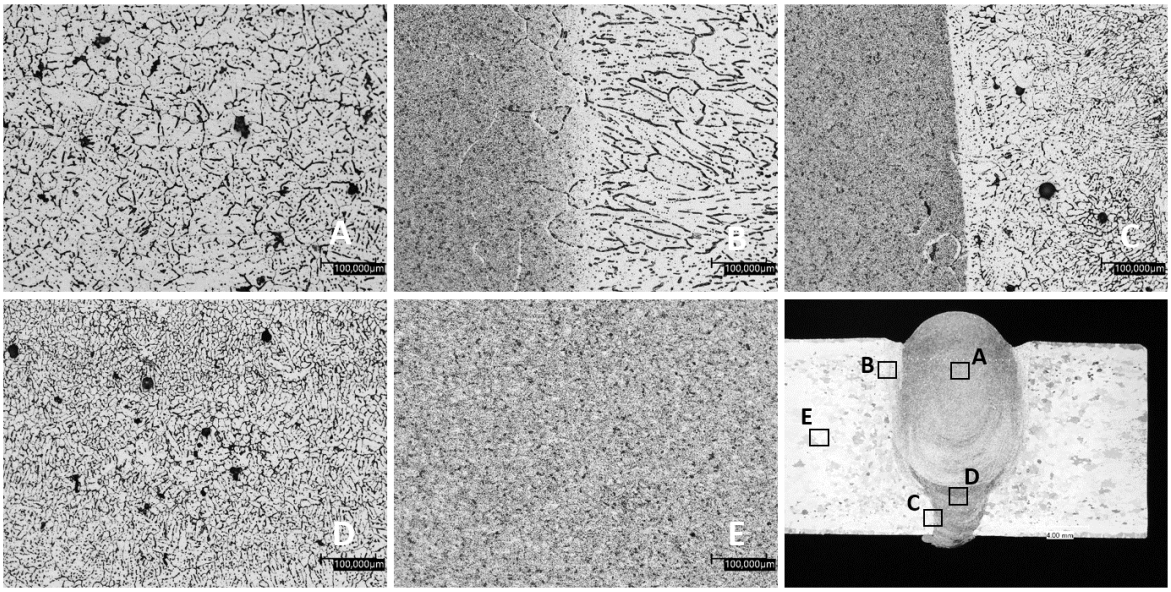

Figure 9.22 - Microstructures of weld beads made by single MIG process. MIG wire feed: 18 m/min. Aluminum joints 15 mm thick.

Mikrostrukturen von Schweißraupen im Einzel-MSG-Verfahren. MSG-Drahtvorschub: 18 m/min. Aluminiumverbindung 15 mm dick.

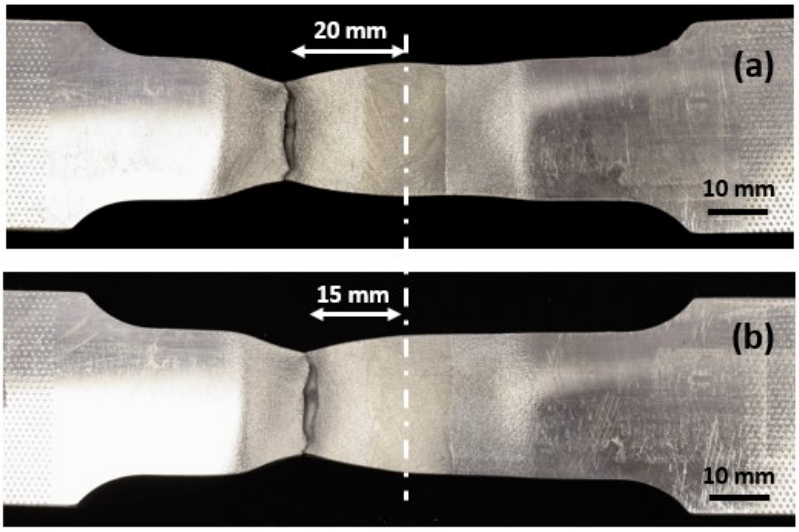

Figure 9.23 - Welding joint samples used in the tensile test for paraxial hybrid plasma-MIG process with plasma (a) direct current (b) alternating current. Aluminum joints 10 mm thick.

Schweißverbindungsproben, die im Zugversuch für das paraxiale Plasma-MSG-Hybridverfahren mit Plasma (a) DC (b) AC verwendet wurden. Aluminiumverbindung 10 mm dick.

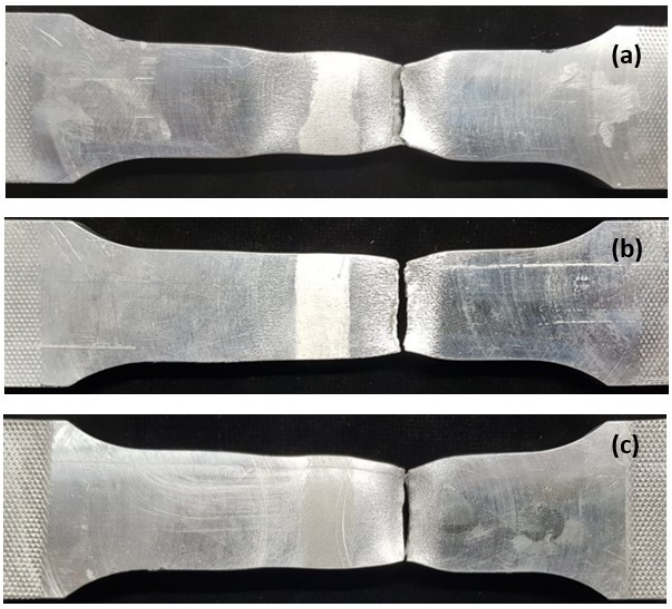

Figure 9.24 - Tensile test samples for (a) SuperMIG (b) MIG (c) paraxial plasma-MIG process. Aluminum joint 15 mm thick.

Zugversuchsproben für (a) SuperMIG (b) MSG (c) Plasma-MSG-Paraxialprozess. Aluminiumverbindung 15 mm dick.

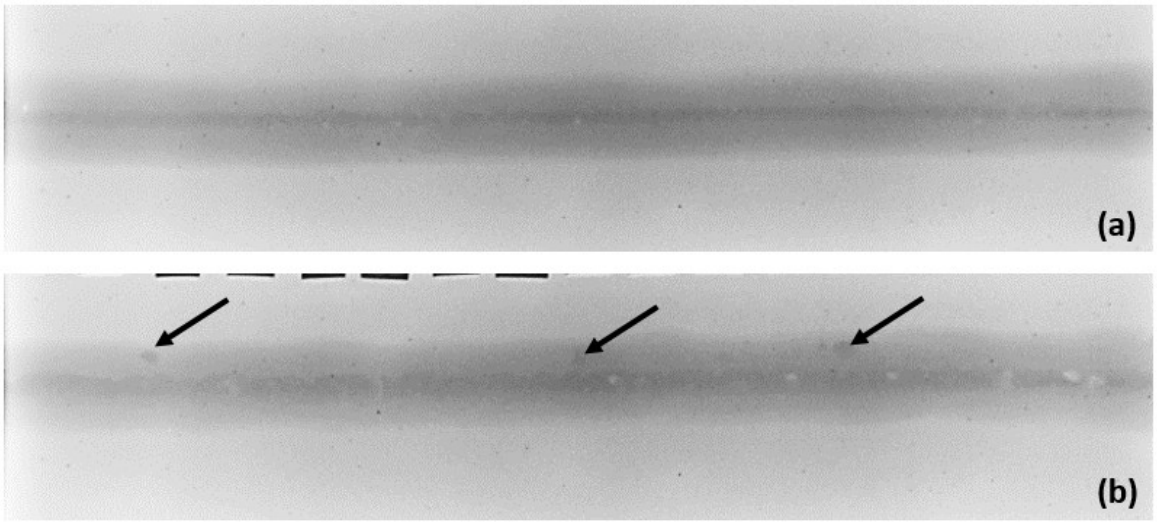

Figure 9.25 - X-ray image for plasma-MIG paraxial process with plasma (a) DC (b) AC. Aluminum joints 10 mm thick.

Röntgenbild für einen paraxialen Plasma-MSG-Prozess mit Plasma (a) DC (b) AC. Aluminiumverbindung 10 mm dick.

ISBN 978-3-8440-8639-3